

*Ion-electron recombination
in merged-beams experiments*

Henning T. Schmidt

Institute of Physics and Astronomy,
Aarhus University.

1994

Table of Contents

1.	<i>Preface</i>	2
2.	<i>Introduction</i>	6
3.	<i>The Merged-Beams Experiments</i>	9
	3.1. <i>The ion beams</i>	10
	3.2. <i>The electron beams</i>	14
	3.3. <i>Electron cooling</i>	29
4.	<i>Radiative Recombination</i>	35
	4.1 <i>RR for fully stripped ions</i>	35
	4.2 <i>RR for non-fully stripped ions</i>	39
	4.3 <i>Laser induced RR</i>	42
5.	<i>Dielectronic Recombination</i>	47
	5.1 <i>Introduction to DR</i>	47
	5.2 <i>DR for ground state Li-like ions</i>	52
	5.3 <i>DR for metastable He-like ions</i> <i>(the single-pass experiment)</i>	57
	5.4 <i>DR for metastable He-like ions</i> <i>(the TSR experiment)</i>	67
	5.5 <i>DR for Be-, B-, and C-like ions</i>	74
6.	<i>Lifetime measurements based on DR</i>	77
	6.1 <i>Lifetime of the 3S metastable state of He-like ions</i>	77
	6.2 <i>The experiment</i>	79
	6.3 <i>Analysis of data from the decay rate measurement</i>	82
	6.4 <i>Discussion of the results</i>	88
7.	<i>Dissociative Recombination</i>	94
	7.1 <i>Earlier DisR experiments</i>	94
	7.2 <i>Some basic concepts of diatomic molecules</i>	96
	7.3 <i>The DisR processes</i>	101
	7.4 <i>The ASTRID H_2^+ experiment</i>	106
	7.5 <i>Results and discussion</i>	112
8.	<i>Summary</i>	121
9.	<i>Dansk resumé</i>	123
10.	<i>Acknowledgments</i>	125

1. Preface

The present thesis serves to fulfil the requirements for the Ph.D. degree at the Faculty of Natural Sciences, Aarhus University. The thesis presents merged-beams experiments, investigating processes of ion-electron recombination. The main part of the work described was performed with the electron cooler at the Institute of Physics and Astronomy, Aarhus University, but the results of a six-month stay at the Max-Planck-Institut (MPI) für Kernphysik in Heidelberg, Germany, are presented as well.

When in the mid-80s, it was decided to build the Aarhus Storage Ring, Denmark (ASTRID), a wise and fruitful decision of building first the electron cooler and installing it at the TANDEM accelerator was made. This way one could gain experience working with ultra-high vacuum systems before constructing the storage ring itself, and at the same time provide an excellent tool for the study of recombination between free electrons and multiply charged ions in a single-pass configuration. Indeed, impressive results were obtained. The first direct tests of the absolute cross sections for radiative recombination (RR) were performed (Andersen 1990), and the dielectronic recombination (DR) measurements (Andersen 1989) had an energy resolution improved by a factor of 30 compared to earlier works.

When I joined the project as a student in the Fall of 1989, these two great successes had been achieved quite recently, and in the spirit of optimism that followed, we decided to try to perform laser-induced radiative recombination (LIR). This attempt was not successful, and after observations of LIR were reported from MPI, Heidelberg

(Schramm 1991) and from University of Western Ontario (Yousif 1991), we stopped this experiment. During the time of our LIR experiment, we continued to study RR for non-fully stripped ions [II,V] and DR with low-energy electrons [I,III,IV,V]. In the Spring of 1992, the electron cooler was 'recombined' with ASTRID. In the following year, technical difficulties had to be solved, and no real electron-cooler experiments were performed. During this year, I spent six months in Heidelberg working on DR with metastable He-like ions measured both as a function of electron energy and as a function of time after injection to deduce the lifetimes of the metastable $1s2s\ ^3S$ states [VI]. In 1993 we made the first experiments with the electron cooler at ASTRID. So far, we have studied electron cooling of D^+ , dissociative recombination (DisR) of H_2^+ , and electron-impact detachment of D^- . For future applications of the electron cooler, we have improved the energy resolution at low relative energies by about one order of magnitude, applying the so-called 'adiabatic expansion' technique first realized at the Stockholm storage ring CRYRING (Danared 1993).

Throughout this thesis, a rather significant variation concerning the amount of details presented on the performance and results of the different experiments will encounter the reader. This is due to a selection based on the following criteria: First of all, previously unpublished material, in particular sec.5.4 on the TSR measurement of DR for metastable He-like ions and ch.7 on the ASTRID experiment on DisR of H_2^+ , is given a high priority. Other criteria also considered in the selection process are the existence of detailed theoretical predictions to compare with our data and the usefulness of a certain

detail in making a point in the presentation.

Parts of the material considered in this thesis has previously been presented in the publications listed in the following.

- I. N R Badnell, M S Pindzola, L H Andersen, J Bolko, and H T Schmidt (1991): *Dielectronic recombination of light Be-like and B-like ions*. Journal of Physics B **24** 4441
- II. L H Andersen, G Y Pan, and H T Schmidt (1992): *Radiative recombination with highly charged Si^{6+} and Si^{11+} ions*. Journal of Physics B **25** 277
- III. L H Andersen, G Y Pan, H T Schmidt, N R Badnell, and M S Pindzola (1992): *State-selective measurements and calculations of dielectronic recombination with Li-like N^{4+} , F^{6+} and Si^{11+} ions*. Physical Review A **45** 6332
- IV. L H Andersen, G Y Pan, H T Schmidt, N R Badnell, and M S Pindzola (1992): *Absolute measurements and calculations of dielectronic recombination with metastable He-like N, F and Si ions*. Physical Review A **45** 7868
- V. H T Schmidt, G Y Pan, and L H Andersen (1992): *Dielectronic recombination with $\Delta n=0$ and $\Delta n=1$ core excitations and radiative recombination for C-like F^{3+} ions*. Journal of Physics B **25** 3165
- VI. H T Schmidt, P Forck, M Grieser, D Habs, J Kenntner, G Miersch, R Repnow, U Schramm, T Schüßler, D Schwalm, and A Wolf (1994): *High-precision measurement of the relativistic magnetic-dipole decay rate of metastable heliumlike carbon ions in a storage ring*. Phys.Rev.Lett. **72**, 1616

The papers listed above will be referred to by roman numbers, whereas other literature cited in the text is referred to by the name of the first author followed by the year of publication. References to other literature will be given at the end of each chapter.

L H Andersen, J Bolko, P Kvistgaard (1990) Phys.Rev.Lett. 64 729.

L H Andersen, P Hvelplund, H Knudsen, and P Kvistgaard (1989) Phys.Rev.Lett. 62 2656

U Schramm, J Berger, M Grieser, D Habs, E Jaeschke, G Kilgus, D Schwalm, A Wolf, R Neumann, R Schuch (1991) Phys.Rev.Lett. 67 22

F B Yousif, P v.d. Donk, Z Kucherowski, J Reis, E Brannen, J B A Mitchell, and T J Morgan (1991) Phys.Rev.Lett. 67 26

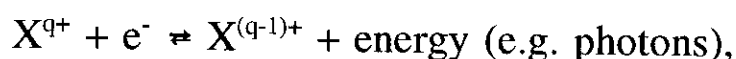
H Danared (1993) NIM A335 397

2. Introduction

From our every-day experience, we all know that matter is found in three phases: The solid phase, the liquid phase, and the gaseous phase. In the ordinary gas phase, matter consists of free neutral molecules. In the situation, where some degree of ionization has taken place, and we have a mixture of atomic and molecular ions and free electrons, we speak of a fourth phase, the plasma phase.

The plasma phase can be reached either by having a very high temperature or by introducing some external ionization mechanism, such as an electrical discharge or irradiation with light with a photon energy exceeding a few eV (i.e. UV, x rays, and γ rays).

When a plasma has been formed, an equilibrium situation can be reached:



where X^{q+} denotes an ion in charge state $q+$. The process from right to left is ionization, while the inverse process is ion-electron recombination, the subject of this thesis. Of course, in a plasma many other processes take place (ion-ion charge exchange, ion excitation induced by collisions with electrons, emission of bremsstrahlung from electrons accelerated by ions, etc.). However, ion-electron recombination remains an essential feature of plasma physics. Plasmas, where these 'atomic physics' processes are dominating, are well known in nature. They can be found in, e.g., stellar atmospheres and in interstellar nebulae; but also in the upper atmosphere of the Earth, where the solar UV radiation leads to ionization. In fact, some of the first experimental

investigations of ion-electron recombination were performed as an attempt to understand the number densities of atomic and molecular ions in the upper atmosphere.

Let us now consider a system consisting of an ion X^{q+} and a free electron e^- . By the conventional definition of the zero point for the total mechanical energy, this system must have a positive energy, while a system forming a stable, bound state of the two (i.e. $X^{(q-1)+}$) must have a negative energy. Hence, in a recombination process, energy in some form must be released. In radiative recombination (RR), the excess energy is emitted in the form of a photon. This is a non-resonant process, having its maximum rate at 0 eV relative energy. Since this process does not require any change of the structure of the initial ion, this will be possible for any positive ion, even a fully stripped one. Another process, also possible for any ion, is referred to as three-body (or ternary) recombination (TR). In this process, the excess energy is given to a second free electron in the form of kinetic energy. Since this process requires the presence of two free electrons, it will have a rate proportional to the electron density n_e squared. This means that when the electron density becomes sufficiently high, the TR rate (which also takes on its maximum value at zero relative energy) will exceed the RR rate. However, for the experiments described in this thesis, the electron density is sufficiently low that the TR contribution is negligible.

For ions carrying electrons, a third recombination mechanism, known as dielectronic recombination (DR), becomes possible. Here the excess energy in the recombination process is used to excite one of the bound electrons, leaving the ion in a doubly excited state which might

autoionize or, alternatively, stabilize radiatively, in which case the DR process has been completed. Since the excitation of the initially bound electron requires a specific amount of energy, the DR process will be resonant.

When the ion, in the initial state, is a molecular ion, new degrees of freedom describing the relative motion of the nuclei are introduced. This makes possible a fourth recombination mechanism, for which the excess energy is transferred to these new degrees of freedom. As a consequence of this, the molecule dissociates. This process is therefore called dissociative recombination.

3. The Merged-Beams Experiments

In this chapter, general features of the merged-beams experiments will be described, postponing some experimental points to the chapters concerning the particular experiments. In sec.3.1 the accelerators and ion beams are briefly described, emphasizing the features relevant to the electron-cooler experiments. Section 3.2 deals with the electron cooler. The electron beam will be described in much more detail than the ion beam since it is the velocity spread of the electrons that determines the energy resolution in the experiments. The final section of this chapter is devoted to electron cooling which, besides being an interesting physical process in itself, is an important tool for understanding other merged-beams experiments performed in storage rings.

The general idea of merged-beams recombination measurements is to overlap two co-propagating beams of electrons and ions of charge q times the elementary charge e over a certain interaction region, and then, as a function of the relative energy, monitor the yield of ions in charge state $(q-1)^+$. The entity determined in the experiments is the recombination rate coefficient $\langle v\sigma \rangle$ (see sec.3.2 eq.3.5). The experimental rate coefficient is determined as

$$\langle v\sigma \rangle = \frac{N^{(q-1)^+} - N_0^{(q-1)^+}}{N^{q+}} \frac{v_i}{\text{Ln } \epsilon}, \quad (3.1)$$

where $N^{(q-1)^+}$ is the yield of ions in the $(q-1)^+$ charge state, with the electron beam tuned to the desired relative energy, $N_0^{(q-1)^+}$ is a background measurement performed by switching off the ion beam (chopping), or changing the energy to a value with zero rate coefficient

(modulating) or, in the case of the storage ring, DR measurements for ions in metastable states waiting for the metastable component to decay to the ground state. L is the length of the interaction region, n_e is the electron density, ϵ is the detector efficiency, and v_i is the ion velocity in the laboratory rest frame.

3.1. The ion beams

The single-pass experiments [I-V] were performed at the Aarhus 6 MV Tandem accelerator. The setup is sketched in fig. 3.1. Positively charged atomic ions were available with typical currents in the range of 200 nA to about 1 μ A for energies of 1-2 MeV per atomic mass unit. From the bending magnet before the electron cooler and on, the pressure was kept below $1\text{-}2 \cdot 10^{-11}$ mBar to reduce the background signal caused by electron capture in collisions with residual-gas molecules. In the interaction region, two sets of electro-static pick-up

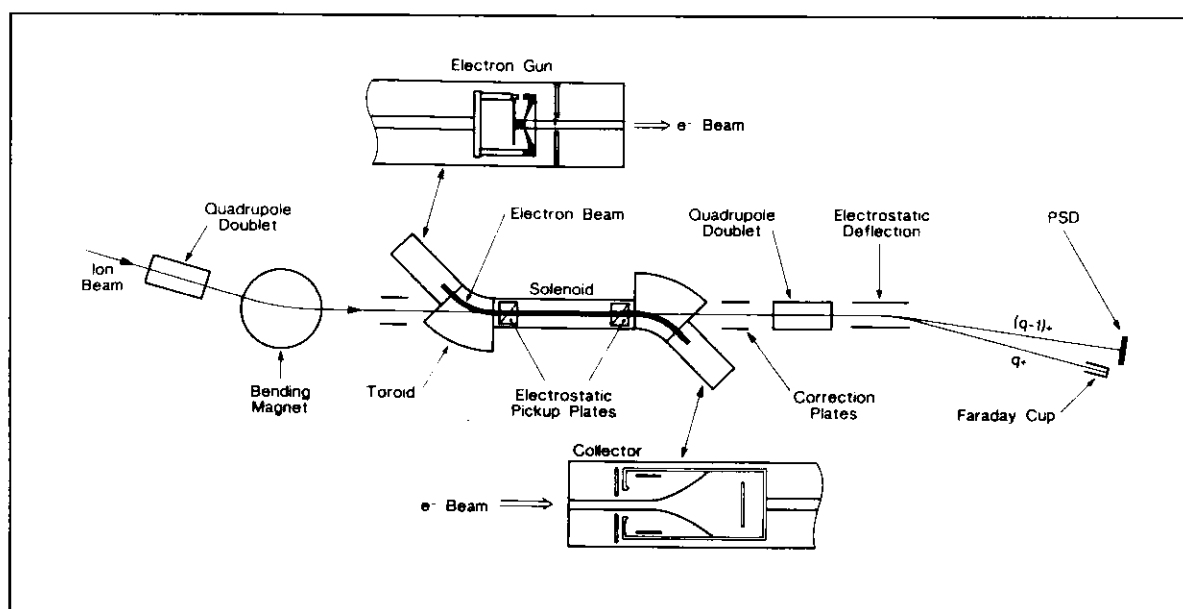


Figure 3.1 *The Aarhus single-pass experiment.*

plates were used to monitor the positions of both the ion and electron beams to ensure full overlap. The ion beam was assumed to be gaussian with a FWHM of 2-3 mm, and the electron beam was 1 cm diameter with uniform density. After the electron cooler, a charge-state separation was performed using a transverse electric field, typically of the order of 10 kV/cm. As a consequence of the traversal of this field, electrons in high Rydberg states were field-ionized and therefore not counted as recombined. The critical principal quantum number, n_{limit} , above which ionization takes place, is given by the following semi-classical expression (Griffin 1989)

$$n_{\text{limit}} = (6.2 \cdot 10^8 q^3/E)^{1/4}, \quad (3.2)$$

where E is the electric-field strength in V/cm. To facilitate the detection, it was necessary to focus the final-state ions onto the position-sensitive channel-plate detector, and therefore no experiments with singly charged ions could be performed since these would result in neutral products.

Figure 3.2 shows the storage ring ASTRID with the parts of greatest interest to the electron-cooler experiments. Beams of singly charged, positive and negative, atomic and molecular ions covering a mass range of 1-1000 atomic mass units have been stored at the injection energy of 50 to 200 keV. However, to perform electron cooler experiments, it is necessary to increase the energy to several MeV, depending on the specific ion beam. The acceleration is achieved by bunching the beam with the RF cavity and then perform a synchronized ramping of the magnetic-dipole fields of the storage ring and the RF frequency. During this ramping, it is necessary to monitor the

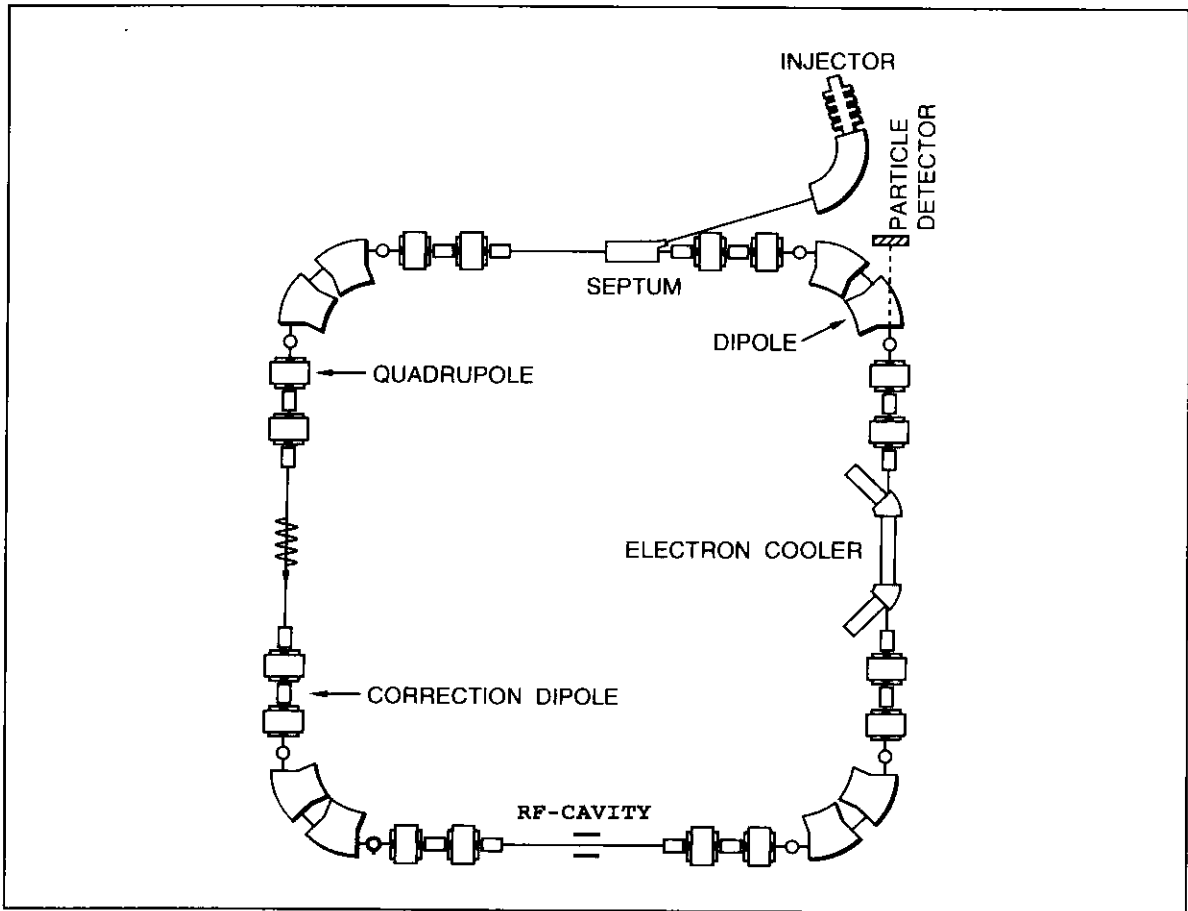


Figure 3.2 *The ASTRID storage ring.*

time structure of the ion beam on one of the pick-up plates to keep the relative phase of the RF and the ion bunches fixed. To perform this monitoring, an ion current of 0.5-1 μA is required. Due to losses during storage and acceleration, it is therefore only possible to perform electron-cooler experiments with ions for which currents from the ion sources of a few μA 's are achievable. For many singly charged positive ions, currents of this magnitude are available from the 'universal' standard plasma ion sources ('Nielsen'-sources). For some negative ions, sputter ion sources (e.g. O^-) or duoplasmatrons (e.g. H^-) can yield the necessary current. An EBIS (Electron Beam Ion Source) that can yield high currents of multiply charged ions is under construction and will be available for future experiments. The ion-beam

position is monitored by the ten sets of electrostatic pick-up plates; two in the electron cooler and one at each end of the four straight sections. The positions can be optimized by adjusting the eight correction dipoles. Charge-state analysis is inherently performed in the dipole magnet following the electron cooler. The effective electric field caused by the transverse magnetic field will lead to field ionization of ions in high Rydberg states according to eq.(3.2). In SI units, the field strength is given as

$$E = \gamma v B = \frac{v B}{\sqrt{1 - v^2/c^2}}, \quad (3.3)$$

where v is the ion velocity. This electric field is typically of the order of 100 kV/cm.

As mentioned in the preface, some of the experiments described in this thesis were performed at the TSR (Test Storage Ring) at the Max-Planck-Institut für Kernphysik in Heidelberg. At the TSR, ions can be injected from a 12 MV Tandem accelerator. This means that electron-cooler experiments can be performed at the injection energy. This point was crucial to these experiments since they concerned ions in metastable states with lifetimes in the millisecond range, leaving no time for ion-beam acceleration. Like in ASTRID, the dipole magnet following the electron cooler acts as a charge-state analyzer. This means that field ionization according to eqs. (3.2) and (3.3) takes place.

3.2 The electron beams

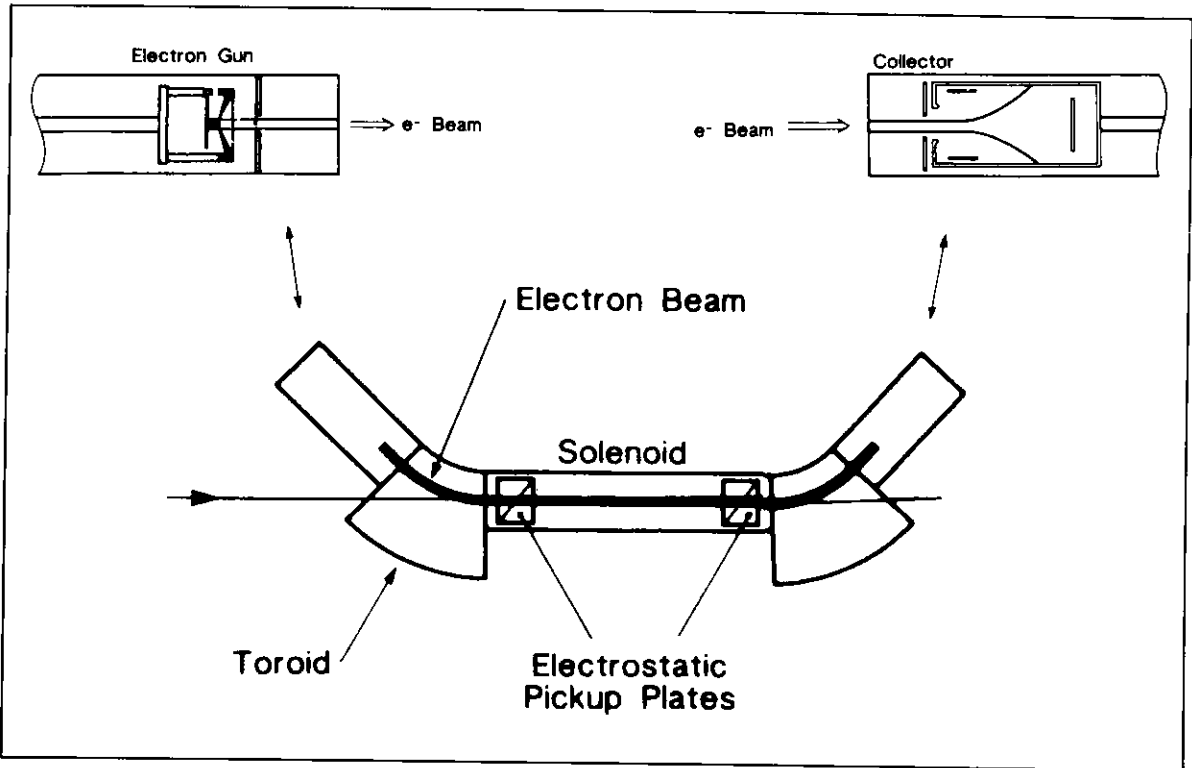


Figure 3.3 *The ASTRID electron cooler.*

Figure 3.3 shows schematically the ASTRID electron cooler. The source of electrons is an indirectly heated disc-shaped BaO-coated tungsten cathode. Cathodes of 10 and 15 mm diameter have been used. The cathode is surrounded by a Pierce shield which can be given a low bias voltage with respect to the cathode potential. From the cathode, the electrons are accelerated towards the anode which is a grid with approximately 80% transmittance. In the case of a space-charge-limited electron beam, the emitted electron current is given by (Poth 1990)

$$I_{\text{electron}} = PV^{3/2}, \quad (3.4)$$

where V is the cathode-anode potential difference, and the constant of proportionality P (the perveance) is inversely proportional to the square

of the cathode-anode distance which can be varied from the outside, allowing for continuous electron-current tuning. The electron beam is guided from the electron gun through the one-meter interaction region to the collector by a solenoid magnetic field. In standard operation, this field is kept constant from the electron gun to the entrance of the collector, leading to a constant beam diameter equal to the cathode diameter. In the collector, the solenoid field decreases, and the beam blows up transversely.

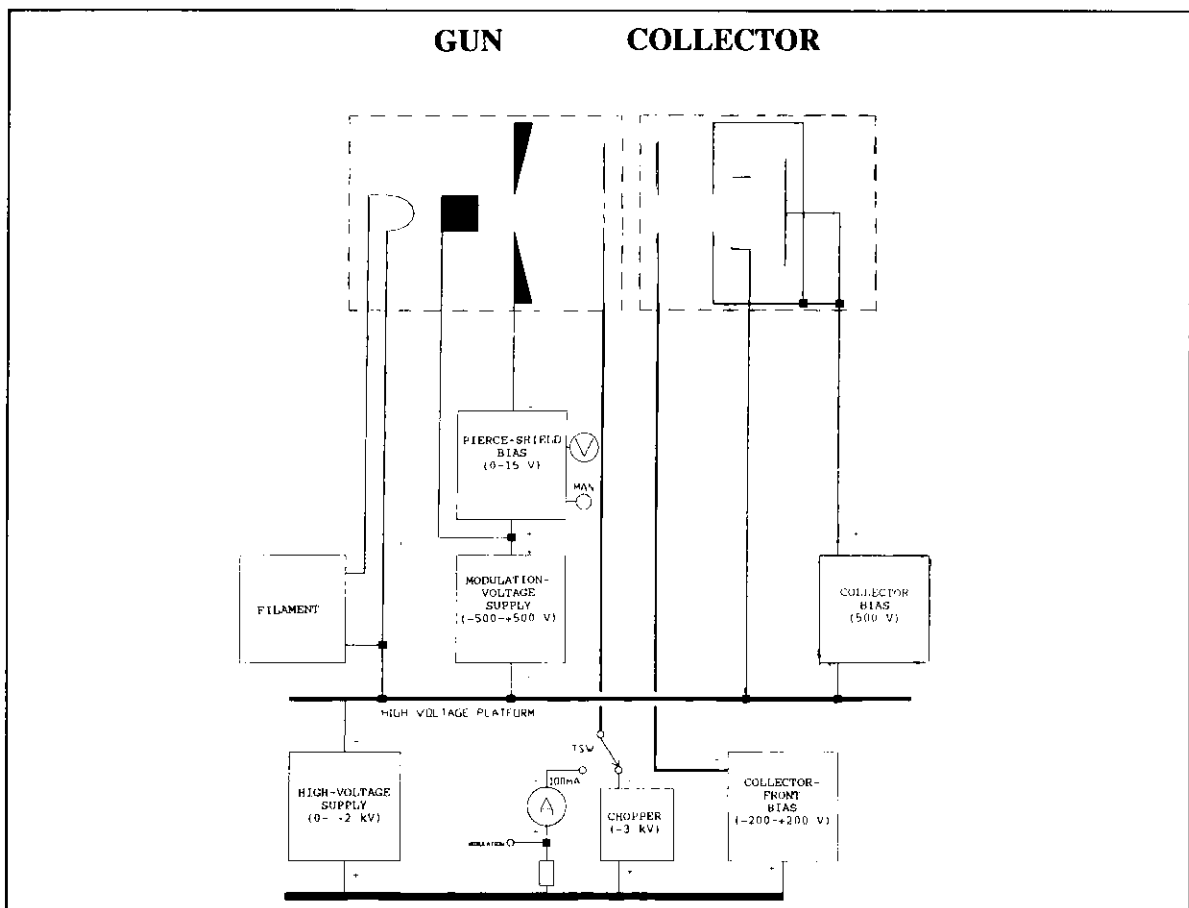


Figure 3.4 *The electrical connections for the electron cooler.*

In fig.3.4 is shown the electrical connections for the electron cooler. The cooler can be run in a DC mode, where the high-voltage platform voltage is equal to the acceleration voltage, but it is often useful to be able to modulate the acceleration voltage between two

values or to switch the beam on and off. For modulation, we have a ± 500 V supply at the high-voltage platform, and for chopping the beam we have a 3 kV supply connected to the anode.

In the remainder of this section, I will discuss the electron-beam velocity distribution since the influence of the ion-velocity distribution on the distribution of relative velocities can be neglected due to the much larger mass of the ions. If the total cross section for recombination as a function of the relative velocity v is known, the rate coefficient $\langle v\sigma \rangle$ in a merged-beams experiment may be expressed as

$$\langle v\sigma \rangle = \int v \sigma(v) f(\bar{v}, \Delta, T_{\perp}, T_{\parallel}) d\bar{v}. \quad (3.5)$$

Here the electron-velocity distribution f in the ion-beam rest frame is a flattened Maxwell distribution, i.e., the product of a two-dimensional transverse and a one-dimensional longitudinal, gaussian velocity distribution,

$$f(\bar{v}, \Delta, T_{\perp}, T_{\parallel}) = \frac{m}{2\pi k T_{\perp}} \exp\left(\frac{-m v_{\perp}^2}{2k T_{\perp}}\right) \cdot \left(\frac{m}{2\pi k T_{\parallel}}\right)^{1/2} \exp\left(\frac{-m v_{\parallel}^2}{2k T_{\parallel}}\right), \quad (3.6)$$

where v_{\parallel} and v_{\perp} are the *random* components of the relative velocity parallel and perpendicular to the ion-beam direction, respectively, T_{\parallel} and T_{\perp} are the associated 'temperatures' of the electron beam, and Δ is the detuning velocity. The relative velocity is related to the detuning velocity through the following 'pythagorean' relation:

$$v^2 = v_{\perp}^2 + (\Delta + v_{\parallel})^2. \quad (3.7)$$

The deviation of the relative energy E_{rel} from the value $E_{\text{rel},0} = m\Delta^2/2$ is

then found to be

$$\delta E_{\text{rel}} = m(v^2 - \Delta^2)/2 = \delta E_{\perp} + \delta E_{\parallel} \pm 2\sqrt{E_{\text{rel},0}} \delta E_{\parallel}, \quad (3.8)$$

where $\delta E_{\perp} = mv_{\perp}^2/2$. For typical electron-beam temperatures of $kT_{\perp} = 100$ meV and $kT_{\parallel} = 1$ meV, we see from eq.(3.8) that for low energies ($E_{\text{rel}} \leq 1$ eV), kT_{\perp} determines the energy resolution, whereas for $E_{\text{rel}} \geq 10$ eV, the last term in eq.(3.8) dominates, and kT_{\parallel} determines the resolution. When low relative energies are considered (i.e. electron-cooling experiments, radiative recombination, dissociative recombination, and low-energy dielectronic recombination), it is therefore of interest to reduce kT_{\perp} .

When the guiding solenoid field is kept constant through the cooler, $kT_{\perp} \approx kT_{\text{cath}}$, where T_{cath} is the temperature of the cathode. One way to reduce kT_{\perp} is then to reduce the temperature of the cathode. At the MPI Heidelberg, experiments have been made with electron beams produced by laser irradiation of a cold semi-conductor cathode (Habs 1988), but so far, sufficient current for electron-cooler operation has not been achieved. Another way of reducing kT_{\perp} is the so-called adiabatic expansion technique, where the magnetic field strength of the guiding solenoid decreases slowly from the electron gun to the interaction region, leading to an almost proportional decrease in kT_{\perp} (Danared 1993). Since we are now applying the second of these methods, I will describe this in more detail.

Because of the guiding magnetic field, the energy in the transverse motion caused by the finite temperature of the cathode, and possibly imperfections in the fields will be 'stored' in the cyclotron motion of the electrons. The energy in the cyclotron motion is given by the subscript c (for cyclotron)

$$E_c = m r_c^2 \omega_c^2 / 2 = B^2 r_c^2 e^2 / (2m). \quad (3.9)$$

If we assume that the relative change in r_c during one cyclotron oscillation is much smaller than unity (adiabatic motion), the electrons will be able to follow the magnetic field lines, and the magnetic flux through a cyclotron loop will be constant. Hence $B r_c^2$ is constant. Comparing this to eq.(3.9), we find that E_c changes proportional to the magnetic field. As a measure of the adiabaticity, we introduce the adiabaticity parameter χ , defined by

$$\chi = \frac{1}{B} T \frac{dB}{dt} = \frac{1}{B} \lambda_c \frac{dB}{dz}, \quad (3.10)$$

where T is the cyclotron period, z is the position coordinate along the beam axis, and the distance travelled in the z direction during one period, λ_c , is given by

$$\lambda_c = \left(\frac{8\pi^2 m E_0}{e^2 B^2} \right)^{1/2}, \quad (3.11)$$

where E_0 is the electron-beam energy. Numerical simulations using the Hermansfeldt computer code (Hermansfeldt 1979) show that the motion remains adiabatic up to $|\chi_{\max}| \approx 0.35$. The new ASTRID gun solenoid can give a magnetic field of 2 kG. The magnetic field on axis and the adiabaticity parameter are shown in fig.3.5 for an electron energy of 1 keV and interaction magnetic fields of 100 G and 200 G.

So far, I have assumed that the transverse motion of the electrons consisted solely of the circular motion caused by the random velocity component perpendicular to the solenoid field. This is not strictly true: Even if an electron is launched from the gun with zero

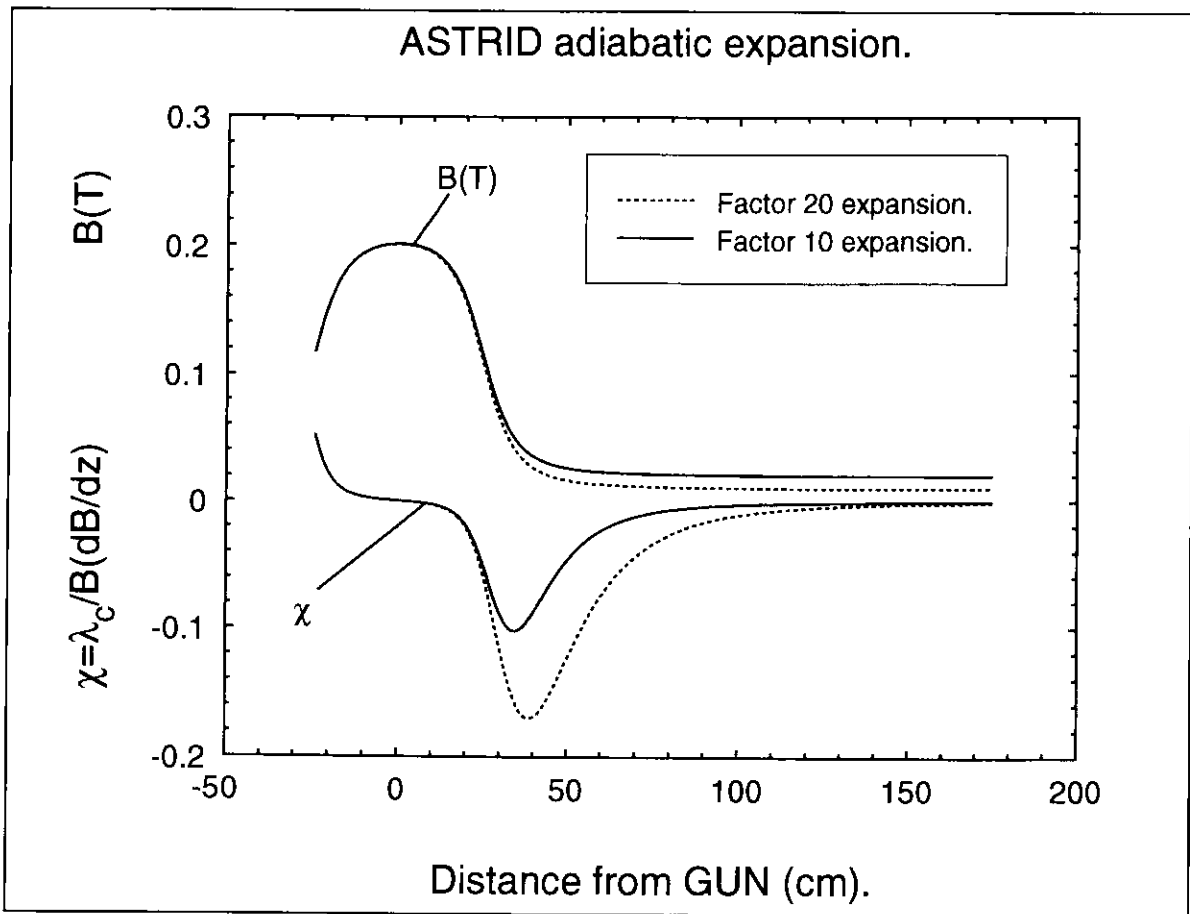


Figure 3.5

transverse velocity, it will start to perform the transverse so-called steady motion. The steady motion is caused by the space-charge electric field, in combination with the solenoid field, and its energy is given by (Poth 1990)

$$E_{ST} = \frac{mr^2\omega_p^4}{8\omega_c^2\gamma^2}, \quad (3.12)$$

where r is the distance from the center of the beam, ω_p is the plasma frequency, and γ is the relativistic Lorentz factor which is close to one for the energy range of about 1 keV of interest to us. A convenient formula for the steady motion energy yields

$$E_{ST}(\text{eV}) = 2.3 \cdot 10^{-14} \left(\frac{r(\text{mm})n_e(\text{cm}^{-3})}{B(\text{G})} \right)^2, \quad (3.13)$$

where n_e is the electron density. Normally $E_{ST} \ll E_c$, but since E_{ST} in the interaction region depends only on the value of the parameters r , B , and n_e in the interaction region, E_{ST} is not affected by the adiabatic expansion and hence sets a limit to the usefulness of this technique. In table 3.1 are shown the cyclotron and steady-motion energies for an electron launched from the gun with a typical transverse energy of 0.13 eV, assuming an interaction-region electron density of $n_e = 5 \cdot 10^6 \text{ cm}^{-3}$.

Table 3.1

Expansion factor	$E_c(\text{meV})$	$E_{ST}(\text{meV})$ $r=5\text{mm}$	$E_{ST}(\text{meV})$ $r=10\text{mm}$	$E_{ST}(\text{meV})$ $r=15\text{mm}$	$E_{ST}(\text{meV})$ $r=20\text{mm}$
10	13	0.4	1.7	3.6	*)-
20	6.5	1.7	6.8	15	23

*) *The 1 cm diameter cathode is used. Therefore the radius after a factor of 10 expansion is only 15.8 mm.*

As can be seen from eq.(3.8), also the longitudinal electron-beam temperature plays a role in determining the energy resolution for $E_{rel} \geq 1 \text{ eV}$, in particular if the transverse-energy spread is decreased by adiabatic expansion. We therefore now turn to the longitudinal electron-beam temperature kT_l . Electrons emitted from the hot BaO-coated tungsten cathode obey a spherically symmetric maxwellian velocity distribution with temperature T_{cath} . The ripple on the acceleration voltage causes an increase in the longitudinal-energy spread, as

observed in the laboratory rest frame. What is interesting from the point of view of the experiments is, however, the velocity distribution in the reference frame moving with the average electron velocity. After transforming to this frame of reference, one finds the following longitudinal temperature (Poth 1990):

$$kT_{\parallel} = \frac{(eV_{\text{ripple}} + kT_{\text{cath}})^2}{4E_0}, \quad (3.14)$$

where E_0 denotes the electron-beam energy.

The longitudinal temperature given above is, however, not the temperature one finds in the interaction region. In particular, the heating mechanisms, known as longitudinal-longitudinal relaxation and transverse-longitudinal relaxation, play a decisive role in determining the longitudinal beam temperature in the interaction region. These two mechanisms will be described in the following.

When the electrons leave the cathode, their spatial distribution will not be uniform. This means that they will have different potential energies determined by the local density of electrons. The phase-space compression caused by the acceleration as indicated in the above formula will, if the electrons are given sufficient time prior to the acceleration to have these variations in potential energy evolve into kinetic-energy variations, make the effect of this mechanism become negligible. If, however, the acceleration is fast compared to the typical plasma time scale, $\tau_p = 2\pi/\omega_p$, where the plasma frequency is given by $\omega_p = \sqrt{4\pi n_e e^2/m}$, the spatial fluctuations will survive until after the acceleration, whereupon this so-called longitudinal-longitudinal relaxation will lead to an increase of the longitudinal temperature of

approximately $e^2 n_e^{1/3}$ (Kudelainen 1982).

The electron beam now produced has a highly oblate velocity distribution ($kT_{\parallel} \ll kT_{\perp}$). In this beam elastic scattering among the electrons will gradually transfer the velocity spread from the transverse degrees of freedom into the longitudinal degree of freedom until eventually $kT_{\parallel} = kT_{\perp}$. If the influence of the guiding magnetic field is neglected, the rate of transverse-longitudinal relaxation pr. unit length is given by (Dikansky 1987)

$$\left(\frac{d(kT_{\parallel})}{dz} \right)_{B=0}^{t-1} = \frac{\pi e^3 j L_c C}{E_0} \sqrt{\frac{m}{kT_{\perp}}}, \quad (3.15)$$

where j is the current density, C is a numerical constant equal to 0.87 for an oblate maxwellian distribution, and L_c is the Coulomb logarithm:

$$L_c = \log \left(\frac{v_{\perp} / \omega_p}{e^2 / kT_{\perp}} \right). \quad (3.16)$$

In more convenient units, the rate of change in the longitudinal temperature is given by

$$\left(\frac{d(kT_{\parallel})}{dz} \right)_{B=0}^{t-1} = \frac{j(\text{A/cm}^2) L_c}{E_0(\text{eV}) \sqrt{kT_{\perp}(\text{eV})}} 8.46 \cdot 10^{-3} \text{eV/cm}. \quad (3.17)$$

The magnetic field restricts the transverse motion of the electrons to distances of the order of the cyclotron radius,

$$r_c = \frac{\sqrt{2mkT_{\perp}}}{eB} = 3.37 \text{ cm} \frac{\sqrt{kT_{\perp}(\text{eV})}}{B(\text{G})}. \quad (3.18)$$

For strong magnetic fields, $r_c \ll n_e^{-1/3}$ and collisions among electrons become improbable, leading to a suppression of the transverse-longitudinal relaxation mechanism. A quantitative measure of this suppression is given by an empirical formula (Kudelainen 1982, Dikansky 1987)

$$\left(\frac{d(kT_{\parallel})}{dz} \right)^{t-1} = \left(\frac{d(kT_{\parallel})}{dz} \right)_{B=0}^{t-1} \exp \left(-2.8 \frac{e^2/r_c}{e^2 n_e^{1/3} + kT_{\parallel}} \right). \quad (3.19)$$

I now want to evaluate the effect of these two heating mechanisms for various configurations relevant to the ASTRID electron cooler. We first consider the time scales involved.

We consider as an example an electron beam accelerated to $E_0=1000$ eV over a distance of $d=2$ cm and transported $s=1$ m.

$$\text{Acceleration time: } \tau_{\text{acc}} = 2d/v = 2.2 \text{ ns.}$$

$$\text{Plasma time scale: } \tau_p = 2\pi/\omega_p = 35 \text{ ns}/\sqrt{n_e/1 \cdot 10^7 \text{ cm}^{-3}}.$$

$$\text{Transport time: } \tau_{\text{tr}} = s/v = 52 \text{ ns.}$$

Since $\tau_{\text{acc.}} \ll \tau_p$, the acceleration is not adiabatic, and we have to take the longitudinal-longitudinal relaxation into account. As the transport time is of the order of the plasma time scale, we will add the extra longitudinal temperature gradually. A reasonable way to do this is to

set the rate of change of kT_{\parallel} due to longitudinal-longitudinal relaxation equal to

$$\left(\frac{d(kT_{\parallel})}{dz} \right)^{1-1} = \frac{e^2 n_e^{1/3}}{v\tau_p} \quad (3.20)$$

for $z < v\tau_p$ and otherwise zero.

Table 3.2

	Tandem	ASTRID (no ad.exp.)	ASTRID (ad.exp.x 20)	ASTRID (ad.exp.x 10)
Energy(eV)	1000	1000	1000	1000
Ripple peak-peak (V)	0.8	0.8	0.8	0.8
kT_{cath} (eV)	0.11	0.11	0.11	0.11
I (mA)	10	2.8	24.5	12.3
j^{GUN} (mA/cm ²)	12.7	1.56	31	15.6
n_e^{GUN} (cm ⁻³)	$4.1 \cdot 10^7$	$5 \cdot 10^6$	$1 \cdot 10^8$	$5 \cdot 10^7$
B^{GUN} (G)	100/200	100/200	2000	2000
$B^{\text{INT.}}$ (G)	–	–	100	200
$j^{\text{INT.}}$ (mA/cm ²)	–	–	1.56	1.56
$n_e^{\text{INT.}}$ (cm ⁻³)	–	–	$5 \cdot 10^6$	$5 \cdot 10^6$
$kT_{\parallel}^{\text{GUN}}$ (eV)	$6.5 \cdot 10^{-5}$	$6.5 \cdot 10^{-5}$	$6.5 \cdot 10^{-5}$	$6.5 \cdot 10^{-5}$
$kT_{\parallel}^{\text{INT.}}$ (eV) *)	$4.5/4.1 \cdot 10^{-4}$	$1.3/1.2 \cdot 10^{-4}$	$2.5 \cdot 10^{-4}$	$1.6 \cdot 10^{-4}$
kT_{\perp} (eV)	0.11	0.11	0.0055	0.011

*) *Halfway through the electron cooler.*

If we now add the contributions from longitudinal-longitudinal and transverse-longitudinal relaxation, we find the total rate of change of the longitudinal temperature. A numerical integration can then be performed to find the longitudinal temperature as a function of the distance from the electron-gun anode. The results of this calculation for some relevant configurations are given in table 3.2. Note that due to the lower electron density in the ASTRID experiments as compared to the Tandem experiments, the longitudinal temperature is expected to be lower.

Figure 3.6 shows the calculated electron beam temperatures for the ASTRID electron cooler in the case of a factor 10 adiabatic expansion as a function of the longitudinal-position coordinate z .

The electron-beam temperatures, kT_{\parallel} and kT_{\perp} , can be deter-

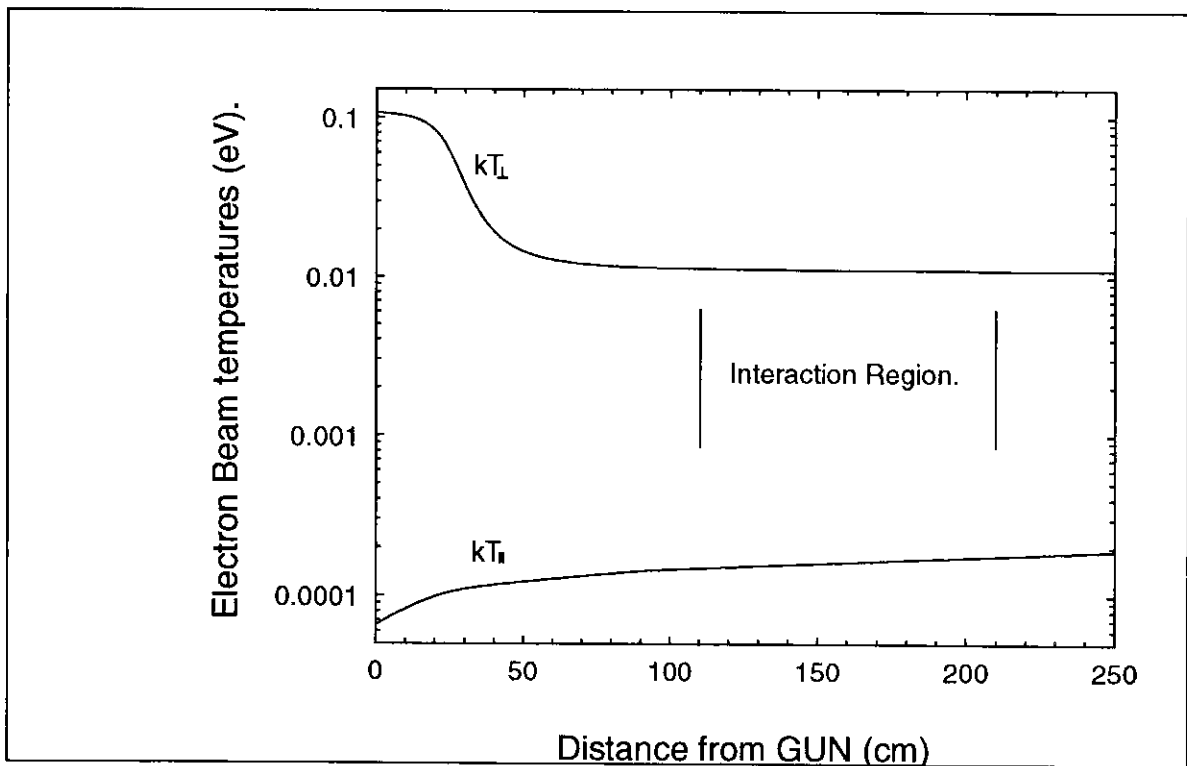


Figure 3.6 *The calculated electron beam temperatures for ASTRID with factor 10 adiabatic expansion.*

mined from the experimental spectra of dielectronic recombination. When a narrow isolated DR resonance is considered, it can be assumed that $\sigma(v)$ is just a δ function. In this case, the integral in eq.(3.5), with f given by eq.(3.6) can be solved analytically in the neighborhood of the resonance, giving $\langle v\sigma \rangle$ as a function of the detuning Δ or, equivalently, as a function of $E_{rel,0}=m\Delta^2/2$

$$\begin{aligned} \langle v\sigma \rangle(E_{rel,0}) = & \text{constant} \cdot \exp\left(-\frac{E_{rel,0}}{kT_{\parallel}} - \frac{E_{res}}{kT_{\perp}} + \frac{E_{rel,0}}{kT_{\parallel}(1-kT_{\parallel}/kT_{\perp})}\right) \\ & \cdot \left[\text{erf}\left(\left|\sqrt{\frac{E_{res}}{kT_{\parallel}}(1-kT_{\parallel}/kT_{\perp})} - \sqrt{\frac{E_{rel,0}}{kT_{\parallel}(1-kT_{\parallel}/kT_{\perp})}}\right|\right) \right. \\ & \left. - \text{erf}\left(\sqrt{\frac{E_{res}}{kT_{\parallel}}(1-kT_{\parallel}/kT_{\perp})} + \sqrt{\frac{E_{rel,0}}{kT_{\parallel}(1-kT_{\parallel}/kT_{\perp})}}\right) \right] \end{aligned} \quad (3.21)$$

where E_{res} is the resonance energy, and erf is the error function defined as

$$\text{erf}(x) = \frac{2}{\sqrt{\pi}} \int_0^x e^{-u^2} du. \quad (3.22)$$

The parameters E_{res} , constant, kT_{\perp} , and kT_{\parallel} can then be varied to obtain the best fit to the data points. Figure 3.7 shows such a fit for the electron beam used in the tandem accelerator experiments. The resonance was $O^{6+}(1s2s^1S) + e^- \rightarrow O^{5+}(1s2p(^1P)11D)$, and the result of the fit was $kT_{\parallel}=10(5) \cdot 10^{-4} \text{eV}$ and $kT_{\perp}=0.135(10) \text{eV}$. In fig.3.8 is shown the corresponding electron-beam-temperature determination for the Heidelberg electron beam performed with a C^{4+} beam. We used the

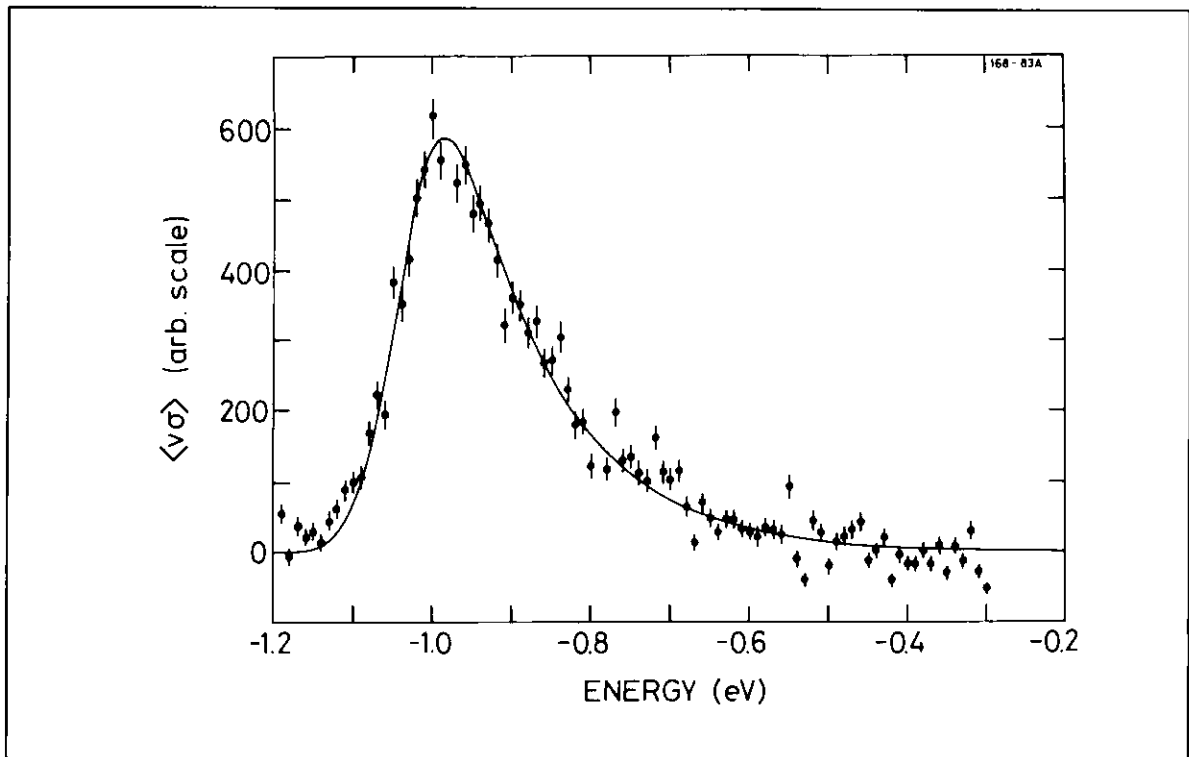


Figure 3.7 *Data points and fit function at the resonance used for the tandem temperature fit. (The negative energy sign just means that the electrons moved slower than the ions).*

resonance $C^{4+}(1s2s\ ^3S) + e^- \rightarrow C^{3+}(1s2s(^1P)7l)$ and found the temperatures $kT_{\parallel} = 6.3(5) \cdot 10^{-4} \text{ eV}$ and $kT_{\perp} = 0.134(10) \text{ eV}$. Due to the larger l splitting for this resonance, a fit was made to *two* δ -shaped resonances. Furthermore, a first-order polynomial was introduced to take into account a slope in the 'background recombination' signal probably caused by the next resonance in the spectrum.

When comparing the measured temperatures for the tandem experiments with the calculated ones, we find reasonable agreement. The slightly higher value for kT_{\perp} can be ascribed to non-uniformity of the solenoid field, but also the ion-beam divergence plays a role since different ions will have slightly different angles with respect to the electron beam, thereby contributing to the spread of relative transverse velocities. Concerning kT_{\parallel} , the effect of the finite size of the ion beam

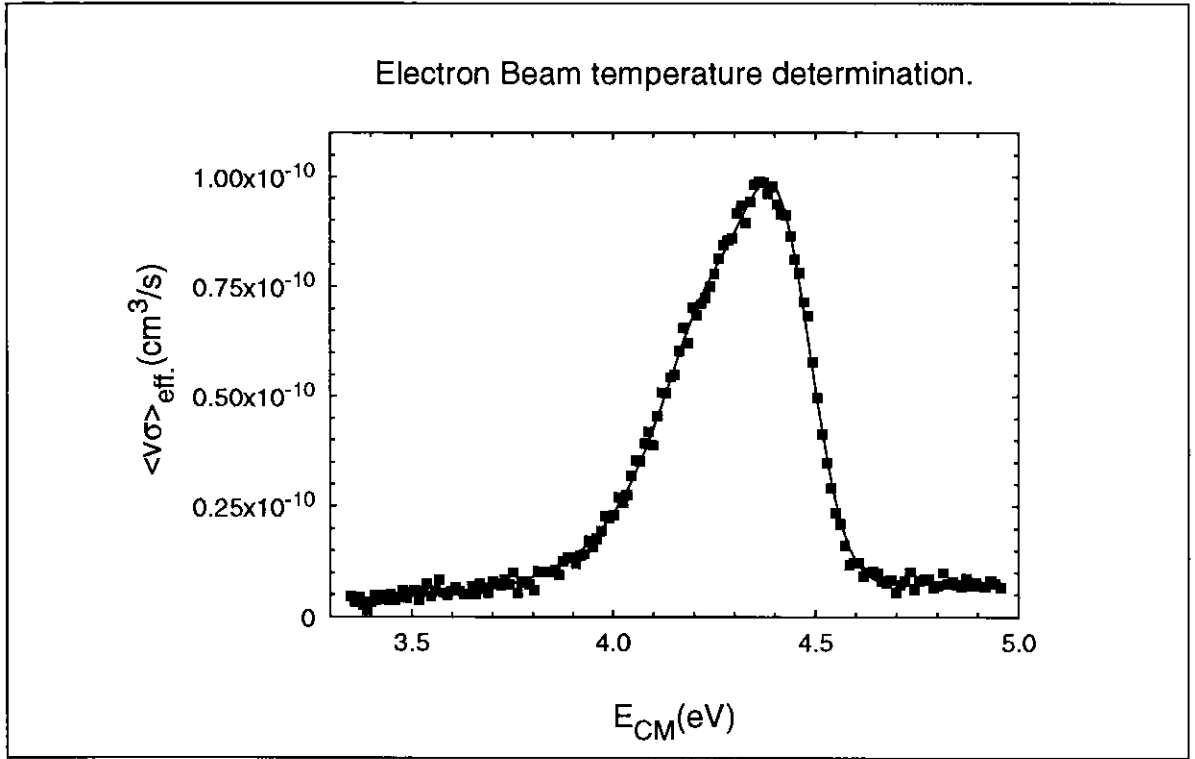


Figure 3.8 *Electron-beam-temperature determination for the TSR electron beam using a C^{4+} beam.*

comes into play since different transverse positions correspond to different values of the electron-beam space-charge potential given by

$$V_{\text{sp}} = \frac{I(\text{A})}{\sqrt{E_0(\text{eV})}} \cdot 1.5 \cdot 10^4 \left[\left(\frac{r}{a} \right)^2 - 1 + 2 \ln \left(\frac{a}{R} \right) \right], \quad (3.23)$$

where a is the electron-beam diameter and R is the diameter of the vacuum chamber. A 1 mm ion-beam radius combined with a 1 mm displacement can then give about 1 V variation in electron space charge across the ion beam for a 10 mA, 1 keV electron beam. This is equivalent to an increase in the peak-to-peak ripple on the acceleration voltage of 1 V. Inserting this in the calculations presented above leads to an increase of almost 50% in kT_{\parallel} . Finally, it is important to bear in mind that electron-beam temperatures measured

with this technique will always be upper limits since any effects of 'non- δ likeness' (e.g finite energy width or l splitting) will lead to apparently higher beam temperatures.

3.3. Electron cooling

Let us consider the electron beam as seen from a reference frame moving with the average electron velocity. If an ion enters this free electron plasma from any direction, it will experience a friction force directed opposite to its velocity vector. The force is known as the drag force and is caused by large-impact-parameter Rutherford scattering between the ions and the electrons. In the single-pass experiments, the influence of the drag force on the recombination experiments could be neglected, but in the storage ring, where the ions pass through the electron cooler several hundred thousand times per second, the accumulated effects of all these passages may be quite significant. In this section, the effects of the drag force relevant to the ion-electron recombination experiments will be discussed qualitatively, and results of cooling of a 4 MeV D^+ beam in ASTRID will be presented.

When the ions and electrons are tuned to the same average velocity, the slower ions are accelerated, and the faster ones are decelerated, leading to a narrowing of the longitudinal velocity distribution of the ions. This is known as longitudinal electron cooling. The process is especially interesting when the initial temperature of the ion beam is so high that the assumption we made in the previous section, that the relative velocity distribution can be well approximated

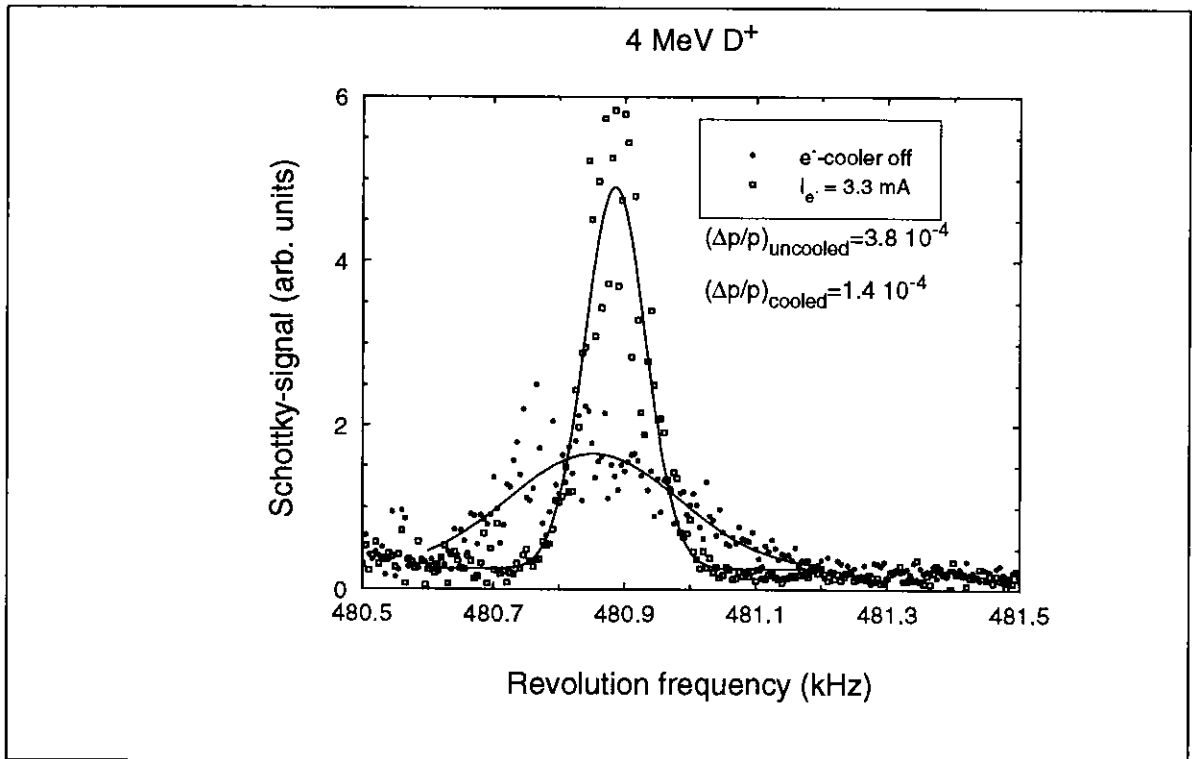


Figure 3.9 Schottky-noise spectra with gaussian fits of a 4 MeV D^+ beam stored in ASTRID. The squares show the cooled beam, and the dots show the uncooled ion beam.

by the electron velocity distribution, no longer holds. In this situation, electron cooling of the ions can practically eliminate the influence from the ion-beam velocity distribution. In fig. 3.9 is shown the Schottky-noise spectrum of a 4 MeV D^+ beam with (squares) and without (dots) electron cooling. This spectrum is the power spectrum of the electrostatic pick-up signal from a cylindrical electrode through which the ion beam passes. Any density fluctuations in the ion beam give rise to a signal at the revolution frequency and its harmonics. The Schottky-noise spectrum hence gives the distribution of revolution frequencies of the ions. To deduce the relative momentum spread from the relative frequency spread, one must divide by the off-momentum factor given by (Poth 1990),

$$\eta = 1 - (v/c)^2 - \alpha, \quad (3.24)$$

where the momentum compaction factor α is defined as

$$\alpha = \frac{\Delta C/C}{\Delta p/p}, \quad (3.25)$$

where C is the circumference of the orbit of a particle with momentum p . For standard ASTRID operation, $\alpha = 0.053$ (Møller 1994), leading to $\eta = 0.943$ for a 4 MeV D^+ beam. For the cooled beam from fig.3.9, we found $\Delta p/p = 1.44 \cdot 10^{-4}$, where Δp is defined as the standard deviation from the mean value of p . Introducing a 'temperature' in analogy to the electron-beam case, we find $kT_{\text{ion}} = 82$ meV, which is much higher than the expected longitudinal *electron* beam temperature of about 1 meV. We see that we do not get complete temperature equilibration between the ions and the electrons. The heating mechanism responsible for this difference is the intra-beam scattering of the ion beam. In the case of equilibrium between intra-beam scattering and electron cooling, $\Delta p/p$ is proportional to $N_i^{0.4}$, where N_i is the number of stored ions (Poth 1990). In table 3.3 is shown $\Delta p/p$ for three different ion intensities, and we see that the $N_i^{0.4}$ dependence is confirmed.

When there is a detuning of the two beam velocities, the drag force will have the same direction for all ions, leading to acceleration or deceleration of the entire ion beam. This can be an obstacle for measuring recombination rate coefficients at very low relative energies, where the drag force is at maximum. This problem is normally circumvented by modulating the electron energy between cooling energy (zero detuning) and the energy at which one wants to measure.

Table 3.3

Ion current $I_i(\mu\text{A})^*$	$\Delta p/p$	$\Delta p/p \cdot (I_i(\mu\text{A}))^{-0.4}$
5	$1.7 \cdot 10^{-4}$	$8.9 \cdot 10^{-5}$
1	$6.9 \cdot 10^{-5}$	$6.9 \cdot 10^{-5}$
0.5	$5.5 \cdot 10^{-5}$	$7.3 \cdot 10^{-5}$

*) *The absolute value of the ion current is only known within a factor of two, but by monitoring the production of neutrals, a relative current measurement with an uncertainty of about 2% could be performed.*

We measured the drag force as a function of the detuning by setting a certain detuning and then watching the drift of the peak in the Schottky spectrum as a function of time. The result of this is shown in

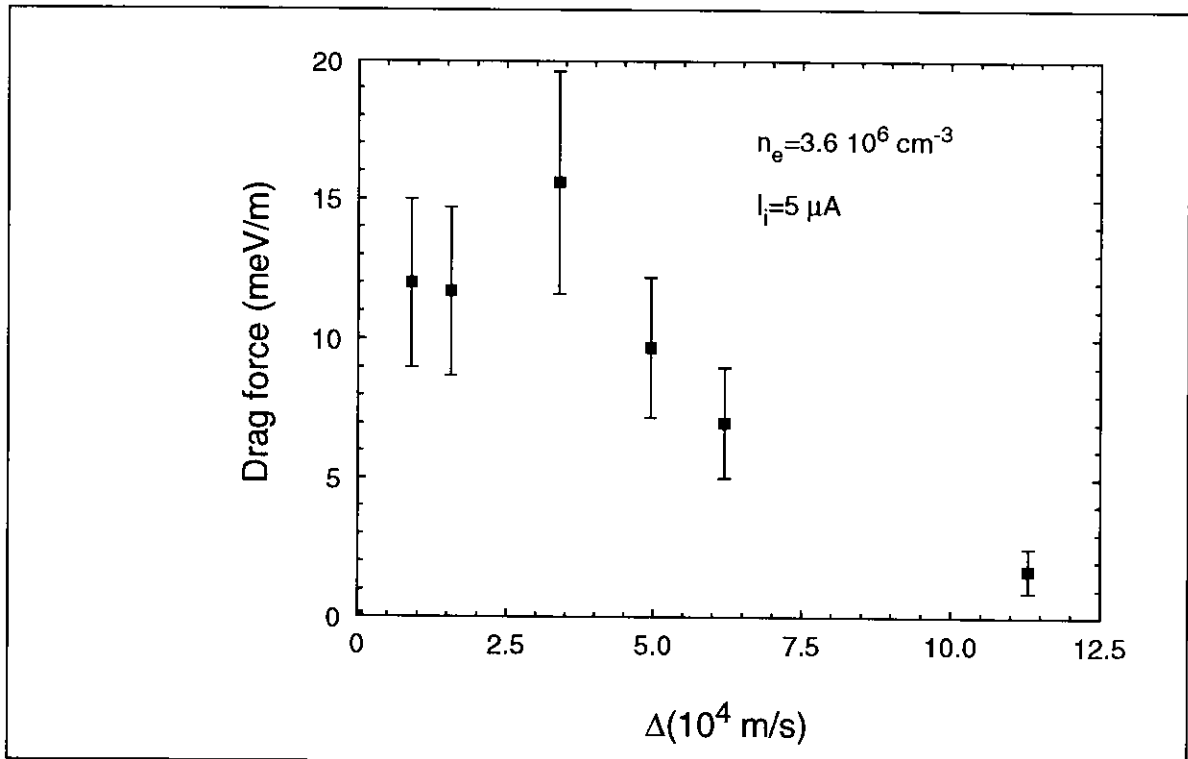


Figure 3.10 *The measured drag force as a function of the detuning velocity Δ .*

fig.3.10.

So far, we have considered only effects of the drag force in the longitudinal direction, but a damping of the transverse motion also takes place. This damping leads to lower transverse ion-beam temperature, smaller beam size, and elimination of the loss of stored particles due to multiple scattering in the residual gas. This last point is illustrated in fig.3.11, where we see that the storage lifetime of a D^+ beam is increased by more than one order of magnitude by applying electron cooling.

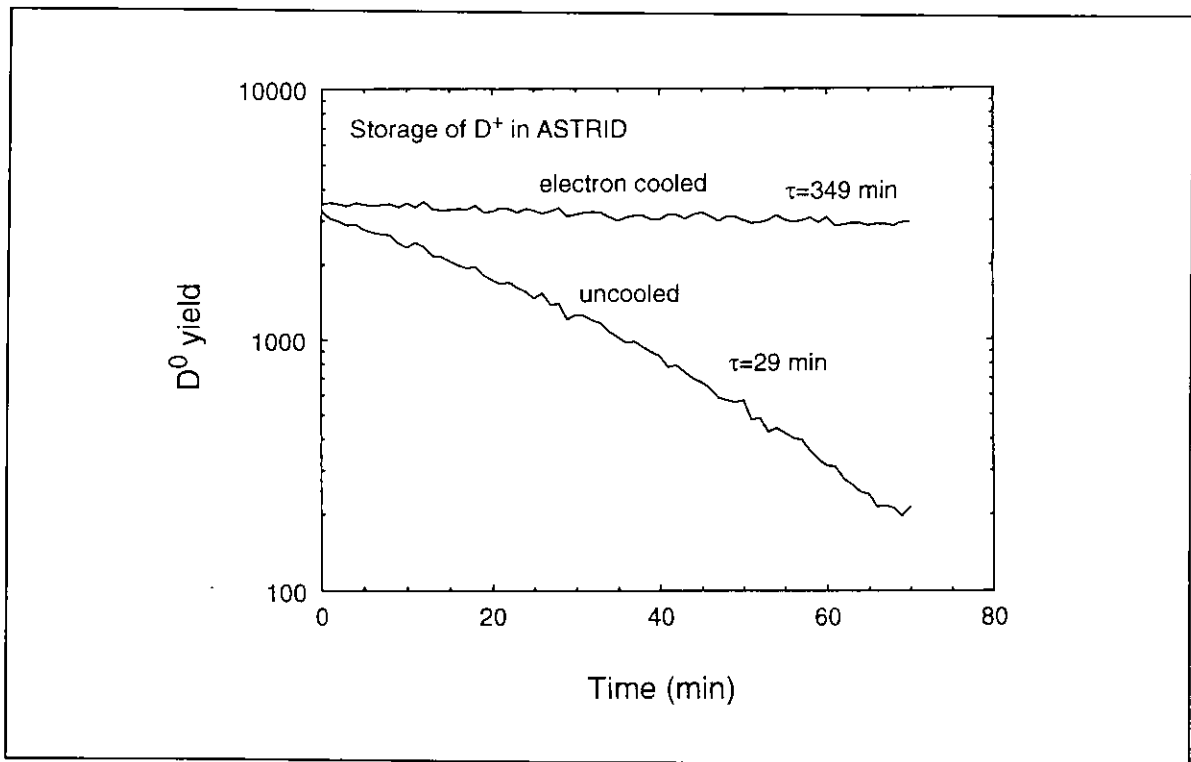


Figure 3.11 Yield of neutrals from stored D^+ beam as a function of time after injection. The upper curve was obtained by applying electron cooling ($n_e = 3.6 \cdot 10^6 \text{ cm}^{-3}$).

H Danared (1993) Nucl.Instr&Methods A335 397

N S Dikansky et al.(1987) Proc. XIII Intern. Conf. on High Energy Accel.- Nauka I 330.

D C Griffin (1989) Physica Scripta T28 17

D Habs, J Kramp, P Krause, K Matl, R Neumann, and D Schwalm (1988) Physica Scripta T22, 269

W Hermansfeldt, SLAC report 226 (Stanford 1979).

V I Kudelainen, V A Lebedev, I N Meshkov, V Parkhomochuk, and B N Sukhina (1982) Sov.Phys.JETP 56 1191.

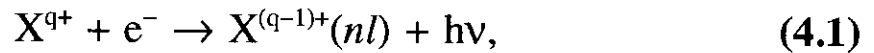
S P Møller (1994) Private communication.

H Poth (1990) Physics Reports 196 135.

4. Radiative Recombination

In this chapter, the process of radiative recombination (RR) is being discussed, and results of the tandem accelerator single-pass experiments are presented. Section 4.1 on RR for fully stripped ions serves as an introduction to the two following sections on RR for non-fully stripped ions (sec.4.2) and on laser-induced recombination (sec.4.3).

The formal prescription of RR is



where q is the ion charge in units of the elementary charge e , n and l are the principal and orbital angular momentum quantum numbers of the captured electron, respectively, and $h\nu$ is the energy of the photon emitted.

4.1 RR for fully stripped ions

We start by considering the case of the initial-state ion being a bare nucleus. For this case, an approximative calculation of the RR cross section was performed by Kramers (Kramers 1923). The Kramers formula gives the cross section for capture to a final state with principal quantum number n ,

$$\sigma_n = 2.10 \cdot 10^{-22} \text{cm}^2 \cdot \frac{Z^4 (e^2 / (2a_0))^2}{n E_{\text{rel}} (Z^2 (e^2 / (2a_0)) + n^2 E_{\text{rel}})}, \quad (4.2)$$

where Z is the nuclear charge in units of e , and a_0 is the Bohr radius.

The derivation of this formula is based on the old quantum mechanics of Bohr and Sommerfeld. The idea is to consider the classical wavelength distribution of the light emitted from an initially free electron, accelerated in the Coulomb field of the nucleus. This wavelength distribution is then modified to take into account the discrete energy levels of the final state, as well as the quantization of light introduced through Einstein's formula,

$$E_{\text{photon}} = h\nu = hc/\lambda. \quad (4.3)$$

With these restrictions, the continuous classical distribution is modified to a series of discrete values. In accordance with the correspondence principle, it is assumed that the integral of the energy emitted in the form of light would be the same as found in the classical calculation. With this assumption, the light emitted in a certain wavelength interval in the classical calculation, can now be associated with radiative recombination into a bound state with a certain principal quantum number n . This procedure leads to the Kramers formula.

After the development of the modern quantum mechanics, exact calculations of the RR cross section for fully stripped ions were performed (Stobbe 1930). These give rise to corrections to the Kramers formula described via the so-called 'Gaunt factors' g_{nl} (Gaunt 1930), defined as the exact cross section divided by the cross section given by the Kramers formula. The l -averaged Gaunt factors may be expressed

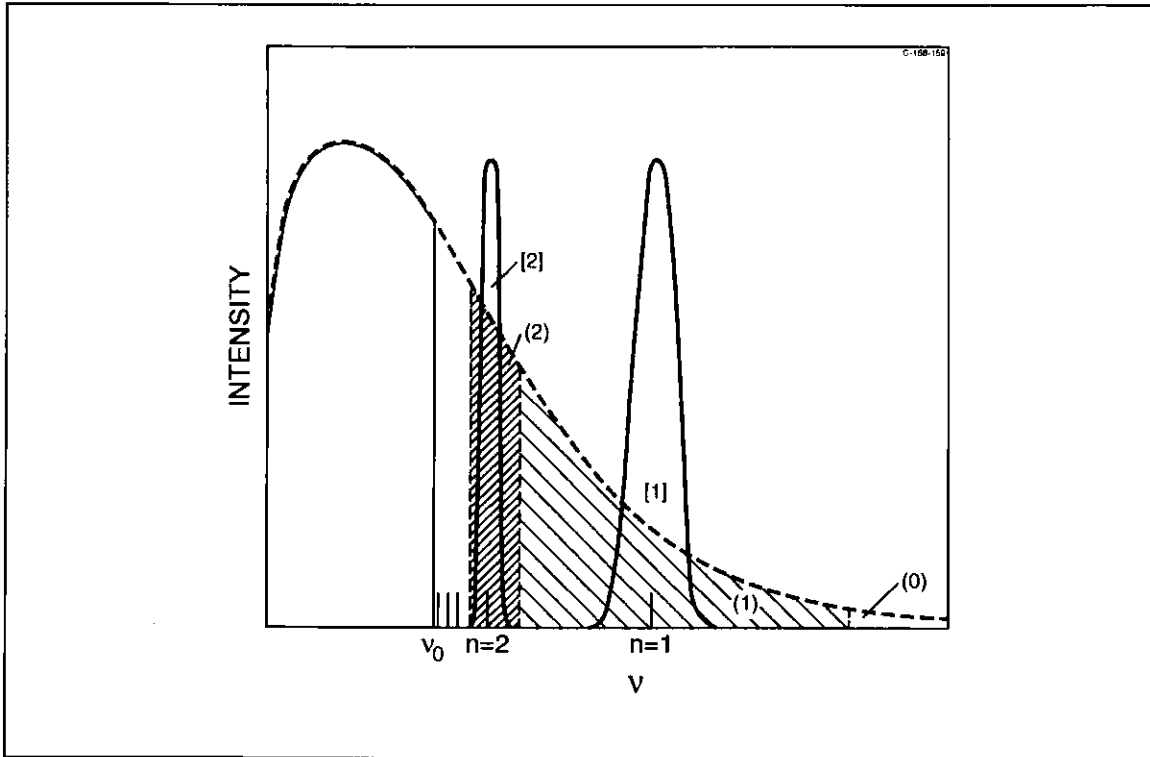


Figure 4.1 *Illustration of Kramers's discretization principle of the emitted radiation.*

by the following asymptotic expansion (Seaton 1959, Griffin 1989):

$$\begin{aligned} \bar{g}_n = & 1 + 0.1728n^{-2/3}(u+1)^{-2/3}(u-1) \\ & - 0.0496n^{-4/3}(u+1)^{-4/3}(u^2+(4/3)u+1) + \dots, \end{aligned} \quad (4.4)$$

where $u = E_{\text{rel}} / (h\nu - E_{\text{rel}})$.

From the quantum mechanical point of view, RR is a radiative transition from a continuum state to a bound state described by the following transition matrix element:

$$T_{fi} = \langle \varphi_{nl}, \bar{k}\rho | H_{\text{int}} | \psi_{\bar{k}}^+, \text{vac} \rangle, \quad (4.5)$$

where the final state is a bound state, φ_{nl} , of the H-like ion plus a photon with wave vector \bar{k} and polarization $\bar{e}_{\bar{k}\rho}$. The initial state is a 'free' electron (distorted by the infinite-ranging Coulomb potential) and

the vacuum state of the electromagnetic field. The interaction Hamiltonian takes on the form (Weissbluth 1978)

$$H_{\text{int}} = -\frac{e}{mc} \cdot \bar{\mathbf{e}}_{\mathbf{k}\rho} \cdot \bar{\mathbf{p}} \left(a_{\mathbf{k}\rho} e^{i\mathbf{k}\cdot\bar{\mathbf{r}}} + a_{\mathbf{k}\rho}^+ e^{-i\mathbf{k}\cdot\bar{\mathbf{r}}} \right), \quad (4.6)$$

where $a_{\mathbf{k}\rho}$ and $a_{\mathbf{k}\rho}^+$ are the photon annihilation and creation operators, respectively. For radiative recombination, only the creation operator yields non-zero matrix elements. For photoionization, which is the inverse process, only the annihilation operator contributes.

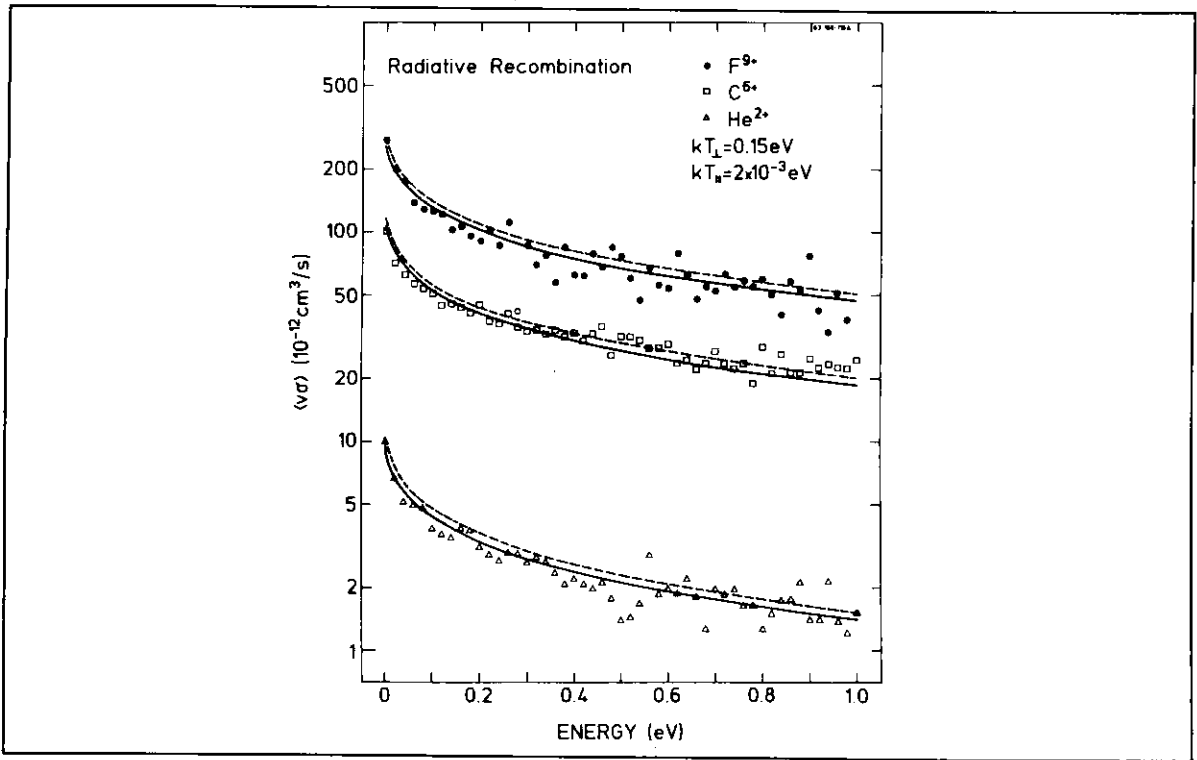


Figure 4.2 RR rate coefficient as a function of relative energy for He^{2+} , C^{6+} , and F^{9+} . Kramers's result with (full curve) and without (dashed curve) Gaunt corrections (Andersen 1990a).

A detailed derivation of the cross section as a function of the relative energy from evaluation of the matrix elements of eq.(4.5) is presented in the thesis of Jakob Bolko (Bolko 1991).

Measurements of RR for He^{2+} , C^{6+} , and F^{9+} in the Aarhus single-pass tandem experiment (Andersen 1990a) confirm these calculations (see fig.4.2) when the effect of field ionization caused by the electric charge-state analyzer field is taken into account. Other experimental studies, performed at the Test Storage Ring (TSR) at the Max Planck Institute Heidelberg, indicate discrepancies of up to 50% for C^{6+} and Cl^{17+} (Wolf 1991), the measured rate coefficient being larger than the theoretically predicted value.

4.2 RR for non-fully stripped ions

For non-fully stripped ions, calculations become more complicated since the final state is no longer a hydrogenic one. However, for states with relatively high n quantum number, the dominating contribution to RR comes from states with $l \geq 2$, and the hydrogenic approximation may be applicable. Since the decrease in the cross section with increasing n given by the Kramers formula is slow for relative energies close to zero, the total cross section will be dominated by contributions from states for which the hydrogenic approximation is good. It is therefore reasonable to use the hydrogenic approximation for the total radiative recombination cross section $\sum_n^{\text{limit}} \sigma_n$, where the summation is restricted to non-occupied levels. It is, however, not clear which charge should be entered in the Kramers formula for this situation. Electrons with high angular momentum will not penetrate the core, and one will expect the effective charge that one should use to be equal to the ion charge. For low- l electrons, however, the incoming electron may penetrate the ion core, leading to an effective charge

higher than the ion charge q and smaller than the nuclear charge Z . A theoretical discussion of the nl dependence of the effective charge derived from Hartree-Fock calculations is given by McLaughlin and Hahn (MacLaughlin 1991), Sunggi and Lin (Sunggi 1991), and Kim and Pratt (Kim 1983). In our measurements, no information on the final state of the recombination products was available. We could, however, deduce an average effective charge q_{eff} by comparing our data to the result of hydrogenic calculations with different values of the charge inserted in the Kramers formula. With this procedure, good agreement with experiments has been found for the H-like ions C^{5+} , O^{7+} , and F^{8+} , as well as for Li-like O^{5+} and Si^{11+} , in all cases using $q_{\text{eff}}=q$ (Andersen 1990b),[II].

Figure 4.3 shows the result of our measurement of the RR rate coefficient for the O-like Si^{6+} ion [II]. Also shown in this figure are the results of the hydrogenic approximation using $q_{\text{eff}}=q=6$ and $q_{\text{eff}}=9$, respectively. We see that in order to reproduce our experimental data, $q_{\text{eff}}=9$ should be used. The fact that $q_{\text{eff}}>q$ we take as evidence of incomplete screening. For F^{3+} [V], we also observed incomplete screening.

Since it has been found that for H-like and Li-like ions, one should use $q_{\text{eff}}=q$, whereas for C-like and O-like ions $q_{\text{eff}}>q$, it is tempting to ascribe the effect of incomplete screening to the presence of 2p electrons in the initial-state ion. This observation is probably related to the fact that p-wave functions extend to larger distances from the nucleus than s-wave functions.

Another measurement of RR for non-fully stripped ions was performed by Müller et al. on U^{28+} ions (Müller 1991). They found a maximum rate coefficient of $r \approx 1 \cdot 10^{-7} \text{cm}^3 \text{s}^{-1}$. This was compared to a

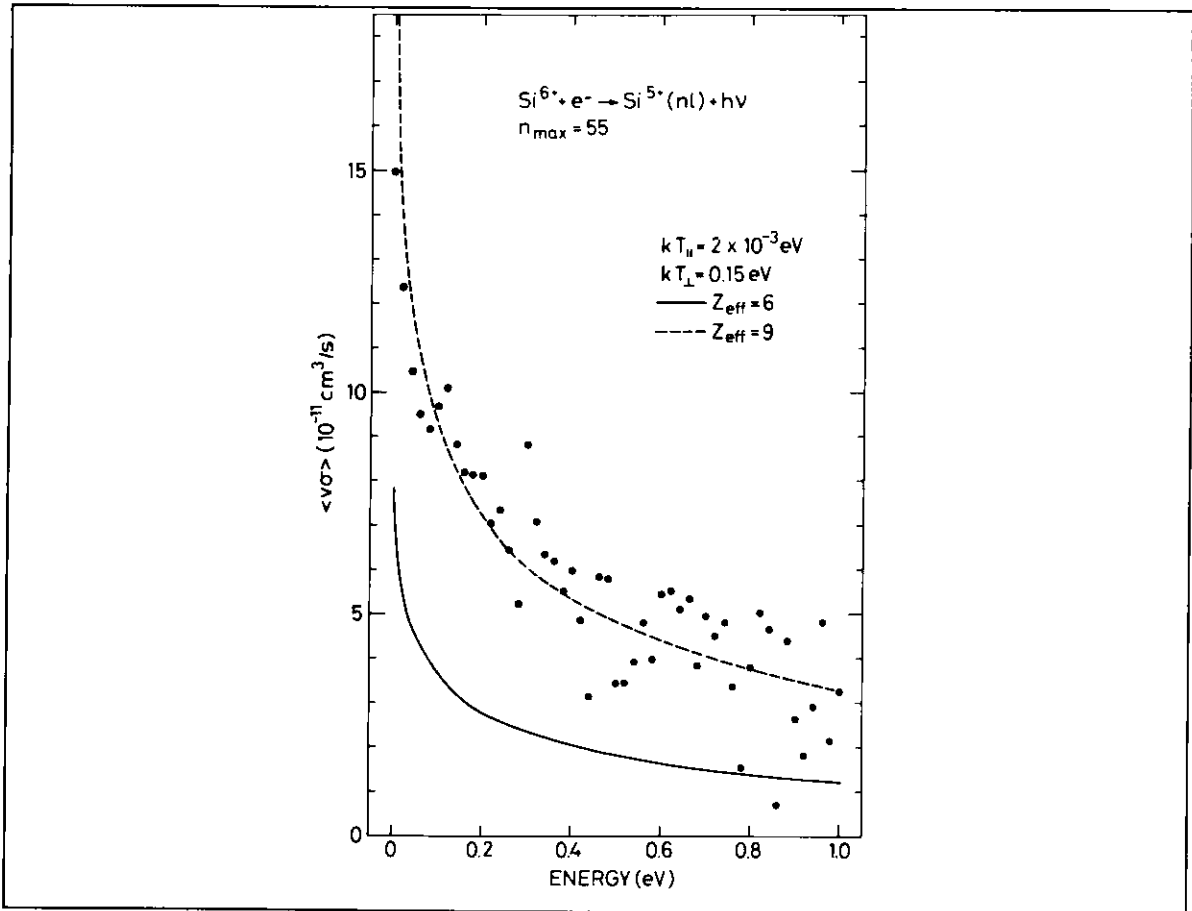


Figure 4.3 *The measured RR rate coefficient for Si^{6+} compared to theoretical values obtained with two different effective charges.*

hydrogenic calculation using $q_{\text{eff}}=60$, and it was found that the experimental result exceeded theory by a factor of five.

We note that since for relative energies close to zero energy, $\sigma_{\text{RR}} \propto Z_{\text{eff}}^2$, the result of Müller et al. would exceed theory by a factor of two, even if they used $q_{\text{eff}}=Z=92$, corresponding to no screening by the 64 electrons on the ion. It is therefore probable that what they saw was not only RR. Some other mechanism must have contributed. One possibility is some DR resonance very close to 0 eV. Another possibility is ternary recombination (see ch.2) since they had very high electron densities, of the order of 10^{10} cm^{-3} . This should be compared to the electron density in our single-pass experiment which was

typically about $5 \cdot 10^7 \text{ cm}^{-3}$.

4.3 Laser-induced RR

In sec.4.1, we considered matrix elements of the form

$$T_{fi} = \langle \varphi_{nl}, \bar{k}\rho | H_{int} | \psi_{\bar{k}}^+, \text{vac} \rangle. \quad (4.7)$$

We now let N denote the number of photons with wave vector \bar{k} and polarization $\bar{e}_{\bar{k}\rho}$ and consider the following matrix element:

$$T_{fi} = \langle \varphi_{nl}, (N+1) | H_{int} | \psi_{\bar{k}}^+, N \rangle. \quad (4.8)$$

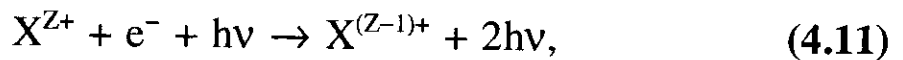
It is a property of the creation operator mentioned in sec.4.1 that

$$a_{\bar{k}\rho}^+ |N\rangle = \sqrt{N+1} |N+1\rangle. \quad (4.9)$$

This leads to

$$|T_{fi}|^2 \propto (N+1). \quad (4.10)$$

In other words, with a laser field of the proper frequency, radiative recombination can be stimulated via the following reaction:



where the two photons in the final state are identical. This possibility was considered by Neumann et al. (Neumann 1983).

If we consider initial-state ions that are fully stripped, the energy

conservation implies

$$h\nu = \frac{1}{2}mv_{\text{rel}}^2 + \frac{Z^2 e^2}{n^2 2a_0} . \quad (4.12)$$

We now let $\Delta\nu$ denote the combined spectral width of the laser field and the n 'th energy level. The stimulated process will then be possible for electrons in the velocity interval $v_{\text{rel}} \pm \Delta v_{\text{rel}}$, where $\Delta v_{\text{rel}} = \frac{h\Delta\nu}{mv_{\text{rel}}}$.

The gain is defined as

$$g_n = \frac{r_n^{\text{IND}}(\Delta v_{\text{rel}})}{r_n^{\text{SPON}}(\Delta v_{\text{rel}})} , \quad (4.13)$$

where $r_n^{\text{IND}}(\Delta v_{\text{rel}})$ and $r_n^{\text{SPON}}(\Delta v_{\text{rel}})$ denote the rates for induced and spontaneous recombination to the state n for electrons in the velocity interval $v_{\text{rel}} \pm \Delta v_{\text{rel}}/2$, respectively. The gain can be determined using Einstein's A and B coefficients. The result is

$$g_n = \frac{Ic^2}{8\pi h\nu^3 \Delta\nu} , \quad (4.14)$$

where I is the laser intensity.

The quantity g_n , however, is not what is measured directly as long as only charge state analysis is used. What influences the measured recombination rate is the total gain G_n defined as

$$G_n = \frac{r_n^{\text{IND}}(\Delta v_{\text{rel}})}{r^{\text{SPON}}} = g_n \frac{r_n^{\text{SPON}}(\Delta v_{\text{rel}})}{r^{\text{SPON}}} , \quad (4.15)$$

where r^{SPON} is the summed rate for all values of n , integrated over the

entire velocity distribution.

r_n^{SPON} can be determined using the Kramers formula and the known velocity distribution. $r_n^{\text{SPON}}(\Delta v_{\text{rel}})$ is determined in the limit $v_{\text{rel}} \rightarrow 0$. Performing these calculations following Neumann et al., leads us to the following expression for G_n at threshold

$$G_n = \frac{1}{n} \frac{4.42 \cdot 10^{-6}}{\sqrt{kT_{\perp}(\text{eV}) kT_{\parallel}(\text{eV})} (h\nu(\text{eV}))^3} I(\text{W}/\text{cm}^2). \quad (4.16)$$

For our LIR experiment at the tandem accelerator, we merged a co-propagating beam from a Nd:YAG laser with a He^{2+} beam and an electron beam tuned to zero relative velocity. This laser had a fixed wavelength of $\lambda=1.0641 \mu\text{m}$, corresponding to a photon energy of $h\nu=1.1652 \text{ eV}$. The wavelength in the ion rest frame depended on the Doppler shift, which we could control by varying the beam energies. For an ion energy of $1.07 \text{ MeV}/\text{amu}$, the photon energy in the ion rest frame is equal to 1.11 eV , which is equal to the binding energy of an electron in the $n=7$ state of He^+ . By applying a Q switch, the laser could be operated in a pulsed mode giving 3.8 mJ pulses of 200 ns duration, with a repetition rate of 2 kHz . The time-averaged intensity of a laser pulse in the interaction region was $68 \text{ kW}/\text{cm}^2$, leading to an expected total gain of $G_n=2.7$ when the previously found electron-beam temperatures of $kT_{\parallel}=1 \text{ meV}$ and $kT_{\perp}=135 \text{ meV}$ (see sec.3.2) were inserted in eq.(4.15).

The measurement was done by having the laser pulse start a time-to-amplitude converter (TAC) which was stopped by the detection at the channelplate of a He^+ ion. In this way, the production of singly charged He ions could be monitored as a function of time in a narrow time window around the time of the laser pulse. Based on earlier RR

measurements with He^{2+} ions, we could estimate the count rates for spontaneous RR as well as for electron capture in collisions with residual gas molecules, which turned out to be the dominating background signal. From this estimate, we should expect a statistically significant peak in the time spectrum to appear after about 30 minutes of measuring. We did, however, not see any effect of the laser, even after 7 hours. The most important reason for this was probably that we did not have the perfect beam overlap we had assumed in our estimates. Furthermore, it was pointed out by Schramm et al. (Schramm 1991) that weak electric fields in the interaction region can lead to a smearing-out of the threshold, which in turn leads to a reduction of the total gain at threshold by up to a factor of two or three.

After our unsuccessful attempts to make laser-stimulated RR, two other groups have succeeded (Schramm 1991, Yousif 1991). Schramm et al. used merged beams of protons, electrons, and laser light. Their laser system was an excimer-laser-pumped dye laser. ($I \leq 18 \text{ MW/cm}^2$). The final state was $n=2$ in hydrogen. Yousif et al. used merged beams of protons and electrons which were crossed by a cw beam from a CO_2 laser ($\lambda=10.535 \text{ }\mu\text{m}$, $P=15 \text{ W}$). They used a field-ionization technique which made it possible to selectively detect hydrogen atoms formed in states with principal quantum numbers in the range of $8 \leq n \leq 19$. By varying the electron-beam energy, they found an enhancement introduced by the laser for RR to $n=11$ and to $n=12$.

L H Andersen and J Bolko (1990a) Phys.Rev.A 42 1184

L H Andersen and J Bolko (1990b) J.Phys.B. 23 3167

J Bolko (1991) Thesis, Institute of Physics and Astronomy, Aarhus University (Unpublished)

- J A Gaunt (1930) Phil.Trans.A 229 163*
- D C Griffin (1989) Physica Scripta T28 17*
- Y S Kim and R H Pratt (1983) Phys.Rev.A 27 2913*
- H A Kramers (1923) Phil. Mag. 46 836*
- D J McLaughlin and Y Hahn (1991) Phys.Rev. A 43 1313*
- Müller et al (1991) Physica Scripta T37 62*
- R Neumann, H Poth, A Winnacker, A Wolf (1983) Z.Phys.A 313 253*
- M J Seaton (1959) Mon. Not. R. Astron. Soc. 119 81*
- U Schramm, J Berger, M Grieser, D Habs, E Jaeschke, G Kilgus, D Schwalm, A Wolf, R Neumann, R Schuch (1991) Phys.Rev.Lett. 67 22*
- M Stobbe (1930) Ann. Phys. 7 661*
- C Sunggi and C C Lin (1991) Phys.Rev.A 43 3433*
- P Van der Donk, F B Yousif, J B A Mitchell and A P Hickman (1991) Phys.Rev.Lett. 67 42*
- M Weissbluth: Atoms and Molecules (1978) Academic Press*
- A Wolf et al (1991) Z.Phys.D 21 69*

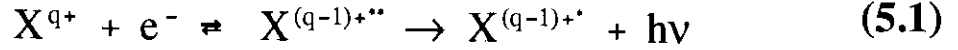
5. Dielectronic Recombination

In this chapter, the process of dielectronic recombination (DR) is being discussed. In particular results from the tandem single-pass experiments on metastable He-like ions [IV], as well as on Li-, Be-, B-, and C-like ions [III, I, V], are considered. Furthermore, previously unpublished results of DR measurements for metastable He-like ions performed at the TSR, MPI-K, Heidelberg are presented.

In sec.5.1 the DR process is introduced, the effects of external electric fields are discussed, and reference is made to other works in the field of DR. Section 5.2 concerns DR for Li-like ions which is a particularly simple case in the sense that no metastable states are involved, and only the 2s-2p excitation is relevant in the energy range considered in these experiments. The remaining sections of this chapter deal with the situation where a fraction of the ions in the beam is formed in electronically excited states which are metastable and hence sufficiently long-lived to be present in the merged-beams experiments. The emphasis will be put on the He-like metastable ions (sec.5.3-4), and in particular on comparisons between the single-pass results [IV] and the results obtained at the TSR.

5.1 Introduction to DR

In the isolated resonance approximation, the DR process is described as a two-step process,

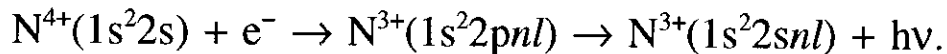


where the doubly excited intermediate state $X^{(q-1)+**}$ in most cases is a Rydberg state with an excited core. The first step will be referred to as the dielectronic capture and has a probability proportional to the autoionization rate A_a of the doubly excited state. The probability for the second step is given as the ratio of the rate for radiative stabilization A_r to the total stabilization rate $A_a + A_r$. The DR cross section is proportional to the product of these two probabilities,

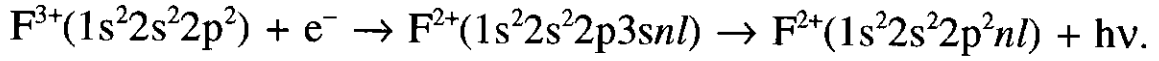
$$\sigma_{nl} \propto \frac{A_a(nl) A_r(nl)}{A_a(nl) + A_r(nl)}, \quad (5.2)$$

where n and l denote the principal and angular-momentum quantum numbers of the captured electron, respectively. After the dielectronic-capture process, the doubly excited state can in general stabilize radiatively or by autoionisation to several different final states. To calculate the DR cross section for a given relative energy, all these rates have to be determined, and eq.(5.2) should therefore only be considered as a formal description.

When discussing DR, one often distinguishes between $\Delta n=0$ and $\Delta n \neq 0$ processes. $\Delta n=0$ denotes a process where the electron, which gets excited as the free electron is resonantly captured, does not change its principal quantum number. As an example of a $\Delta n=0$ process, consider



An example of a $\Delta n \neq 0$ process is

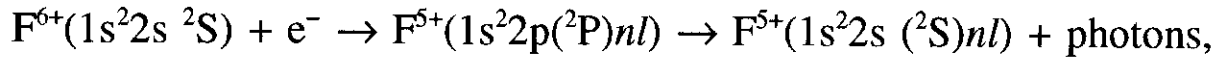


This distinction becomes very important when the effect of external electric fields in the interaction region is considered. The presence of weak electric fields [primarily caused by the electron-beam space charge (see eq.3.23)] in the interaction region is found to dramatically enhance the rate for DR ($\Delta n=0$), whereas only small effects can be found for DR ($\Delta n \neq 0$).

The electric-field enhancement for $\Delta n=0$ processes can be understood qualitatively by the following argument: The radiative stabilization rate is practically independent of the n and l quantum numbers of the captured electron in the doubly excited state since the dominant radiative stabilization (except for the lowest values of n and l) is usually a core stabilization, with the Rydberg electron acting merely as a spectator. The rate for autoionisation, however, is decreasing dramatically when l is increased, so that for low l , $A_a \gg A_r$, while for high l , $A_a \approx 0$ (Griffin 1989). For this reason, only low-to-moderate values of l contribute to the DR cross section.

In the presence of electric fields, the spherical symmetry will be broken, and l is no longer a good quantum number. The physical states will then become linear combinations of states with different l , and all states will have admixtures of low- l states. As a consequence, A_a , and hence the DR cross section, will be increased for states dominated by high- l components as compared to the field-free case, whereas no change is found in the cross section when states dominated by low- l components are considered. For low values of n (typically $n \leq 15$), all possible l states are to be considered low in this context, and therefore field effects are not important. However, for higher n , the field effect

is increasing, so that the contribution from the high Rydberg states can be substantially increased. As an example, we mention that for the following $\Delta n=0$ reaction:



an enhancement of the summed rate coefficient from $n=20$ to $n=58$ by a factor of three to four is found by considering an electric field of 15 V/cm rather than a zero field [III].

For the $\Delta n \neq 0$ transitions, the field effects will be much weaker than for the $\Delta n=0$ transitions. This is due to the fact that for $\Delta n \neq 0$, the value of σ_{nl} will be substantial only for states with relatively low principal quantum numbers n , for which the field effect is known to be insignificant (Griffin 1989). To explain this, we note that the rate A_r is practically independent of n , whereas A_a is approximately proportional to n^{-3} . According to eq.(5.2), this means that there will be a critical principal quantum number n_{crit} for which $\sigma_n = \sum_{l=0}^{n-1} \sigma_{nl}$ is constant if $n < n_{\text{crit}}$ and $\sigma_n \propto n^{-3}$ if $n > n_{\text{crit}}$. For $\Delta n \neq 0$, A_r is in general much larger than for $\Delta n=0$ because of the v^3 dependence in the radiative rate, whereas A_a will be smaller than for $\Delta n=0$ because of the larger energy of the electron in the continuum state. As a consequence, n_{crit} will be much smaller for $\Delta n \neq 0$ transitions than for $\Delta n=0$ transitions, and therefore the high- n states, which have the largest field dependence, will not contribute much to the DR signal (Griffin 1989).

Several DR measurements have been performed using merged beams. The first measurements considered 2s-2p excitations in C^+ ions

(Mitchell 1983). Shortly after this, 2s-2p excitations in Li-like boron and carbon ions were studied (Dittner 1983). With the construction of the Aarhus tandem single-pass experiment, better resolution was achieved, allowing state-selective measurements of DR for He- and Li-like carbon and oxygen ions (Andersen 1990). Since 1990, many experimental results on DR have been published. The most widely used techniques are the merged-beams technique in storage rings (see, e.g., Wolf 1991, Spies 1992) and the electron-beam ion-trap (EBIT) technique (Beiersdorfer 1991, Ali 1991).

The first evidence of the field effect for $\Delta n=0$ processes was reported by Müller et al. (Müller 1987). Crossed beams of ions and electrons were used. The DR process considered was:

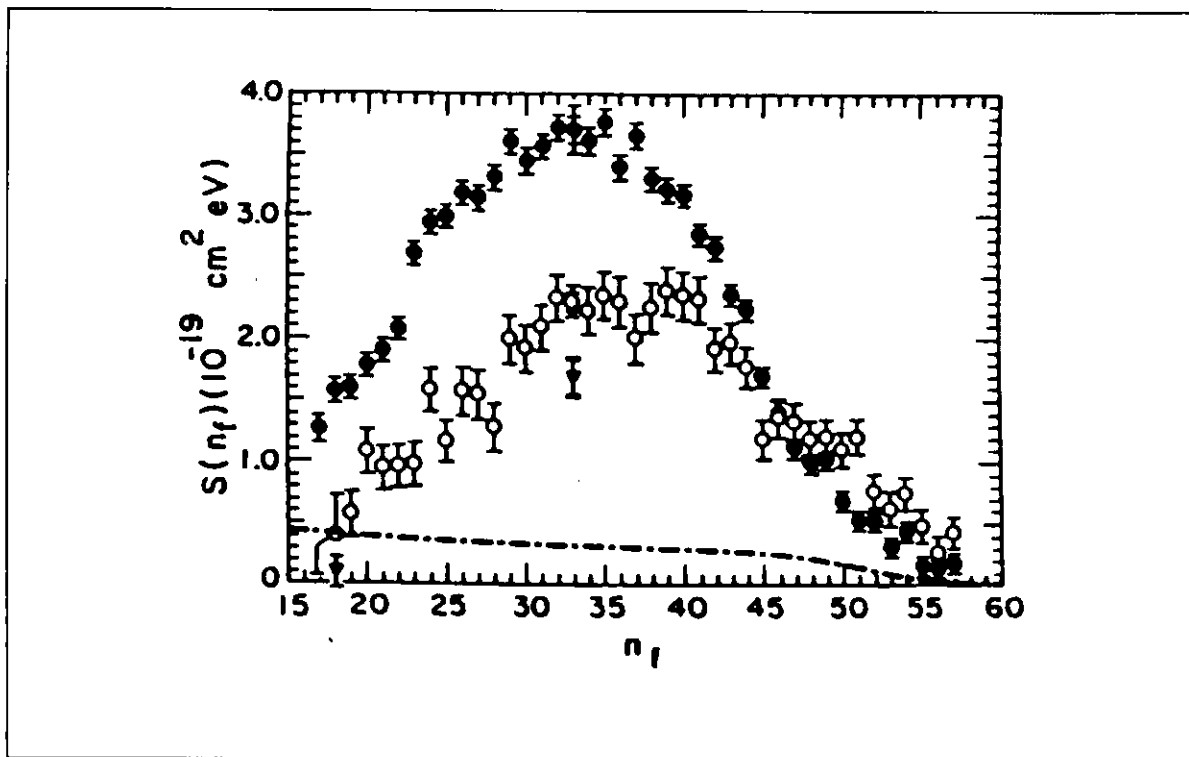
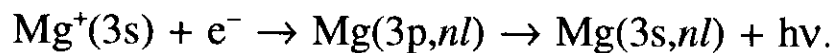
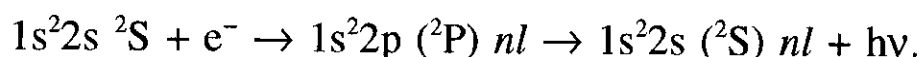


Figure 5.1 Collision strength as a function of the final state n quantum number for fixed relative energy (Müller 1987).

The dominating contribution to the electric field in the interaction region was the motionally induced electric field, caused by the solenoid field, which was applied to confine the electron beam. Müller et al. performed the experiment with two different solenoid fields so that the electric field was 7.2 V/cm and 23.5 V/cm, respectively. For detection, they used a field-ionization technique, so that the final state n could be determined for states with $n \geq 17$. Their result, the yield for constant relative energy as a function of the principal quantum number for the two different field strengths, is shown in fig.5.1 together with a zero-field calculation.

5.2 DR for ground-state Li-like ions

As mentioned in the beginning of this chapter, only one particular electronic excitation is relevant to the DR process for Li-like ions in the low-energy regime, namely the 2s-2p excitation. Therefore the discussion is restricted to DR processes of the following form:



What we expect to see is then a Rydberg series of resonances converging to the 2s-2p excitation energy of the Li-like ion involved. Since this is a $\Delta n=0$ process, we expect a substantial field dependence for the higher- n -states.

In figs.5.2, 5.3, and 5.4 we present our data for N^{4+} , F^{6+} , and Si^{11+} , respectively, together with calculations by Badnell and Pindzola including Stark l -mixing effects for varying electric field strengths

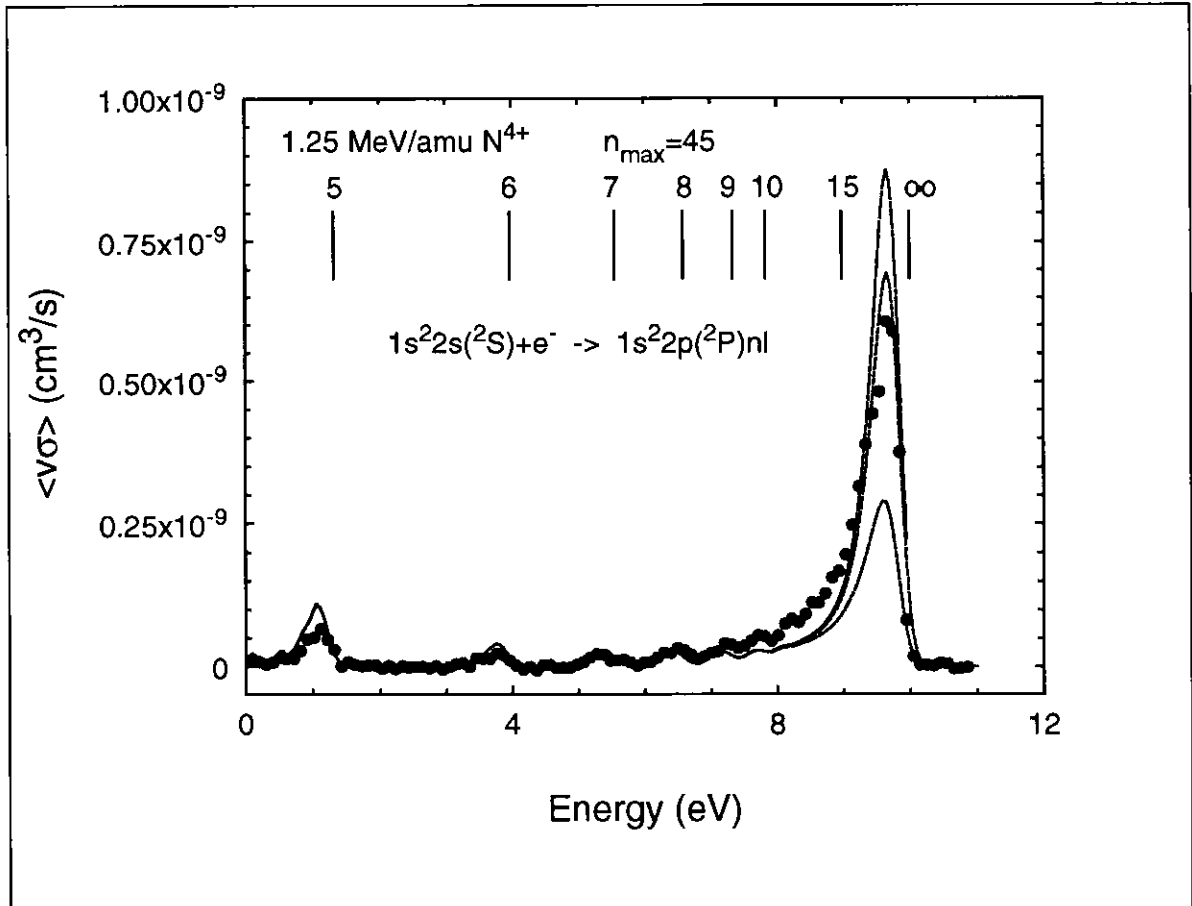


Figure 5.2 Measured and calculated rate coefficients as a function of energy for N^{4+} . The calculations assume electric fields of 0 V/cm, 5 V/cm, and 10 V/cm, respectively.

[III]. The expected resonance positions marked by vertical lines are calculated from the known 2s-2p excitation energy and the assumption that the binding energy of the captured electron is well described by the Rydberg formula without quantum defects. The peaks are always found at a slightly lower energy. This is primarily due to the flattened electron-velocity distribution, as described in sec.3.2, but also non-zero quantum defects for the lowest l values will give a displacement to the low-energy side.

For N^{4+} and F^{6+} , good overall agreement is found. We do, however, notice that theory tends to overestimate the lowest-energy resonances and to underestimate the DR signal for energies just below

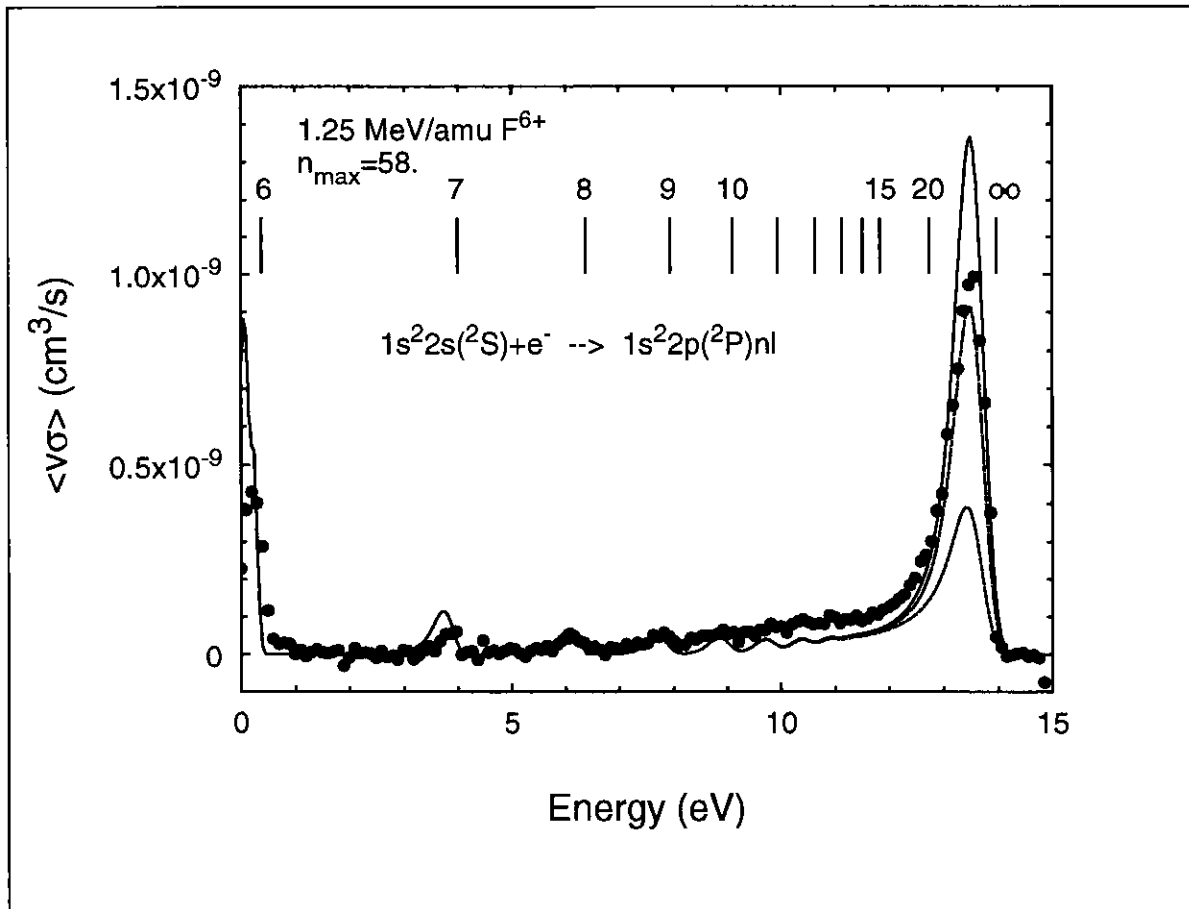


Figure 5.3 Measured and calculated rate coefficients as a function of energy for F^{6+} . The calculations assume electric fields of 0 V/cm, 5 V/cm, and 15 V/cm, respectively.

the Rydberg peaks. The gravest discrepancy appears to be related to the contribution from the $2p6l$ configurations of F^{6+} . These are, however, found to straddle the threshold, making it very difficult to determine which states should be included in the theoretical treatment [III]. It has been proposed (Hahn 1994) that the recombination rate just below the Rydberg peak not accounted for in the DR theory could be due to a 'new' recombination-mechanism; radiative dielectronic recombination, which is a DR process where the initial capture is accompanied by a simultaneous emission of a photon. However, no detailed calculations concerning this contribution have been performed.

For N^{4+} , it seems that the average electric field is a little below

5 V/cm, while for F^{6+} , it seems to be a bit more than 5 V/cm. This agrees with the expected values from the space-charge field and the motionally induced electric field due to small angles between the ion trajectories and the magnetic solenoid field.

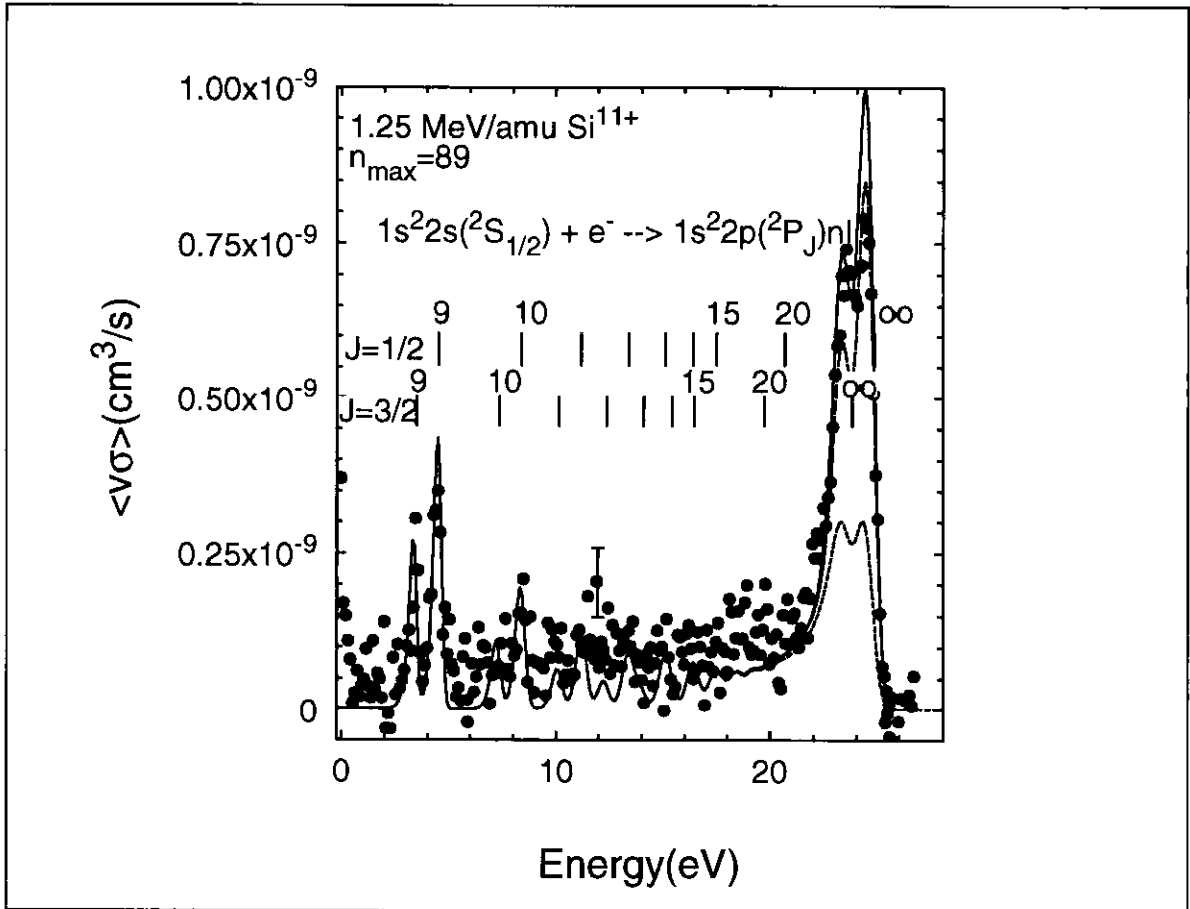


Figure 5.4 Measured and calculated rate coefficients as a function of energy for Si^{11+} . The calculations assume electric fields of 0 V/cm, 5 V/cm, and 10 V/cm, respectively.

For Si^{11+} , the beam current was so low that the statistical errors became rather large. The double structures in this spectrum are due to the fine-structure splitting of the $1s^2 2p \ ^2P$ state (for N^{4+} and F^{6+} , this splitting was too small to be resolved). Considering the double Rydberg peak, the calculations indicate that not only the total rate coefficient, but also the relative height of the two peaks depend on the field strength. If we want to get the relative height right, we must use

an electric field between 0 V/cm and 5 V/cm, but if we want the total recombination rate coefficient to be right, we have to use a somewhat larger field (5-10 V/cm). This discrepancy indicates that either is the electric field dependence not treated correctly in the calculations, or some other mechanism is involved. One mechanism could be radiative stabilization of some of the high Rydberg states before they reach the charge-state analyzer, where they were expected to be field-ionized and therefore not counted as recombined. When discussing the relative height of the two peaks, it should be pointed out that the possibility for the high- n Rydberg levels with a $^2P_{1/2}$ core to autoionize to the $^2P_{3/2}$ continuum has been taken into account in the calculations.

We performed a systematic investigation of the field dependence for N^{4+} . An ion beam was set up and left unchanged, while the integrated DR Rydberg contribution for energies from 8 eV to 10.5 eV was measured. Three different electron currents, corresponding to three different space-charge electric field strengths, were used.

The result of this measurement is shown in fig.5.5. The fields in the experiments were estimated under the assumption that the ion-beam width was $2\sigma=0.2$ cm, and the displacement of the ion beam with respect to the electron beam was between 0 and 0.1 cm. This uncertainty led to the horizontal error bars in the figure. The vertical error bars reflect a 15% uncertainty on the absolute scale. Motionally induced electric fields due to the solenoid magnetic field are not considered. Within the experimental error, agreement with theory is found. We note that this would probably still be the case if the motionally induced field was included since this would on the average displace the experimental points towards higher electric fields.

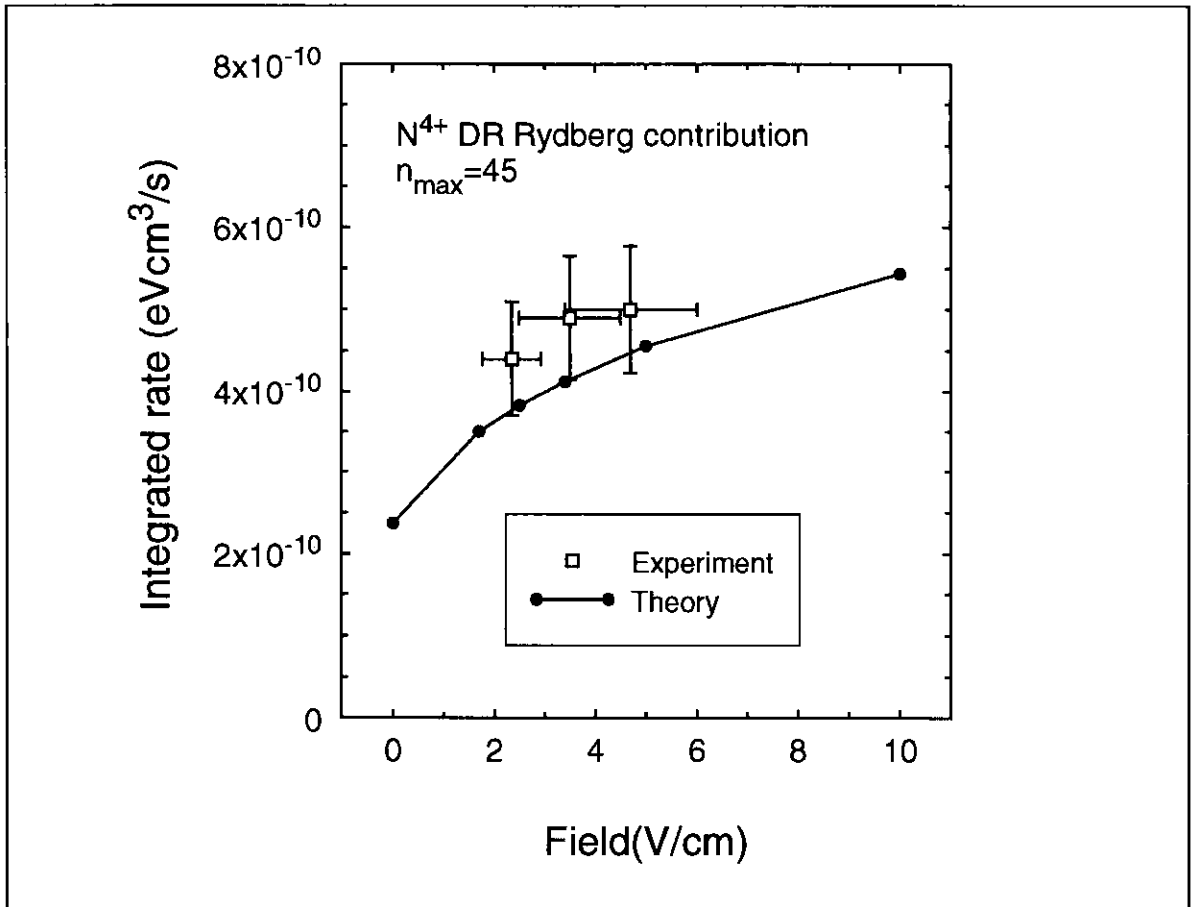


Figure 5.5 *The experimental and theoretical rate coefficient of the high- n contribution for N^{4+} integrated from 8 to 10.5 eV as a function of the calculated space-charge field.*

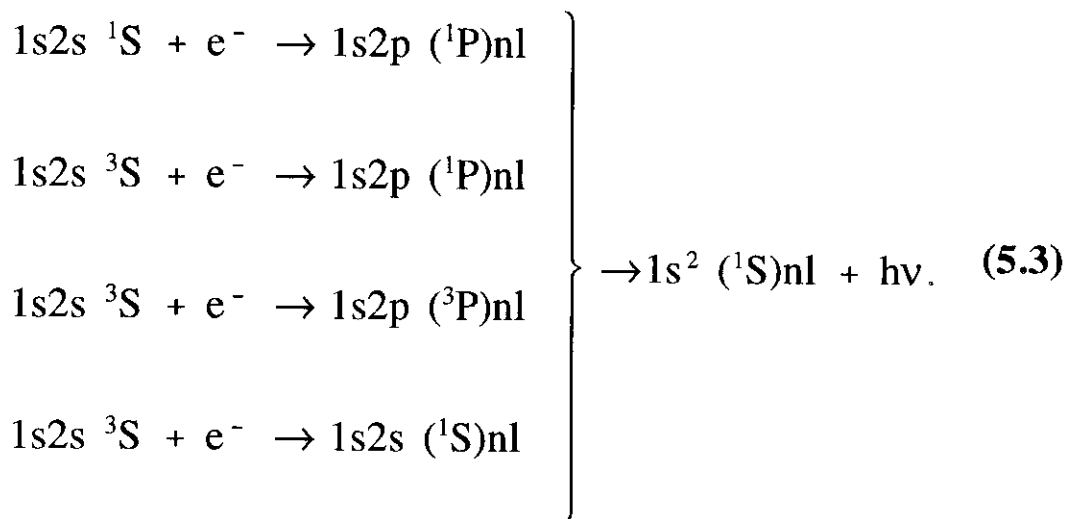
5.3 DR for metastable He-like ions (the single-pass experiment)

In this and the following section, DR for metastable He-like ions is discussed. We start by considering the single-pass experiment and then go on to the Heidelberg storage-ring experiment. The comparison of the two will yield new information concerning the interpretation of the results of the single-pass experiments.

In the single-pass experiment, the He-like ions were produced in a stripping target (gas or foil) placed at the terminal of the tandem

accelerator or, in the case of high nuclear charge, in a stripping target placed right after the tandem accelerator. This production method leads to population of a large number of electronic states. However, most of these states are rather short-lived, so that within a micro-second, all ions are found either in the ground state $1s^2 \ ^1S$, or in one of the two metastable states $1s2s \ ^1S$ or $1s2s \ ^3S$. For the ions considered here (N^{5+} , F^{7+} and Si^{12+}), the $1s2s \ ^3S$ states live much longer than the flight time from the place of production to the interaction region (Drake 1971). Hence, contribution from the $1s2s \ ^3S$ -state to the observed recombination spectrum is expected for all these ions. The $1s2s \ ^1S$ lifetimes, on the other hand, are comparable to the flight time (for N^{5+}) or much shorter (for F^{7+} and Si^{12+}).

We measured DR in the range of relative energies 0 eV - 28 eV, where no structures related to the ground state was expected. The following DR reactions could be expected in this energy region: (We expect the first two of these to be dominant since their radiative core stabilization process is dipole-allowed.)



To be able to extract absolute rate coefficients from the measurements, it is necessary to know which fraction of the incoming

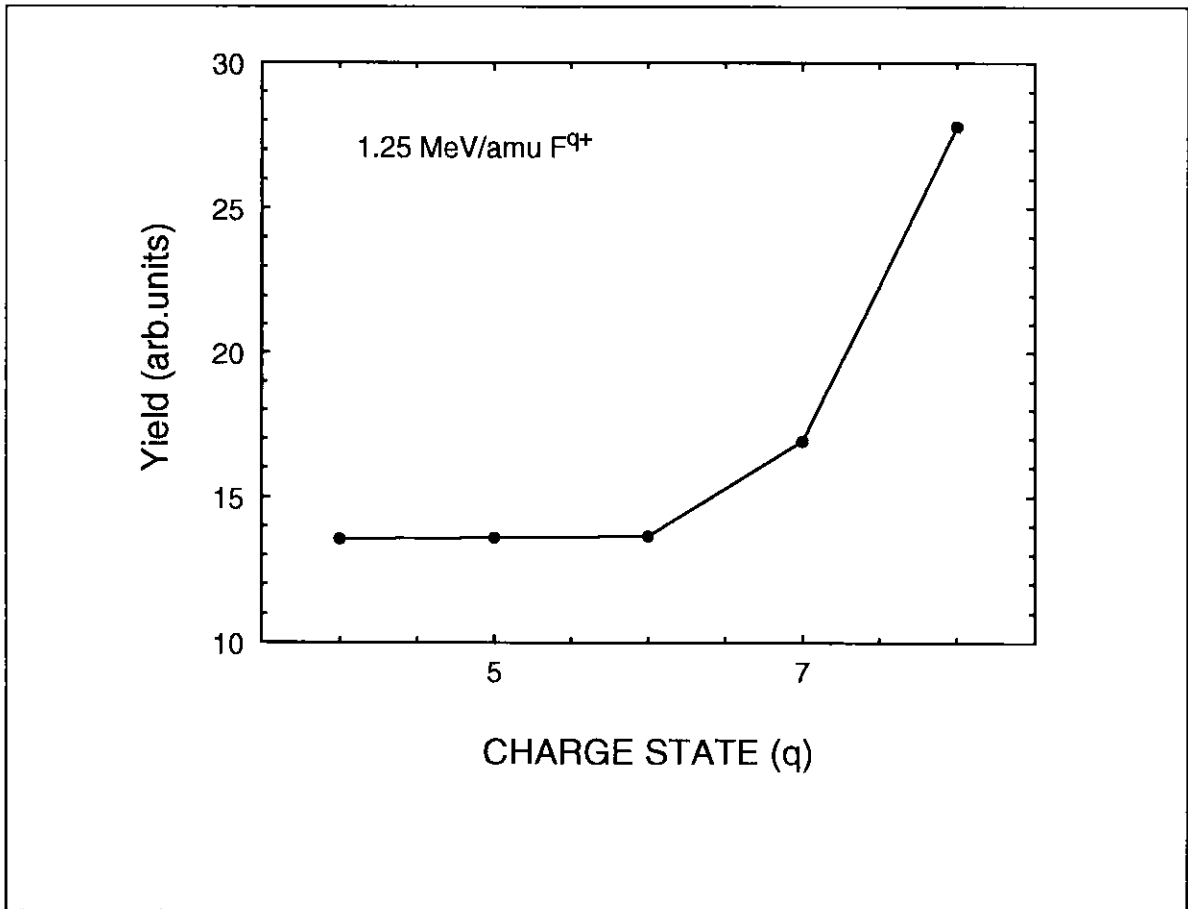


Figure 5.6 *Relative yield of Al K x rays for beams of fluorine ions in different charge states q as a function of q .*

ions is in the different states. In order to enlighten this question, we performed a series of x ray experiments. The ion beam from the tandem accelerator was passed through a carbon foil coated with a thin layer of aluminum. The emitted Al K x rays were detected at a right angle using a Si(Li) x ray detector. The idea was to take advantage of the fact that the yield of K x rays is dramatically increased when ions with only one electron in the K shell are used. The result of a series of measurements with fluorine ions in different charge states is shown in fig.5.6. We note that the yield is constant for F ions with 3, 4, and 5 electrons, corresponding to no K-shell holes. If we now assume that the increase in the yield is solely due to the presence of K-holes, the

fraction of He-like ions in the 1s2s configuration can be determined by

$$\text{metastable fraction} = \frac{Y_{(\text{He-like})} - Y_{(\text{Li-like})}}{Y_{(\text{H-like})} - Y_{(\text{Li-like})}}. \quad (5.4)$$

Note that this gives the fraction at the Al target, and that no information is achieved as to how large a fraction of the ions in the 1s2s configuration is in the ^1S or ^3S state, respectively.

If the lifetimes of the 1s2s ^1S states (Drake 1969) as well as the ion flight times to the Al target and to the electron cooler, respectively, are taken into account, the assumption of statistical population in the production mechanism (three times as many ions in the 1s2s ^3S state as in the 1s2s ^1S state), leads to the following metastable fractions in the electron cooler.

Table 5.1

ion term	C ⁴⁺	N ⁵⁺	O ⁶⁺	F ⁷⁺	Si ¹²⁺
1s2s ^1S	3 % (foil)	2 %	1 %	0.2 %	0.004 %
1s2s ^3S	16 % (foil) 7 % (gas)	15 %	20 %	23 %	12 %

C⁴⁺ and O⁶⁺ were included in these measurements because DR for these ions had been studied earlier without knowledge of the metastable fractions (Andersen 1990, Badnell 1990).

Figure 5.7 shows the result of our DR measurement for N⁵⁺ together with an LS-coupling calculation performed by Badnell and Pindzola [III]. A ^3S population of 15% as determined above was used. The ^1S population had to be adjusted to 0.8% for the theory to fit the

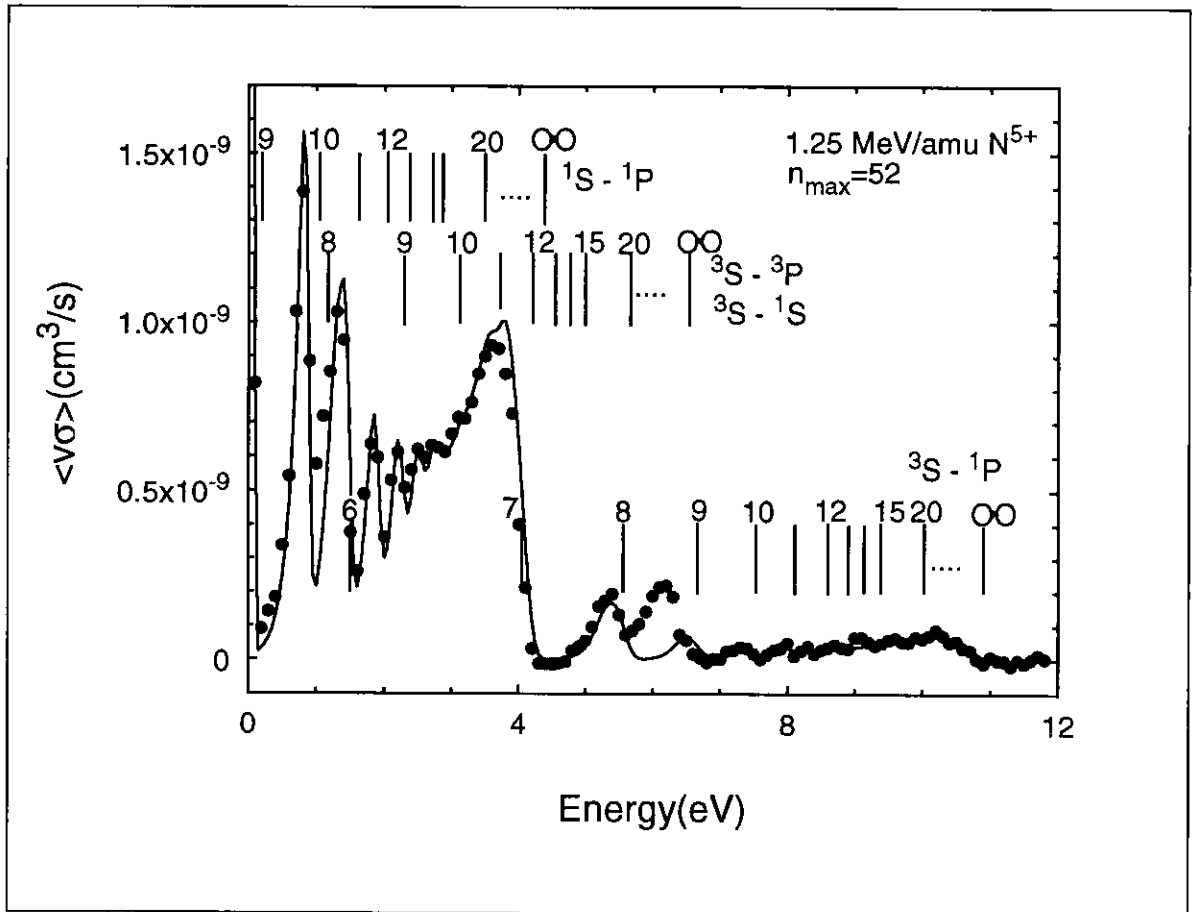


Figure 5.7 Measured and calculated rate coefficient of DR for N^{5+} ions. Metastable fractions of 0.8 % ($1s2s\ ^1S$) and 15 % ($1s2s\ ^3S$) were assumed in the calculations.

experiments on an absolute scale. If we assume that these are the right metastable fractions, agreement between theory and experiment is found except for an extra peak at about 6 eV. Except for this peak, what we see are two Rydberg series, one associated with the $1s2s\ ^1S \rightarrow 1s2p\ ^1P$ excitation, the other associated with the $1s2s\ ^3S \rightarrow 1s2p\ ^1P$ excitation. We notice that the contribution from the last of these two series is decreasing dramatically when states above the 3P and 1S series are considered. This is due to the fact that autoionization into these two open channels can now take place.

Concerning the extra peak at about 6 eV, we notice that also for

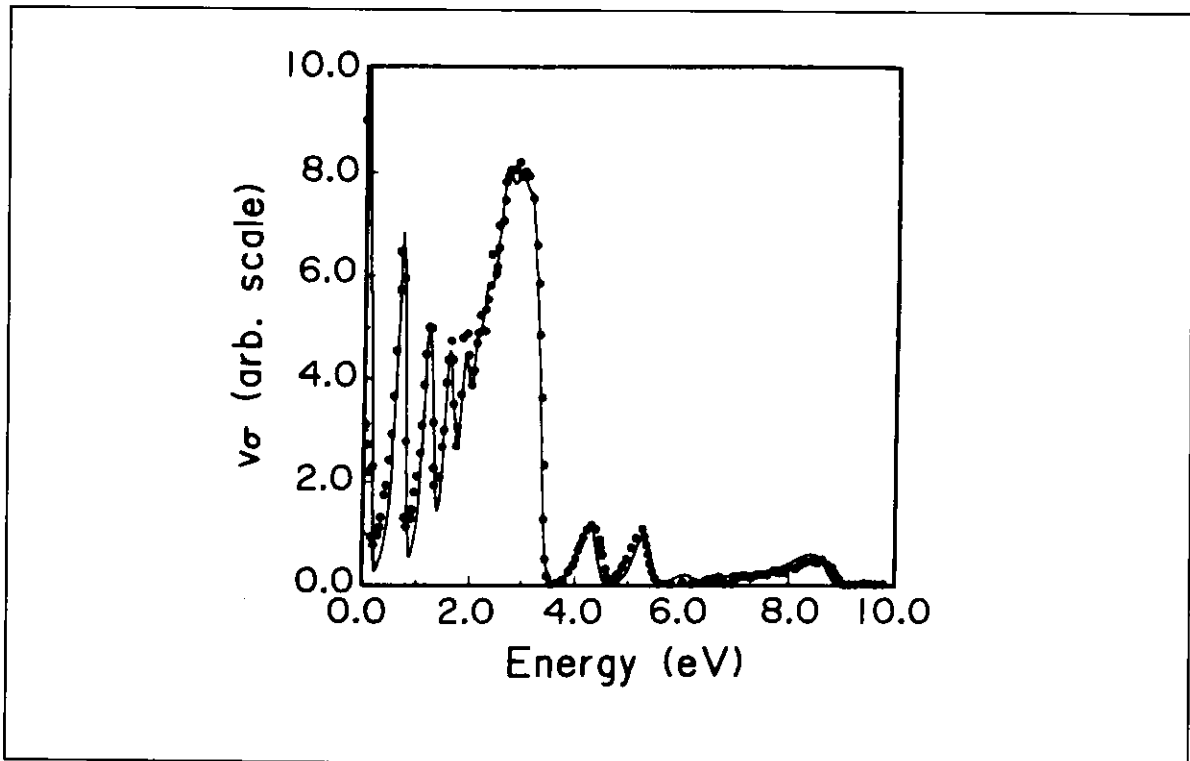
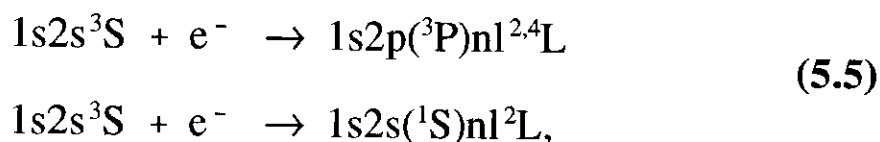


Figure 5.8 Illustration from (Badnell 1990) showing the apparently perfect agreement between theory and experiment for C^{4+} ions.

O^{6+} (Andersen 1989, Andersen 1990) and F^{7+} [III], an unexplained feature is seen just below the almost coincident 3P and 1S thresholds. It was therefore almost disturbing that for C^{4+} , absolutely perfect agreement was found between theory and experiment (see fig.5.8 and Badnell 1990). The key to this 'problem' turned out to be the $1s2p(^1P)8l$ configurations which were assumed to be responsible for the peak at about 5 eV in fig.5.8. All these configurations are found to be very close in energy to the $1s2s\ ^1S$ threshold (for $l=1$ or 2 ; too close for the theorists to determine which terms are above the $1s2s\ ^1S$ threshold). The terms higher in energy than the $1s2s\ ^1S$ threshold have a very high autoionization rate to the $1s2s\ ^1S$ continuum, and the DR cross section will be strongly reduced. In the original calculations (Badnell 1990), all the terms of the $1s2p(^1P)8p$ and $1s2p(^1P)8d$ configurations were found to be bound with respect to $1s2s\ ^1S$, and since

this gave results which agreed with experiment, it was of course believed to be correct. Later it turned out, however, that for theory to be able to account for the observed cross sections for DR for *ground state* C^{4+} (Kilgus 1991), it had to be assumed that all these terms were in fact *above* the $1s2s\ ^1S$ limit and could therefore autoionize into this continuum. This means that also for C^{4+} , there is a peak in the experimental data close to the 1S and 3P thresholds, not properly accounted for in the calculations.

In the following, possible explanations of this extra structure will be discussed. Since the energy position of a DR signal is determined by the initial capture process, and since the structure we want to account for is found just below the 1S and 3P thresholds, the responsible capture process(es) must be found among the following



where the principal quantum number of the captured electron must be larger than 20 for the energy-position to fit in the observed spectra. The problem with these capture processes is that the doubly excited intermediate states formed cannot decay directly to the $1s^2(^1S)nl$ configuration via an allowed electric-dipole transition. This means that we have to look for some other stabilization mechanism.

One such stabilization mechanism was proposed by Taulbjerg and Macek (Taulbjerg 1989) just after the first high-resolution DR measurement of O^{6+} (Andersen 1989). Their idea was that the intermediate states as described here were not pure states, but they

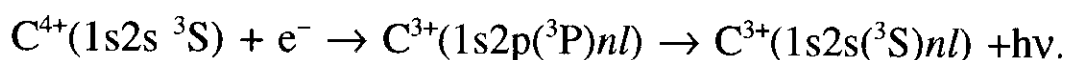
were 'contaminated' with close-lying levels of $1s2p(^1P)n'l'$ via configuration interaction. The states formed can formally be described as follows:

$$\begin{aligned} & [1s2p(^3P)nl + \varepsilon \cdot 1s2p(^1P)n'l']^2L \\ & [1s2s(^1S)nl + \varepsilon \cdot 1s2p(^1P)n'l']^2L \end{aligned} \quad (5.6)$$

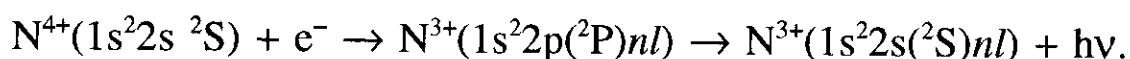
Here ε is meant to indicate that only a weak mixing is assumed. $L=l, l\pm 1$, $l'=l, l\pm 1$, and n' is 8 for C^{4+} , 9 for N^{5+} , and probably 10 for O^{6+} . Because of the presence of the $1s2p(^1P)$ core, these states can then stabilize radiatively to $1s^2(^1S)n'l'$. And this was then assumed to be the stabilization mechanism responsible for the observed DR signal.

For the first of the capture processes of eq.(5.5), another stabilization process could be the allowed electric-dipole transition to $1s2s(^3S)nl\ ^2L'$, $L'=L, L\pm 1$. This is not really a stabilization process since this state can still autoionize to the ground state $1s^2\ ^1S$ and a high-energy electron (≈ 300 eV for C^{4+}), but in particular the quartet terms may be sufficiently long-lived to survive until after the charge-state analysis and therefore be counted as recombined. Dielectronic capture, followed by transitions to metastable autoionizing states, has also been seen in other DR measurements. As an example of this, we mention the situation for Be-like ions [I], where it was found that about 50% of the ions that ended up in the metastable autoionizing $1s^2s2p(^3P)nl$ state were actually counted as recombined because they had not autoionized before the charge-state analyzer. The idea that this mechanism could also be responsible for the extra structure in the He-like ions is in fact mentioned in [I], but based on a qualitative comparison with the dominant series caused by the 3S metastables

($1s2s\ ^3S + e^- \rightarrow 1s2p(^1P)nl \rightarrow 1s^2(^1S)nl$), it was concluded that this mechanism could be neglected. Nevertheless, the following considerations will show that assuming a large survival probability of the metastable autoionizing states, the proposed mechanism does indeed give rise to a DR signal of the right order of magnitude. For C^{4+} , the maximum rate coefficient in the extra peak amounts to approximately $8 \cdot 10^{-10}$ cm³/s with the experimental velocity distribution. The proposed mechanism is the following:



We now assume that a reasonable measure of the rate coefficient for this process can be obtained by considering the situation, where an inactive 1s electron is added to the electronic core, and to compensate for the charge of this electron, a proton is added to the nucleus. This system is Li-like nitrogen which was already considered in the previous section



We see that apart from possible effects of spin, these two processes are very similar, and the maximum of the experimental rate coefficient found for N^{4+} was $6 \cdot 10^{-10}$ cm³/s, indicating that the proposed mechanism may give rise to a DR rate coefficient of the right strength.

This means that we have now two different explanations of the extra structure, and on the basis of the experimental results presented so far, we are not able to tell which one is correct. But there is an important difference between the two proposed mechanisms. In the

case of configuration interaction, the final state is a Rydberg state with $n \leq 10$ ($n=8$ for C^{4+}), whereas the proposed metastable autoionizing states will have a Rydberg electron keeping the same principal quantum number that it was captured into, and this must be $n \geq 20$. This means that if the experiment is done again, and this time with a stronger analyzer field, leading to field ionization for all ions with $n \geq 20$, the extra structure will disappear if the mechanism is radiative transition to a metastable autoionizing state, whereas in the case of the configuration-interaction mechanism, this structure will remain unchanged.

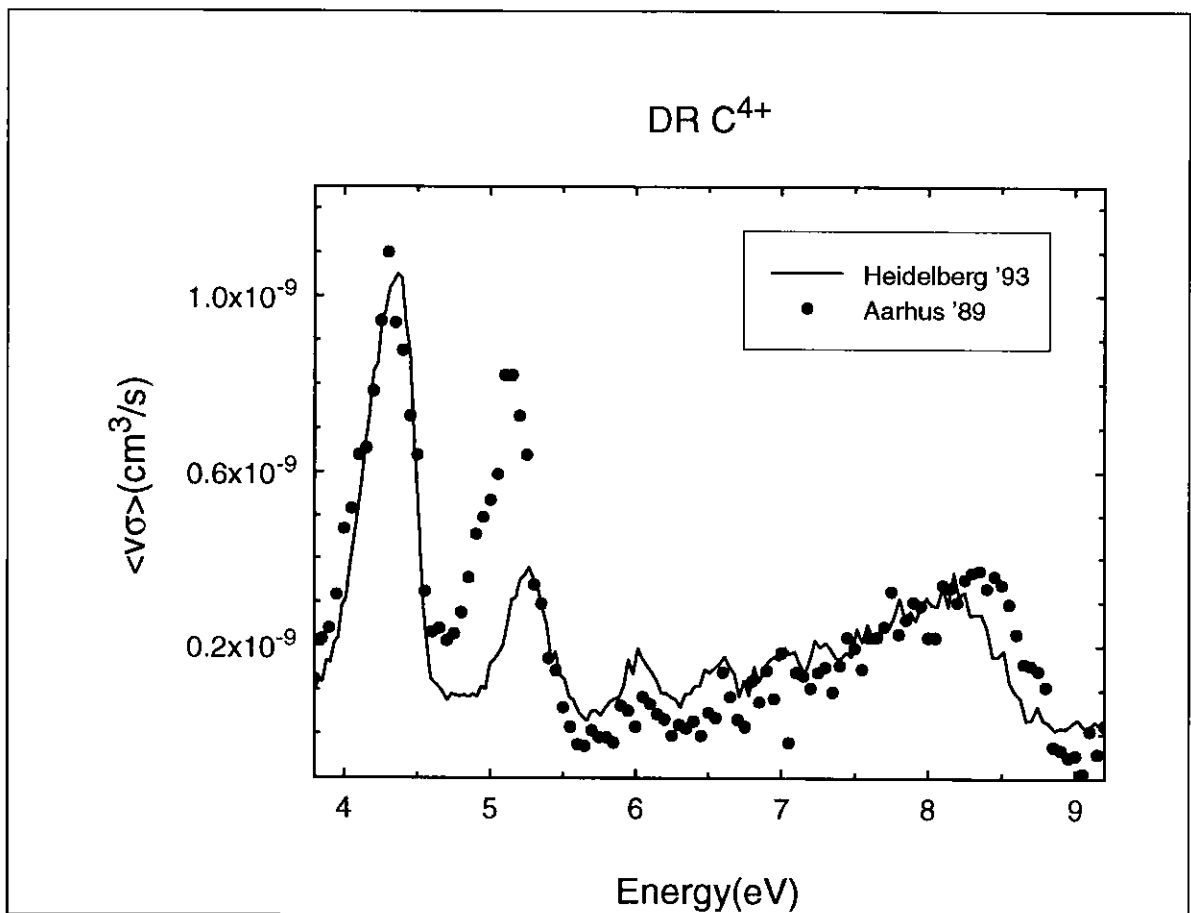


Figure 5.9 Comparison of the two results of DR measurements for He-like C^{4+} . The strong reduction of the peak at 5 eV is taken as evidence for the proposed mechanism (see text).

The storage-ring experiments described in the following section

represent just this new measurement of DR for He-like boron, carbon, and oxygen ions in the $1s2s\ ^3S$ state. In fact, in the case of C^{4+} , the limit for field ionization as given by eq.(3.2) amounts to $n_{\text{limit}}=20$. Figure 5.9 shows the measured DR rate coefficient for C^{4+} in the vicinity of the structure just discussed. We see that this structure is strongly reduced in the storage-ring experiment as compared to the earlier single-pass result. Following the discussion given above, we therefore conclude that the extra structure observed in the single-pass experiment is caused by initial capture to $1s2p(^3P)nl$ states, followed by a radiative transition to metastable autoionizing states of the form $1s2s(^3S)nl$ rather than by configuration interaction.

5.4 DR for metastable He-like ions (the TSR experiment)

For the TSR experiments, the He-like ions were created in the stripping target of the 12 MV tandem accelerator used as injection accelerator for this facility. Just as in the single-pass experiment, this leads to population of the metastable $1s2s\ ^{1,3}S$ states, but since the metastable singlet states of the ions involved (B^{3+} , C^{4+} , and N^{5+}) have lifetimes only of the order of a few μs , we get a pure spectrum of contributions only from the metastable triplet state by waiting about one ms after injection into the storage ring before we start taking data. The beam energies applied were 44 MeV for B^{3+} , 55 MeV for C^{4+} , and 60 MeV for N^{5+} . And the storage lifetimes limited by collisions with residual gas molecules (typical vacuum $5\cdot 10^{-11}$ mBar) were in all cases of the order of one to three minutes.

When usual experiments with ions in the ground state are

performed at the TSR, one applies the so-called multi-turn injection which makes the intensities of stored ion beams larger than the intensity in the injection accelerator beam by a factor of up to 40 (Bisoffi 1990). This leads to a very large horizontal ion-beam width, which is normally not a problem since a very narrow beam can be obtained by applying electron cooling for a few seconds before starting the actual measurement. However, in our case, where we want to measure the DR signal for ions in metastable states with lifetimes in the ms range this method is not applicable. On the other, hand if we tried to do the experiment with a normal multi-turn-injected ion beam, we would find ourselves in the rather unpleasant situation of having an ion beam which had a larger diameter than the aperture of our detector (2.5 cm in the horizontal direction). To circumvent this problem, we take advantage of the fact that in a normal multi-turn injection, those ions first injected will have the smallest amplitude in their oscillations around the ideal closed orbit of the storage ring (betatron oscillations). It is therefore possible to reduce the size of the ion beam in the horizontal direction by interrupting the injection at a properly chosen time. By doing so, the horizontal ion-beam width could be reduced from about 4 cm to about 1.2 cm, as observed on the TSR beam-profile monitor, making it simple to ensure that all particles, which had captured an electron on the electron-cooler straight section of the storage-ring, would be detected on the moveable multi-channel-plate detector.

The beam-profile monitor works in the following way: The passage of multiply charged ions through the residual gas leads to ionization of residual-gas molecules, which can then be electrostatically accelerated towards a position sensitive channel-plate

detector, thereby yielding the projection of the beam profile onto one of the transverse directions (Hochadel 1990). At the same time, the total count rate on the beam-profile monitor will be proportional to the ion current and may therefore be used as a relative measure of this.

With the injection scheme described above, typical currents of the stored ion-beams were a few μA 's, which is slightly too low for a reliable ion-current measurement to be performed with the DC current transformer installed for this purpose. We therefore made a calibration of the counts from the beam-profile monitor versus the DC current transformer by going to high currents, applying the normal multi-turn injection. We could then use the beam-profile monitor for measuring the currents in the experiments within systematic errors of approximately 30%.

For C^{4+} and N^{5+} with metastable lifetimes of 20 ms and 4 ms, respectively, ions were injected at the maximum injection rate of 4.8 Hz to optimize the time-averaged number of metastable ions in the storage ring. For B^{3+} with a metastable lifetime of about 150 ms, a new injection was made every 800 ms.

To match the velocities of the ion beams just described, the electron energies were typically about 2.5 keV. Typical electron currents were around 250 mA, which with a beam diameter of 5 cm corresponds to an electron density of $2\text{-}3 \cdot 10^7 \text{ cm}^{-3}$. This is similar to the electron densities in the Aarhus single-pass experiment (sec.3.2). The electron-beam position was optimized by making electron cooling of a stored ion beam. The relative positions of the ion and electron beams could be optimized by finding a minimum, for a given electron-beam acceleration voltage, of the ion-revolution frequency, as observed in the Schottky spectrum. This minimum corresponds to the situation

where the ions pass through the center of the electron beam where the space-charge potential given by eq.(3.23) is at maximum (numerically), and therefore the electron velocity is at minimum. The angular alignment was made by minimizing the ion-beam width, as observed on the beam-profile monitor, since better alignment means lower average relative velocity and hence more effective transverse cooling, leading to smaller beam size. After this alignment procedure, the acceleration voltage corresponding to the cooling energy could be determined, and it was checked that taking into account the space-charge potential as given by eq.(3.23) gave the proper electron velocity. This indicated that the space-charge correction was done correctly, and the ion beam was in fact passing through the center of the electron beam. With this information, it is possible to deduce the relative energies from the recorded values of the acceleration voltages and electron currents.

The DR measurement was performed as follows: The acceleration voltage was set to a given value by the electron-cooler control computer. After each injection, the number of particles detected by the channel-plate detector were counted in two time windows. One starting about one ms after the injection and lasting for a time corresponding to about one lifetime of the 3S state of the He-like ion to measure the DR signal, and another time window starting after several 3S lifetimes to measure the background contribution which was typically about 10% of the DR signal at a major resonance. This was repeated for about 20 injections, whereupon the number of counts in the two time gates, the actual gate times, the electron acceleration voltage, the electron current, and the ion current in terms of the total number of counts on the beam profile monitor were stored on a μ -

VAX computer, and the electron acceleration voltage was stepped to the next value for measuring.

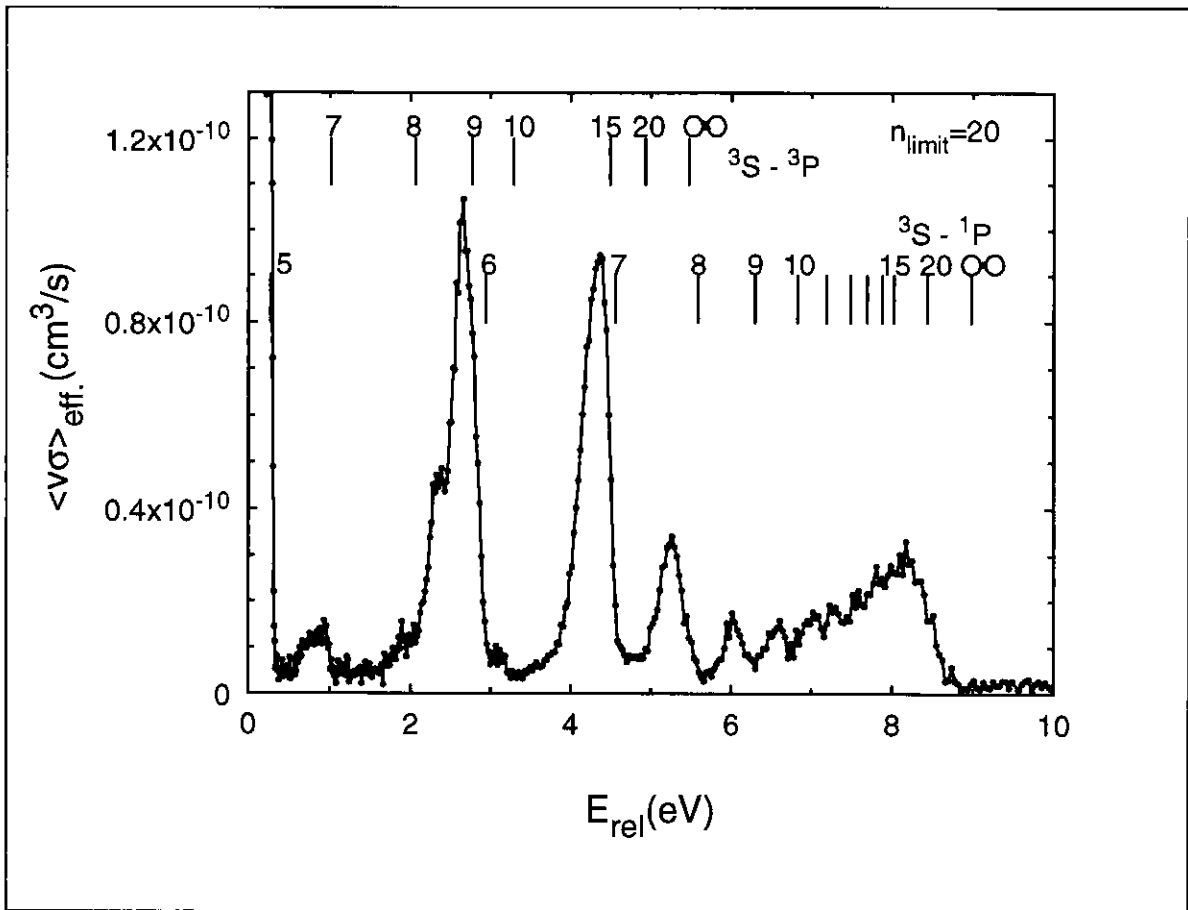


Figure 5.10 The measured effective rate coefficient for DR for C^{4+} ions in the metastable $1s2s\ ^3S$ state.

Figure 5.10 shows the result of the DR measurement for C^{4+} in terms of the *effective* rate coefficient obtained by pretending in the analysis that the unknown average fraction of metastables during the signal time window is 100%. By comparing this to the theoretical rate coefficient (Badnell 1990), which was confirmed in the single-pass experiments, the average metastable fraction can be deduced, and from knowledge of the metastable lifetime and the gate-open and -close times, the initial metastable fraction is found. The result for C^{4+} was 18(6)%, where the main source of error comes from the ion-current

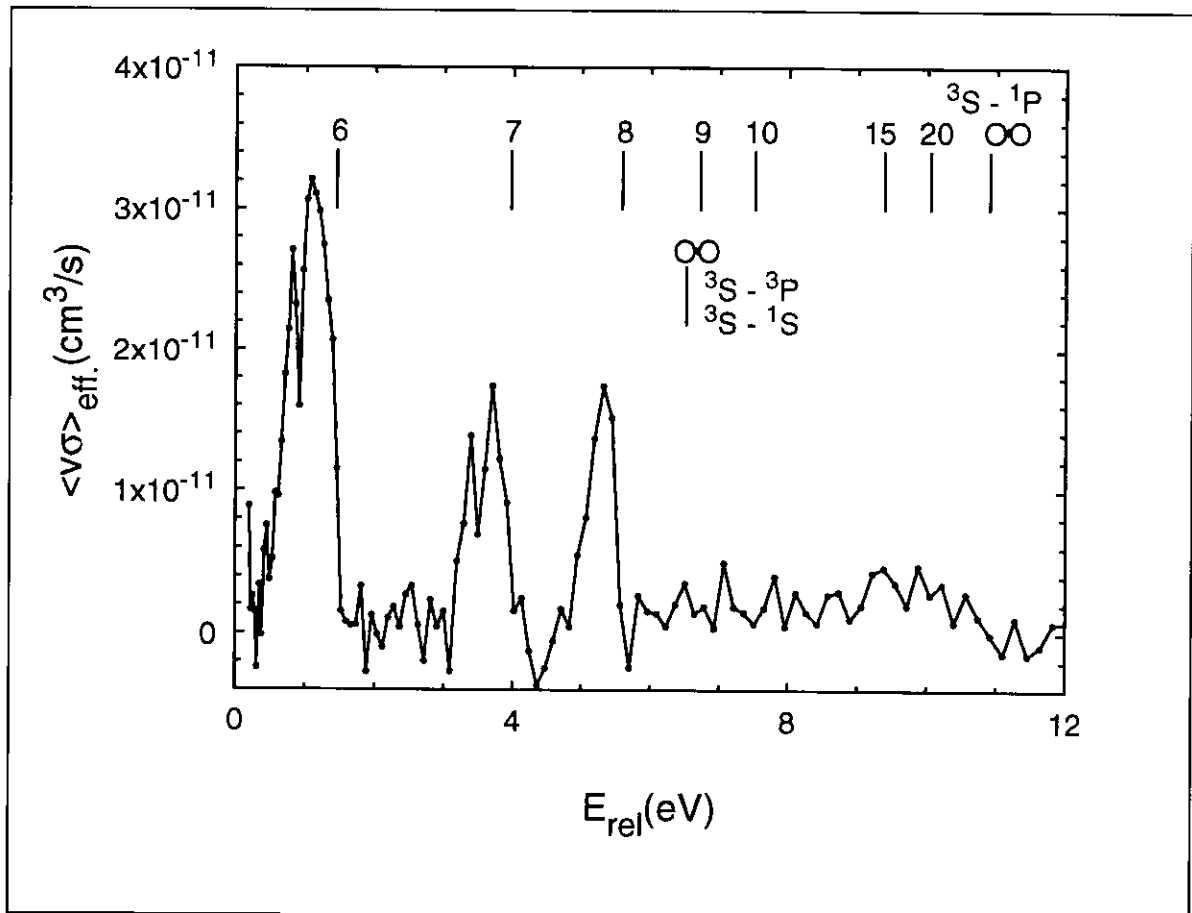


Figure 5.11 The measured effective rate coefficient for DR for N^{5+} ions in the metastable $1s2s\ ^3S$ state.

measurement.

With no contribution from the 1S metastables, the observed DR spectrum is dominated by the series of resonances related to the excitation from $1s2s\ ^3S$ to $1s2p\ ^1P$. Single resonances can be resolved up to the principal quantum number of the captured electron $n'=12$. Details of the $n'=5$ peak close to 0 eV could not be observed due to the substantial drag force at low energy. For the $n'=6$ peak, we observe a splitting caused by the different l -quantum numbers of the captured electrons. The DR signal for $n' \geq 8$ is reduced because of the opening of new autoionization channels, as discussed in the previous section. The high- n' contribution is only slightly reduced due to the stronger

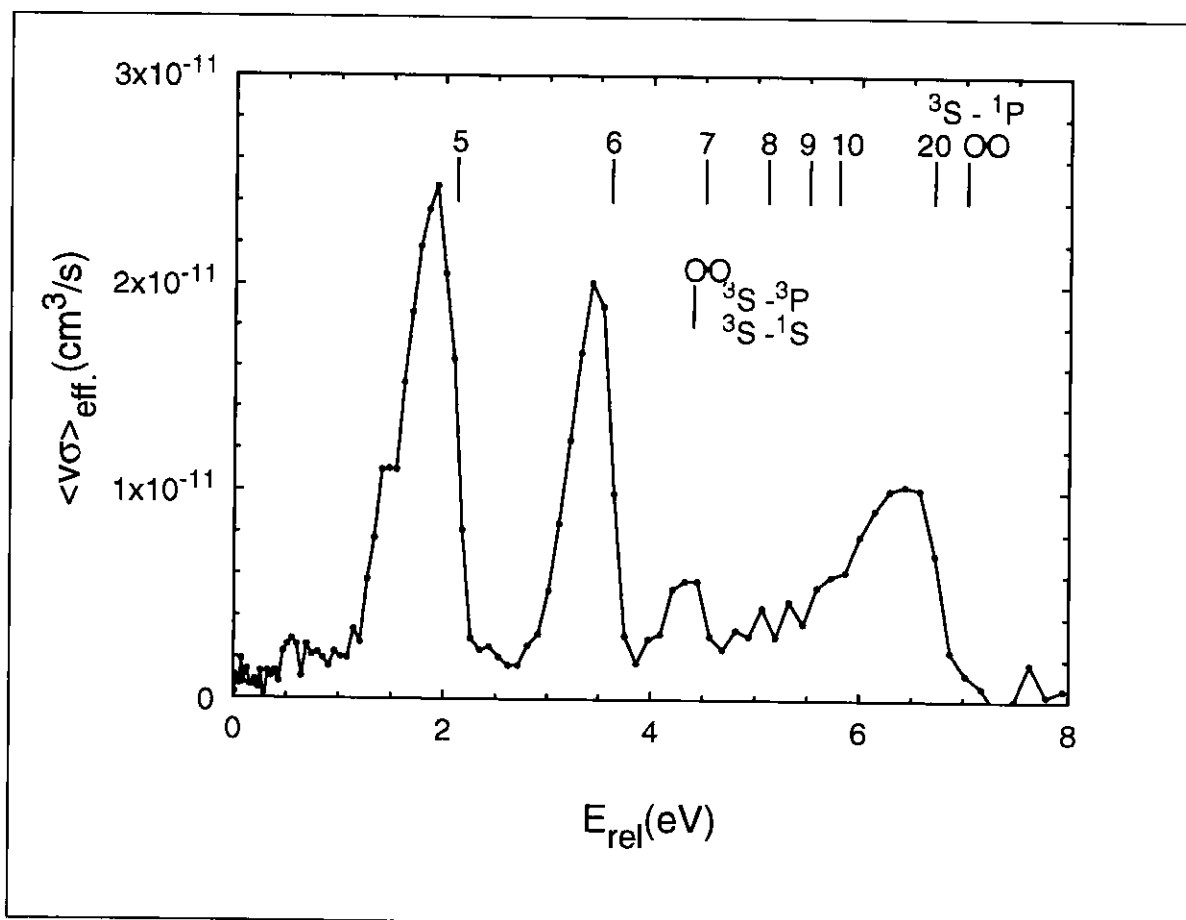


Figure 5.12 The measured absolute rate coefficient for DR for B^{3+} ions in the metastable $1s2s\ ^3S$ state.

field-ionization effects as compared to the single-pass experiment. This is because the stabilization mechanism is a $\Delta n=1$ process, where the high- n' contribution is known to be small (see sec.5.1).

This is in strong contrast to the high- n' contribution related to the 3S - 3P excitation which, as discussed in sec.5.3, becomes strongly reduced going to the lower n_{limit} of the storage-ring experiment, yielding yet an indication that the stabilization for this process is in fact a $\Delta n=0$ transition (i.e. a transition to $1s2s({}^3S)nl$). The only structure related to this excitation, which can be seen clearly in fig.5.10, is the peak just below 1 eV which we ascribe to the $n'=7$ -resonance of this excitation. The other resonances are hidden by the

much stronger DR signal related to the $^3S-^1P$ excitation.

In figs.5.11 and 5.12, the equivalent results for B^{3+} and N^{5+} are shown. For N^{5+} , the metastable fraction could be determined by comparing with the theoretical spectrum. When using a stripper gas at the tandem terminal (as was done for C^{4+}), the metastable fraction was as low as 3.1(1.0)%, whereas replacement of the gas by a thin foil leads to an increase to 11(4)%. For B^{3+} , no detailed calculation was available for comparison, but by extrapolating the rate coefficients from the known values for He-like carbon, nitrogen, and oxygen, the metastable fraction was found to be of the order of 10%.

Let us end this section on the DR measurements of stored, metastable He-like ions by concluding that they appear to be well understood and have shed light on a five year old controversy regarding certain anomalies observed in the Aarhus single-pass experiment.

5.5 DR for Be-, B-, and C-like ions

This short section on DR for Be-, B-, and C-like ions is only added for completeness. For a detailed discussion of these, reference is made to the original articles [I,V].

As was the case for the He-like ions, the presence of ions in metastable states in the single-pass experiment was found to strongly influence the observed DR spectra. But unlike the situation for He-like ions, the excitation to the metastable states is an intra-shell ($\Delta n=0$) excitation which requires only a small amount of energy. This means that at low relative energies, both DR for metastable and ground states

will be observed.

As an example I show here the observed recombination spectrum for C-like flourine ions (fig.5.13). DR related to ions initially in all three terms (3P , 1D , and 1S) of the ground-state configuration $1s^22s^22p^2$ is observed. The observed spectrum relates to the following three single-electron excitations: $2s-2p$, $2p-3s$, and $2p-3d$.

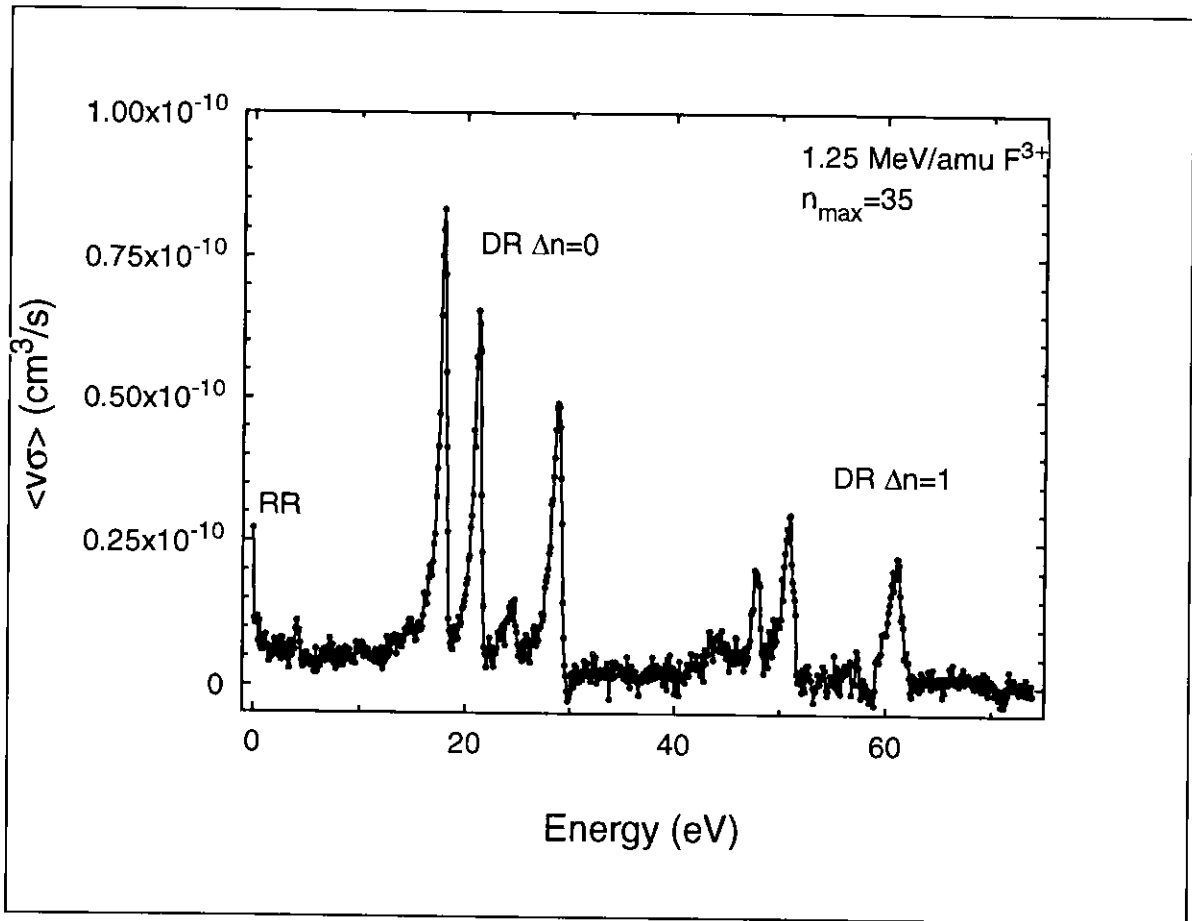


Figure 5.13 Complete recombination spectrum of F^{3+} in the energy range of 0 eV to 74 eV. Contributions from RR, DR($\Delta n=0$), and DR($\Delta n=1$) can be observed.

- R Ali, C P Bhalla, C L Cocke, M Schulz and M Stockli (1991) Phys.Rev.A 44 223*
- L H Andersen, P Hvelplund, H Knudsen, and P Kvistgaard (1989) Phys.Rev.Lett. 62 2656*
- L H Andersen, J Bolko and P Kvistgaard (1990) Phys.Rev. A 41 1293*
- N R Badnell, M S Pindzola, and D C Griffin (1990) Phys.Rev.A 41 2422*
- P Beiersdorfer, M H Chen, R E Marrs, M B Schneider and R S Walling (1991) Phys.Rev.A 44 396*
- G Bisoffi, M Grieser, E Jaeschke, D Krämer, and A Noda (1990) NIM A287 320*
- P F Dittner, S Datz, P D Miller, C D Moak, P H Stelson, C Bottcher, W B Dress, G D Alton, N Neskovic and C M Fou (1983) Phys. Rev. Lett. 51 31*
- G W F Drake, G A Victor and A Dalgarno (1969) Phys.Rev. 180 25*
- G W F Drake (1971) Phys.Rev.A 3 908*
- D C Griffin (1989) Physica Scripta T28 17*
- Y Hahn (1994) Submitted to Phys.Rev.A*
- B Hochadel (1990) Thesis entitled: "Ein Strahlprofilmonitor nach der methode der Restgasionisation für den Heidelberger Testspeicherring TSR, Max-Planck Institut für Kernphysik, Heidelberg."*
- G Kilgus, D Habs, D Schwalm, A Wolf, R Schuch, N R Badnell (1993) Phys.Rev.A 47 4859*
- J B A Mitchell, C T Ng, J L Forand, D P Levac, R E Mitchell, A Sen, D B Miko, and J Wm McGowan (1983) Phys.Rev:lett. 50 335*
- A Müller, D S Belic, B D DePaola, N Djuric, G H Dunn, D W Mueller and C Timmer (1987) Phys.Rev.A 36 599*
- W Spies, A Müller, J Linkemann, A Frank, M Wagner, C Kozuharov, B Franzke, K Beckert, F Bosch, H Eickhoff, M Jung, O Klepper, W König, P H Mokler, R Moshhammer, F Nolden, U Schaaf, P Spaedtke, M Steck, P Zimmerer, N Grun, W Scheid, M S Pindzola, N R Badnell (1992) Phys.Rev.Lett. 69 2768*
- K Taulbjerg and J Macek (1989) Phys.Rev.Lett. 62 2766*
- A Wolf, J Berger, M Bock, D Habs, B Hochadel, G Kilgus, G Neureither, U Schramm, D Schwalm, and E Szmola (1991) Z.Phys.D 21 69*

6. Lifetime measurements based on DR

For the TSR DR measurements described in sec.5.4, we took advantage of the fact that the ions in the metastable states decayed to the ground state and therefore no longer contributed to the DR signal in the energy range considered. This allowed us to isolate the background signal by waiting for (practically) all the ions in the metastable state to decay to the ground state. In this chapter, experiments are discussed in which we determine the lifetimes of the metastable states by recording the time dependence of the recombination signal.

In sec.6.1, an introduction to this subject is given, and earlier experimental results are quoted. Section 6.2 describes the experimental procedure, and in sec.6.3, the data analysis is described. Finally, discussion and comparison with theory are presented in sec.6.4. The results for carbon and nitrogen were presented in [VI], whereas the boron result has not been published before.

6.1 Lifetime of the 3S metastable state of He-like ions

We consider spontaneous radiative transitions in the He-like atomic systems from the lowest excited state $1s2s\ ^3S_1$ to the ground state $1s^2\ ^1S_0$. Due to conservation of the total angular momentum of the entire system (including the radiation field), a triangle inequality of the final and initial total angular momentum J of the atomic system and the multipole order of the emitted radiation must be fulfilled (Marrus 1978). As J goes from one to zero, this means that the emitted

radiation is of order one, i.e. we have a dipole transition. As the parity does not change, an electric-dipole (E1) transition can be excluded, and we are left with a magnetic-dipole (M1) transition as the only possible one-photon mechanism. A spin-forbidden two-photon E1 transition cannot be ruled out and was in fact for almost 30 years believed to be dominating (Breit 1940). But after the identification of spectral lines associated with the M1 decay of He-like ions in the radiation emitted from the solar corona (Gabriel 1969, 1970), theoretical studies of the M1 decay were actively pursued (Beigman 1971, Drake 1971, Feinberg 1971, Johnson 1974). It was then found that the M1 decay was the dominating decay mode of the 2^3S state for all He-like ions, and in particular for the ions of boron, carbon, and nitrogen considered here, it was found that the ratio of the rate of the two-photon E1 transition to that of the M1 transition is about $2 \cdot 10^{-4}$ (Drake 1969, 1971).

The 2^3S decay rates of He-like ions with high nuclear charge ($Z \geq 16$) in the range $> 10^6 \text{ s}^{-1}$ were measured in a number of experiments using the beam-foil technique (Marrus 1978, Hubricht 1987, Marrus 1989). This yielded results with experimental errors of $\geq 3\%$ which did not distinguish between the different theoretical approaches to the problem. Much less data are available for He-like systems with lower Z , where the M1 decay rate, scaling roughly as $\propto Z^{10}$, becomes small ($\approx 10^{-4} \text{ s}^{-1}$ for He). On the other hand, especially for the low- Z systems, the Coulomb interaction between the two electrons is expected to have large effect and to add a further complication to the calculation of the M1-transition matrix element, whereas in the high- Z systems mainly studied experimentally until now, two-electron effects lead to small corrections only.

Measurements of the 2^3S decay rate in low- Z He-like systems

have so far been performed for He atoms (Woodworth 1975) and Li^+ ions (Knight 1980). Due to the very low decay rates for these two ions, it was not possible to use the time dependence of a signal related to the 2^3S states. Instead, the decay rate was deduced from observation of the emitted photons from the M1 decay, in combination with a probe measurement to determine the number of ions in the metastable state. Here, the correction to the transition matrix element due to the electron-electron interaction (Drake 1971) is of the order $\approx 30\%$, but experiments have confirmed the expected size of this correction with low precision only, limited by errors of 15-20%. Recently, an experiment on Ne^{8+} ions was performed with an electron-beam ion trap (Wargelin 1993). Here the two-electron correction is $\approx 5\%$, and with an experimental error of 1.7%, this experiment has somewhat improved the situation for low-Z He-like ions.

The experiments treated in this chapter for boron, carbon, and nitrogen have relative errors of 2.8‰, 2.3‰, and 1.2‰, respectively, and for the first time, distinction between the theories of Drake (Drake 1971) and of Johnson and Lin (Johnson 1974) can be made.

6.2 The experiment

The lifetime measurements were performed at the TSR during the same beam times as the DR measurements described in sec.5.4. When the DR spectrum was recorded for the currently studied He-like ion, the electron acceleration voltage was fixed at a value corresponding to one of the resonances, and we changed data taking system to a multichannel scaler which, recorded as a function of time after the

injection, the number of particles hitting the channel-plate also used for the DR-measurement. The time scale was shown to be reproducible within relative deviations of $<10^{-3}$ for carbon and nitrogen. Prior to the boron experiment, this was improved to $<2 \cdot 10^{-5}$. Measurements were performed at different resonances to exclude a dependence of the measured decay rate on the relative energy, which might be suspected due to the small drag force exerted on the ions by the electron beam (see sec.3.2).

The decay curve measured on the C^{4+} , $n'=6$ peak after adding up

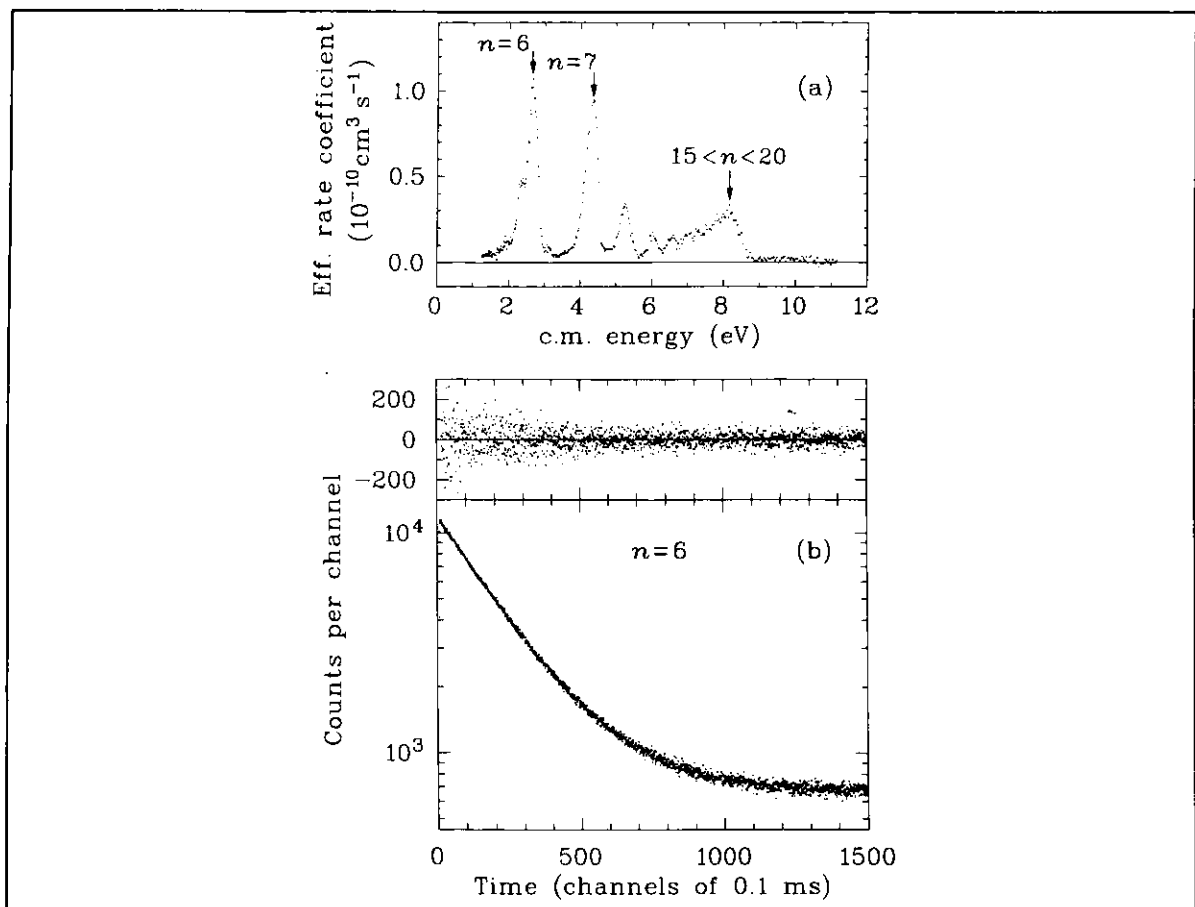


Figure 6.1 (a): The C^{4+} DR spectrum, with indications of the resonances where decay curves were recorded. (b): Decay curve recorded at the $n'=6$ resonance and deviations from the fit to eq.(6.4).

approximately 70 000 injections is shown in Fig.6.1. Because of the long beam lifetime of ≈ 2 min and the small influence of any collisional processes, the signal features a very clean exponential decrease due to the radiative decay of the 2^3S state.

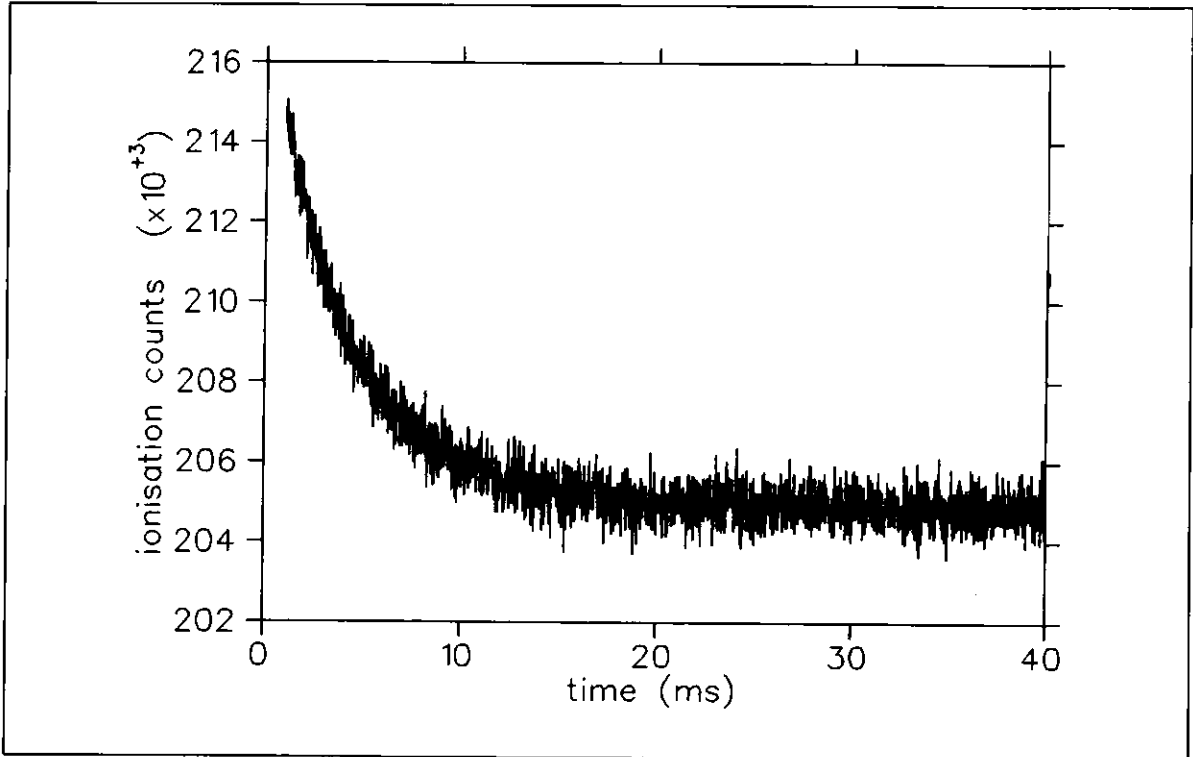


Figure 6.2 Yield of N^{6+} ions formed in residual-gas collisions in the electron-cooler straight section as a function of time after injection of a N^{5+} beam.

In the case of C^{4+} and N^{5+} , an additional detector was counting the ions which had lost an electron due to ionizing collisions with residual-gas molecules, and this information was recorded by the multi-channel scaler as well. It was demonstrated that due to the large difference in the ionization cross sections of ions in the metastable and ground states, lifetime measurements of poorer but comparable quality could have been performed by considering this signal rather than the DR signal. Figure 6.2 shows the yield of N^{6+} ions as a function of time after injection of a N^{5+} beam. Note the poorer 'signal-to-background'

ratio as compared to fig.6.1.

6.3 Analysis of data from the decay rate measurement

To extract from the data a precise value of the total radiative decay rate observed in laboratory rest frame, we must consider the following set of rate equations:

$$\begin{aligned} \frac{dN^m}{dt} &= -(A_r + A_l^m + A_q + A_{DR})N^m + A_e N^g, \\ \frac{dN^g}{dt} &= (A_r + A_q)N^m - (A_l^g + A_e)N^g, \end{aligned} \tag{6.1}$$

where N^m and N^g denote the population of the metastable $1s2s\ ^3S$ state (m) and the $1s^2\ ^1S$ ground state (g), respectively, and A_r is the radiative decay rate of the 3S state. All other rates in these equations are much smaller than A_r and describe the loss of ions from the storage ring for the two states ($A_l^{g,m}$), the collisional excitation from g to m (A_e), the collisional quenching from m to g (A_q), and the dielectronic recombination of the metastable ions (A_{DR}). The beam loss-rates $A_l^{g,m}$ are dominated by ionization of the circulating ions in collisions with residual-gas molecules. Different loss rates are assumed for the two state, since the ionization cross sections are larger for ions in the metastable state than for ground-state ions.

To solve these equations, we shall write them in the simpler form:

$$\begin{aligned} \mathbf{u}' &= \mathbf{a}\mathbf{u} + \mathbf{b}\mathbf{v}, \\ \mathbf{v}' &= \mathbf{c}\mathbf{v} + \mathbf{d}\mathbf{u}, \end{aligned} \quad (6.2)$$

where differentiation with respect to time is denoted by a prime and $\mathbf{u}=\mathbf{N}^m$, $\mathbf{v}=\mathbf{N}^g$, $\mathbf{a}=-(\mathbf{A}_r+\mathbf{A}_1^m+\mathbf{A}_{DR}+\mathbf{A}_q)$, $\mathbf{b}=\mathbf{A}_e$, $\mathbf{c}=-(\mathbf{A}_1^g+\mathbf{A}_e)$, and $\mathbf{d}=\mathbf{A}_r+\mathbf{A}_q$.

The solution to these equations is that both \mathbf{u} and \mathbf{v} will be linear combinations of the two exponentials $\exp(\mathbf{X}^+t)$ and $\exp(\mathbf{X}^-t)$ where

$$\mathbf{X}^\pm = \frac{1}{2} \left(\mathbf{a} + \mathbf{c} \pm (\mathbf{a} - \mathbf{c}) \sqrt{1 + 4\mathbf{b}\mathbf{d}(\mathbf{a} - \mathbf{c})^{-2}} \right). \quad (6.3)$$

The observed count rate, consisting of the dielectronic-recombination signal and a background contribution primarily caused by electron capture in residual-gas collisions, will again be a linear combination of \mathbf{u} and \mathbf{v} and can hence be represented as a function of time by the following two-component exponential:

$$\mathbf{F}(t) = \mathbf{C}_1 \exp(\mathbf{X}^+ t) + \mathbf{C}_2 \exp(\mathbf{X}^- t), \quad (6.4)$$

where \mathbf{C}_1 and \mathbf{C}_2 are arbitrary constants.

So far, we have made no approximations. To proceed, we now take advantage of the known orders of magnitude of the single terms. $\mathbf{A}_r \approx 7 \text{ s}^{-1}$, 50 s^{-1} , and 250 s^{-1} for B^{3+} , C^{4+} , and N^{5+} , respectively. For all the three ions considered here $\mathbf{A}_1^{g,m}$ are of the order 10^{-2} s^{-1} , $\mathbf{A}_{DR} \approx 10^{-3} \text{ s}^{-1}$, and $\mathbf{A}_{e,q} \leq 10^{-4} \text{ s}^{-1}$.

In the limit $\mathbf{A}_e = \mathbf{A}_q = 0$, we find $\mathbf{X}^+ = \mathbf{a} = -(\mathbf{A}_r + \mathbf{A}_1^m + \mathbf{A}_{DR})$ and $\mathbf{X}^- = \mathbf{c} = -\mathbf{A}_1^g$. This relation between \mathbf{X}^+ and \mathbf{X}^- means that we can

determine X^- by considering $F(t)$ after a few seconds when the first term has vanished. We therefore made a few long-time scans to determine X^- which was then kept fixed when the data from short scans of 5-10 radiative lifetimes were analyzed. A χ^2 method was applied to find X^+ with statistical errors from the data set.

Expanding eq.6.3 to first order in $A_{e,q}/A_r$ we find $X^+ \approx a + bd(a-c)^{-1} \approx -(A_r + A_1^m + A_{DR} + A_q + A_e(1 + A_1^m/A_r + A_{DR}/A_r + A_1^g/A_r)^{-1})$. We neglect terms of relative order $A_e A_1^{g,m}/(A_r)^2$ and find $X^+ \approx -(A_r + A_1^m + A_{DR} + A_q + A_e)$. Hence, to find A_r , we have to make estimates of A_1^m , A_{DR} , A_q , and A_e and subtract these from $|X^+|$.

For nitrogen, the result of the fit was $|X^-| = 6.0(2) \cdot 10^{-3} \text{ s}^{-1}$, and $|X^+| = 254.9(3.1) \text{ s}^{-1}$ (the errors stated here and throughout this section are one standard deviation). The leading correction A_1^m is of the same order as $A_1^g \approx |X^-|$ and thus more than two orders of magnitude smaller than the statistical uncertainty of X^+ . We therefore neglect the corrections and find $A_r = |X^+| = 254.9(3.1) \text{ s}^{-1}$. Correcting for the relativistic time dilation of the 60 MeV $^{14}\text{N}^{5+}$ beam yields the result $A_{CM}^N = 256.1(3.1) \text{ s}^{-1}$.

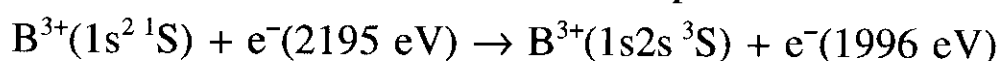
For carbon, the result of the fit was $|X^-| = 7.8(7) \cdot 10^{-3} \text{ s}^{-1}$, and $|X^+| = 48.350(95) \text{ s}^{-1}$. The loss rate A_1^m of the metastable ions relative to that of the ground state ions ($A_1^g \approx |X^-|$) was deduced from the ionization-rate measurement mentioned in sec.6.2. From the ratio of the ionization count rate right after the injection and after a few seconds, when practically all ions are in the ground state, and from the initial metastable fraction derived from the DR analysis of sec.5.4, we deduce $A_1^m/A_1^g = 2.1(8)$ and hence $A_1^m = 1.6(6) \cdot 10^{-2} \text{ s}^{-1}$.

To evaluate the total influence of the pressure-dependent terms in X^+ ($A_1^m + A_q + A_e$), we repeated the measurement at an effective residual-gas pressure higher by a factor of 10(1), achieved by switching off the ion pumps in the entire storage ring. The long-time decay rate $|X^-|$ was used as a measure of the effective ring pressure. The decay constant measured at the high residual-gas pressure is $|X^+|^{\text{high}} = 48.44(28) \text{ s}^{-1}$. The difference $|X^+|^{\text{high}} - |X^+|$, scaled down assuming a linear pressure dependence, together with the earlier result for A_1^m yields $A_q + A_e = -0.006(34) \text{ s}^{-1}$ at the lower pressure. Since A_q and A_e cannot be negative, we just get the upper limit $A_q + A_e < 0.028 \text{ s}^{-1}$ and hence $A_1^m + A_q + A_e = 0.016^{+0.028}_{-0.006} \text{ s}^{-1}$. The loss of ions due to dielectronic recombination represents an even smaller correction of $A_{\text{DR}} = 1.0(1) \cdot 10^{-3} \text{ s}^{-1}$. The measured decay rate of the stored metastable ions therefore amounts to $A_r = 48.33(11) \text{ s}^{-1}$, where the error includes the relative error of 10^{-3} of the multichannel scaler clock. Correcting for the relativistic time dilation of the 55 MeV $^{12}\text{C}^{4+}$ beam yields the result $A_{\text{CM}}^{\text{C}} = 48.57(11) \text{ s}^{-1}$.

In the case of N^{5+} , the corrections were less than one per cent of the statistical error of $|X^+|$ and could safely be ignored. For C^{4+} , the corrections were still only about 20% of the statistical error. For B^{3+} , however, the corrections amount to several times the uncertainty of the final result. Therefore correct estimates of these corrections become important if we want to find a result as accurate as the one found for C^{4+} . We have two measurements of the long-time decay rate, $|X^-|^{\text{I}} = 0.0184(4) \text{ s}^{-1}$, and $|X^-|^{\text{II}} = 0.0147(3) \text{ s}^{-1}$. Since an error in X^- influences the final result both through the value of X^+ found and through the pressure-dependent corrections, and since these influences tend to

cancel, we would overestimate the total error if we just used one value of X^- with errors large enough to contain both $|X^-|^I$ and $|X^-|^II$ and treated the errors introduced as if they were independent. Rather than doing so, we make the entire data evaluation for both cases I and II and then give a final result in accordance with the results of both analyses. For the two cases I and II, we found $|X^+|^I=6.6921(124) \text{ s}^{-1}$, and $|X^+|^II=6.6796(124) \text{ s}^{-1}$.

We start by estimating the size of the rate of excitation in collisions with the residual-gas molecules A_e . Since the residual gas consists primarily of molecular hydrogen ($\geq 90\%$), we estimate the cross section for excitation in collision with H_2 . The electrons in the H_2 molecule move with velocities in the order of $v_0=\alpha c \approx 1/137 c \approx 7.3 \cdot 10^{-3} c$. This should be compared to the velocity $v_{ion}=9.2 \cdot 10^{-2} c$ of the 44 MeV $^{11}B^{3+}$ beam. Having $v_{ion} \gg v_0$, we approximate the excitation cross section for collisions with H_2 with twice (because of the *two* electrons in the molecule) the excitation cross section for electrons moving with the same velocity relative to the ions as the H_2 molecules. We hence consider the collision process:



Kato and Nakazaki (Kato 1989) give the cross sections in terms of the collision strengths for a number of He-like systems. The collision strength Ω_{if} is defined through the relation:

$$\sigma_{exc.}^{el.} = \frac{\Omega_{if}}{\omega_1 E(\text{Ry})} \pi a_0^2 \quad (6.5)$$

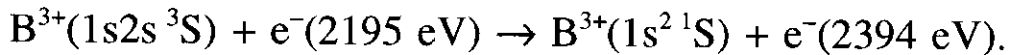
where $\sigma_{\text{exc}}^{\text{el}}$ is the electron impact excitation cross section, ω_i is the statistical weight of the *initial* state, E is the electron energy in Rydberg units, and a_0 is the Bohr length unit. The collision strength is stated as

$$\Omega_{\text{if}} = \alpha + \beta/x + \gamma/x^2 + \delta/x^3, \quad (6.6)$$

where α , β , γ , and δ are tabulated coefficients and x is the electron energy in units of the excitation energy (199 eV for B^{3+}). The coefficients are not given for B^{3+} , but the coefficients of the dominating terms (β and γ) decrease with increasing nuclear charge. We therefore find an upper limit by using the Li^+ - β and γ . This leads to the result:

$\sigma_{\text{exc}}^{\text{H}_2} \approx 2 \cdot \sigma_{\text{exc}}^{\text{el}} \leq 2.2 \cdot 10^{-21} \text{ cm}^2$. At a residual-gas pressure of $p = 5 \cdot 10^{-11} \text{ mBar}$, this corresponds to $A_e \leq 7.3 \cdot 10^{-6} \text{ s}^{-1}$, which is negligible compared to the statistical error of $|X^+|$.

To evaluate A_q , we again compare with a collision involving a free electron:



Applying the principle of detailed balance and the fact that the excitation cross section is decreasing with increasing electron energy, we immediately see that $A_q < A_e/3$, where the factor of 1/3 is the ratio of final-state statistical weights of the two processes. We therefore also ignore A_q .

For the loss rate of ions in the metastable state, we have two independent estimates. We can estimate A_1^m by assuming that the ratio of $A_1^m/A_1^g = 2.1(8)$ found for C^{4+} can also be used here, or we can use a pressure variation giving A_1^m alone since A_e and A_q can be disregarded.

Using the weighted average of these two values of A_1^m (see table 6.1) and subtracting also $A_{DR}=8(1)\cdot 10^{-4} s^{-1}$, we find for cases I and II $A_r^I=6.6483(173) s^{-1}$ and $A_r^{II}=6.6438(157) s^{-1}$. We give the result containing the full confidence interval of the two values:

$A_r=6.6469(188) s^{-1}$. As for N^{5+} , and C^{4+} we must take into account the relativistic time dilation, which lead to the result $A_{CM}^B=6.675(19) s^{-1}$.

Table 6.1

A_1^m	Case I	Case II
Assuming A_1^m/A_1^g as for C^{4+}	$0.0386(147) s^{-1}$	$0.0309(118) s^{-1}$
Applying the pressure variation	$0.0525(215) s^{-1}$	$0.0424(165) s^{-1}$

6.4 Discussion of the results

The decay rates derived from the data in the previous section are total spontaneous-decay rates, including both contributions from the M1 and 2E1 transitions discussed in sec.6.1. Since the M1 contribution is by far the dominating one we subtract the theoretical value for the small 2E1 contribution to derive an experimental rate for the M1 transition which we compare with the theoretical prediction for this. In table 6.2, our results are presented together with other low-Z experimental results as well as the theories by Drake (Drake 1971) and Johnson and Lin (Johnson 1974).

When comparing our results with those of Drake, we find satisfactory agreement. The carbon result is right on the theoretical value, whereas the results for boron and nitrogen are both about one

standard deviation off, the experimental decay rate being lower than theory for boron and higher for nitrogen. In contrast, the results of Johnson and Lin are found to be three standard deviations higher

Table 6.2 *Experimental and theoretical results for the magnetic dipole decay rate A_{M1} for He-like ions with low nuclear charge Z .*

Z	Experiment	Drake	Johnson&Lin	Units	Exp. reference
2	1.11(33)*)	1.272	1.253	10^{-4} s^{-1}	Woodworth 1975
3	1.71(38)*)	2.039	2.037	10^{-2} s^{-1}	Knight 1980
5	6.674(19)	6.695	6.731	s^{-1}	This work
6	48.56(11)	48.56	48.87	s^{-1}	This work
7	256.0(3.1)	253.2	255.1	s^{-1}	This work
10	1.105(18)	1.087	1.098	10^4 s^{-1}	Wargelin 1993

*): *Error 2 standard deviations*

than our results for both carbon and boron, indicating that for the range of nuclear charges considered here, Drake's values are the most reliable. This is not very surprising when the applied theoretical approaches are considered. Drake used highly correlated, nonrelativistic radial-wave functions and left out higher-order relativistic effects of the relative order of $(Z\alpha)^2$ in the transition-matrix elements (here α denotes the fine-structure constant) (Drake 1971). In contrast, Johnson and Lin performed a fully relativistic Dirac-Hartree-Fock (DHF) calculation but took into account effects of electron correlation only to relative order Z^{-1} (Johnson 1974). Since electron correlation is most important for low Z , whereas relativistic effects increase with Z , it is therefore expected that for low Z , Drake's results will be the most

accurate, whereas for high Z , Johnson and Lin will get the most accurate results. Johnson and Lin estimated the limiting Z value Z_{lim} for which their theoretical prediction became more accurate than that of Drake by assuming that the coefficients of the terms of order Z^{-2} omitted in their DHF calculation were equal to the coefficients of the terms of order $(Z\alpha)^2$ omitted in Drake calculation! The limiting Z value was then found by setting $Z_{\text{lim}}^{-2} = (Z_{\text{lim}}\alpha)^2 \Leftrightarrow Z_{\text{lim}} = \alpha^{-1/2} \approx 12$ (Johnson 1974). The plausibility of this prediction lies somewhere between a very crude estimate and a pure guess, but at least the present experiments have shown that $Z_{\text{lim}} > 6$.

A formal recipe of the theoretical decay rate is:

$$A_{M1} = (4\omega^3/\hbar c^3) |T_{M1}|^2, \quad (6.7)$$

where $|T_{M1}|^2 = |\langle 1s^2 \ ^1S | \vec{\mu} | 1s2s^3S \rangle|^2$ is the squared transition-matrix element, and $\vec{\mu}$ is the magnetic dipole-moment operator (Drake 1971). Since accurate theoretical values of the transition energies in He-like systems are available (Drake 1988) and have been confirmed experimentally to very high accuracy (Martin 1981), ω is known, and our measurement of the M1 decay rate A_{M1} can be regarded as a sensitive test of theoretical predictions for the M1 transition-matrix element $|T_{M1}|^2$ and, more specifically, the two-electron correction contained in it. When the electron-electron interaction is neglected, a prediction for the matrix element $|T_{M1}^0|^2$, valid to leading order in $Z\alpha$, is given by (Drake 1971):

$$|T_{M1}^0|^2 = (2/3) |\langle 1s | \vec{\mu} | 2s \rangle|^2 = (4/3) [(8/81)(Z\alpha)^2 \mu_B]^2, \quad (6.8)$$

where $\langle 1s | \vec{\mu} | 2s \rangle|^2$ is the hydrogenic M1 matrix element, μ_B is the Bohr magneton, and the factor of 2/3 accounts for the suppression of the nonspin-flip transitions between the magnetic substates of the active electron, as required by the Pauli principle. By inserting $|T_{M1}^0|^2$ in eq.6.7, we find an expression for the decay rate with electron-correlation-free transition-matrix elements:

$$A_{M1}^0 = (4\omega^3/3\hbar c^3) [(16/81)(Z\alpha)^2 \mu_B]^2. \quad (6.9)$$

As a measure of the electron correlation effects contained in the

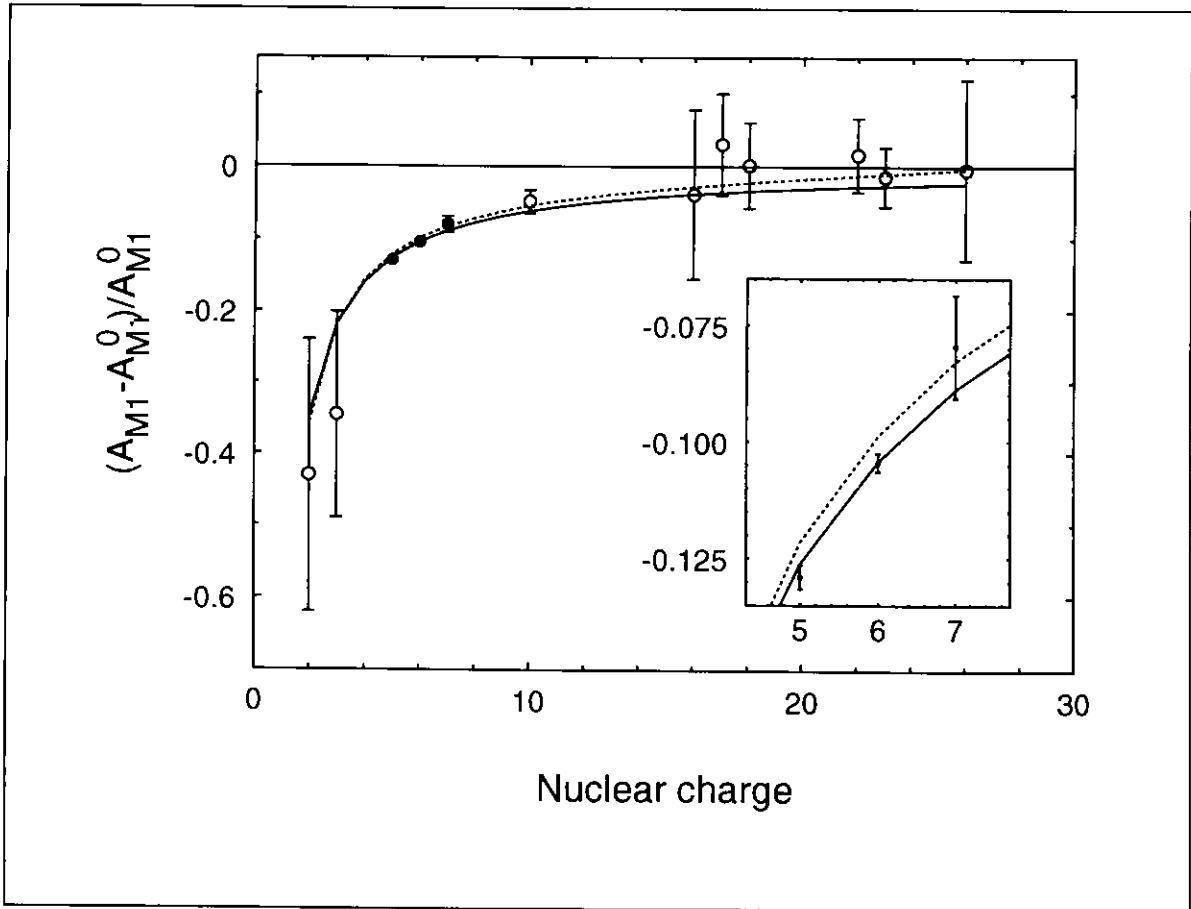


Figure 6.3 *Relative deviation of the decay rate from the single-electron approximation (see text) as a function of Z. Circles: Other experiments. Dots: Our results. Full curve: Drake. Dashed curve: Johnson and Lin.*

transition-matrix elements, we introduce $(A_{M1} - A_{M1}^0)/A_{M1}^0$. Values of this correction for various experimental values of A_{M1} at low and intermediate Z are shown in fig.6.3, together with the theoretical values of Drake and of Johnson and Lin.

In summary, we have presented a new experimental method by which the radiative decay rate of the metastable $1s2s^3S$ state can be measured with high precision for low- Z He-like ions, where it assumes very small values and is strongly influenced by the Coulomb interaction between the two atomic electrons. The results suggest that for $Z \leq 6$, calculations based on accurate nonrelativistic two-electron wave functions are reliable to within ≈ 0.2 percent, whereas the available fully relativistic calculations do not reach this precision in this Z range. We estimate that the technique described can be used for high-precision measurements of decay rates of 10^0 - 10^3 s^{-1} ($5 \leq Z \leq 8$ for the 2^3S state of He-like ions). Dielectronic resonances suitable for similar measurements exist also in systems with more than two electrons, although the count rate in general will be at least one order of magnitude smaller, so that very accurate measurements will become more difficult. Nevertheless, considering the strong limitations of previous decay-rate measurements on long lived atomic levels and the larger uncertainties of theoretical calculations for these systems, this technique appears to be useful also for a number of metastable states in more complex atomic ions.

I L Beigman and U I Safranova (1971) Sov.Phys.JETP 33, 1102

G Breit and E Teller (1940) Astrophys.J. 91, 215

G W F Drake, G A Victor, and A Dalgarno (1969) Phys.Rev 180, 25

G W F Drake (1971) Phys.Rev.A 3, 908

G W F Drake (1988) Can.J.Phys. 66, 586

G Feinberg and J Sucher (1971) Phys.Rev.Lett 26, 681

A H Gabriel and C Jordan (1969) Nature (London) 221, 947

A H Gabriel and C Jordan (1970) Phys.Lett. 32A, 166

G Hubricht and E Träbert (1987) Z.Phys.D 7, 243

W R Johnson and C Lin (1974) Phys.Rev.A 9, 1486

T Kato and S Nakazaki (1989) At. Data and Nucl. Data Tables 42, 313

R D Knight and M H Prior (1980) 21, 179

R Marrus and P J Mohr (1978) Adv.At.Mol.Phys 14, 181

R Marrus et al. (1989) Phys.Rev.A 39, 3725

W C Martin (1981) Phys.Scr. 24, 725

B J Wargelin, P Beiersdorfer, and S M Kahn (1993) Phys.Rev.Lett. 71, 2196

J R Woodworth and H W Moos (1975) Phys.Rev.A 12, 2455

7. Dissociative Recombination

In this chapter, we return to the main subject of the present thesis, namely the recombination of electrons with positive ions. In doing so, we leave the atomic ions and enter the field of molecules to describe the first ASTRID recombination experiments — dissociative recombination (DisR) measurements for molecular hydrogen ions.

In sec.7.1, a brief review of DisR experiments is given. Without going into details sec.7.2 presents, some of the fundamental concepts of diatomic molecules necessary in understanding the DisR mechanisms. In sec.7.3, the DisR process is introduced, and a simplified model for the so-called direct mechanism, which dominates our spectra, is presented. Our experiment on H_2^+ is described in sec.7.4, and in sec.7.5, our results are presented and discussed in the light of other experimental works.

7.1 Earlier DisR experiments

In going from atomic to molecular ions, new degrees of freedom are introduced, leading to a rich and complicated structure of the recombination spectra. In particular, one complication concerning the initial states populated in the experiments should be mentioned here. Where we found that for atomic ions, we had all the population in the ground state and in some cases in one or two metastable states, the situation for molecules is much more complicated since now *vibrational* and possibly *rotational* sub-levels must be considered. It is therefore of great importance in DisR experiments to find ways to

determine and/or control the distribution of population in the various sub-levels.

On the other hand, due to the very high rates for the DisR process, together with the relative simplicity in producing molecular ions in comparison to highly charged atomic ions, measurements of molecular recombination predate atomic recombination experiments by more than three decades.

The first DisR measurements (Biondi 1949) were made by measuring with a microwave technique the density of electrons in a gas as a function of time after a discharge in the gas was made. Having recombination as the dominant mechanism for the loss of free electrons, a recombination rate coefficient could be derived from the time dependence of the electron density. At the time of this experiment, it was not yet realized that molecular recombination rate coefficients could be significant, and the very large rate coefficients observed were ascribed to atomic recombination processes in the afterglow plasma. But the following year, Bates proposed what is now known as the *direct* mechanism for DisR and showed that this process had much larger rate coefficients than atomic recombination, and was the true origin of the observed rate coefficients (Bates 1950). A modernized version of the afterglow technique is still in use in DisR studies (Adams 1984). An advantage of this technique is the fact that due to the high density in the experiment, ions in higher vibrational levels are likely to be quenched to lower levels. The rate coefficient obtained from this type of experiments is a convolution of the reaction cross section with a spherical Maxwellian velocity distribution characterized only by the temperature of the plasma. This is exactly what is needed in the diagnostics of astrophysical and laboratory

plasmas, but when the interest is focussed not on the applications but rather on the recombination process itself, more detailed information of the reaction cross section as a function of the relative energy is needed. Another limitation of the afterglow technique is the fact that the simplest of all molecular ions H_2^+ evades this type of investigation since H_2^+ ions formed in a dense hydrogen gas will react with H_2 molecules and form H_3^+ and neutral hydrogen atoms.

To circumvent these two limitations, interacting particle beams are required. Peart and Dolder (Peart 1974) used inclined beams, and Auerbach et al. (Auerbach 1977) used a single-pass, high-resolution, merged-beams technique, which allowed them to measure at very low relative energies. Lately, a number of DisR measurements of molecular ions stored in heavy-ion storage rings have been published, some of which concerned H_2^+ and the isotopes HD^+ and D_2^+ (Forck 1993, Zajfman 1993, Larsson 1994). We shall return to the results of these measurements in the discussion of our own results in sec.7.5.

7.2 Some basic concepts of diatomic molecules

The purpose of the present section is to introduce a few basic concepts of diatomic molecules of importance for the understanding of DisR. This presentation relies to a large extent on the presentation of Bransden and Joachain (Bransden 1983), where many of the details not considered here may be found.

Let us consider the simplest of all molecules, H_2^+ . The coordinates with respect to the center of mass of the constituents of the molecule are denoted \mathbf{r} for the electron and \mathbf{R}_A and \mathbf{R}_B for the two

nuclei of mass M_A and M_B , respectively (we are explicitly not excluding the replacement of one of the protons by a deuteron). The non-relativistic, time-independent Schrödinger equation for this system is:

$$(T_N + T_e + V(\mathbf{R}, \mathbf{r}))\psi(\mathbf{R}, \mathbf{r}) = E\psi(\mathbf{R}, \mathbf{r}), \quad (7.1)$$

where $\mathbf{R} = \mathbf{R}_B - \mathbf{R}_A$, $T_N = -\hbar^2/(2\mu)\nabla_{\mathbf{R}}^2$ is the nuclear kinetic energy operator, $T_e = -\hbar^2/(2m)\nabla_{\mathbf{r}}^2$ is the electronic kinetic energy operator, and V is the potential-energy operator $V(\mathbf{R}, \mathbf{r}) = -e^2/|\mathbf{r} - \mathbf{R}_A| - e^2/|\mathbf{r} - \mathbf{R}_B| + e^2/R$. Here μ is the reduced mass of the nuclei, and R is the internuclear distance (i.e. the length of the vector \mathbf{R}).

Equation 7.1 can be solved by considering first the situation where the coordinate \mathbf{R} is kept fixed. The solutions in terms of eigenfunctions $\Phi_q(\mathbf{R}, \mathbf{r})$ and eigenenergies $E_q(\mathbf{R})$ to this *electronic* wave equation will then depend on the fixed value of \mathbf{R} . In the Born-Oppenheimer approximation, the problem of *nuclear* motion is solved independently for each electronic state, with $E_q(\mathbf{R})$ as found from the electronic-wave equation acting as the potential in which the nuclear motion takes place. When $E_q(\mathbf{R})$ has a minimum, this potential can accommodate a number of bound states characterized by the vibrational and rotational quantum numbers v and J . For other solutions to the electronic wave equation, $E_q(\mathbf{R})$ forms a purely repulsive potential, in which case the electronic state is a dissociating state.

It is worth noting that with the separation of electronic and nuclear motion sketched above, the nuclear masses do not enter the electronic-wave equation. This means that the electronic structure will be identical for H_2^+ , HD^+ , and D_2^+ . However, the nuclear motion is

strongly affected. The splitting of vibrational levels becomes smaller for heavier nuclei, and for HD^+ , a permanent electric-dipole moment is introduced. As a consequence of this the lifetime of the longest-lived vibrationally excited state of the electronic ground state, is only about 60 ms (Amitay 1994), whereas in the case of H_2^+ , it is longer than one week! (Mitchell 1990).

As for atoms, the electronic levels are classified according to the symmetry properties of the electronic wave function. Due to the breaking of the spherical symmetry, we cannot find common eigenfunctions of the Hamiltonian H , L^2 , and L_z , where L is the electronic orbital angular-momentum operator. It is, however, possible to find common eigenfunctions of H and L_z if the quantization axis is chosen along the internuclear axis. This is due to the invariance of the electronic Hamiltonian with respect to rotations about this axis. The numerical value of the eigenvalue of L_z in units of \hbar is denoted by Λ , and states with $\Lambda=0$ are called Σ states, states with $\Lambda=1$ are called Π states, etc., in analogy with S,P,D,F,.. states of atomic-energy levels.

Another symmetry operation, under which the electronic Hamiltonian is invariant, is a reflection of the electronic coordinates in a plane containing the internuclear axis (e.g. the xz plane). The operator A_y that performs this operation does not commute with L_z for $\Lambda \neq 0$, but reverses the sign of M_L , the eigenvalue for L_z . For Σ states, however, common eigenfunctions of H , L_z , and A_y can be formed. One therefore distinguishes among Σ states according to the eigenvalue of A_y . States for which the wave function does not change sign are called Σ^+ states, and states for which the wave function does change sign are called Σ^- states.

For homonuclear molecules, one defines a parity operation reflecting the electronic coordinates in the midpoint between the two nuclei. This parity operator also commutes with both H and L_z . States for which the wave function is unchanged after this operation has been performed are called *gerade* states and are marked by a subscript g. In the case, where the wave function changes sign upon this operation, the state is called an *ungerade* state and is marked by a subscript u.

In analogy with the labelling of atomic single-electron orbitals, the molecular single-electron orbitals are labelled according to their value of λ ($\lambda=0:\sigma$, $\lambda=1:\pi$, etc.), which is the one-electron analogue of Λ . When molecules with more than one electron are considered, an approach known as the Hund-Mulliken method, which is similar to the Hartree-Fock method of atomic physics, is used to form multi-electron wave functions from the single-electron wave functions. The terms of these multielectron configurations are then found by coupling the λ 's of the single electrons to form the total Λ , and by coupling the spins of the single electrons to form the total spin S .

In the LCAO approximation (linear combination of atomic orbitals), the single electron molecular orbitals are formed as linear combinations of atomic wave functions. In the two limits *united* atom ($R \rightarrow 0$) and *separated* atoms ($R \rightarrow \infty$), the molecular wave function converges to a single atomic wave function. We consider as an example the ground state of H_2^+ which is a Σ_g state. In the united-atom limit, this corresponds to $He^+(1s)$, and in the separated-atom limit, it corresponds to a proton plus $H(1s)$. The lowest Σ_u excited state converges to the same limit for $R \rightarrow \infty$, but for $R \rightarrow 0$ it converges to the lowest odd-parity level $He^+(2p)$ since it is an ungerade level.

The molecular states are often labelled by their united-atom

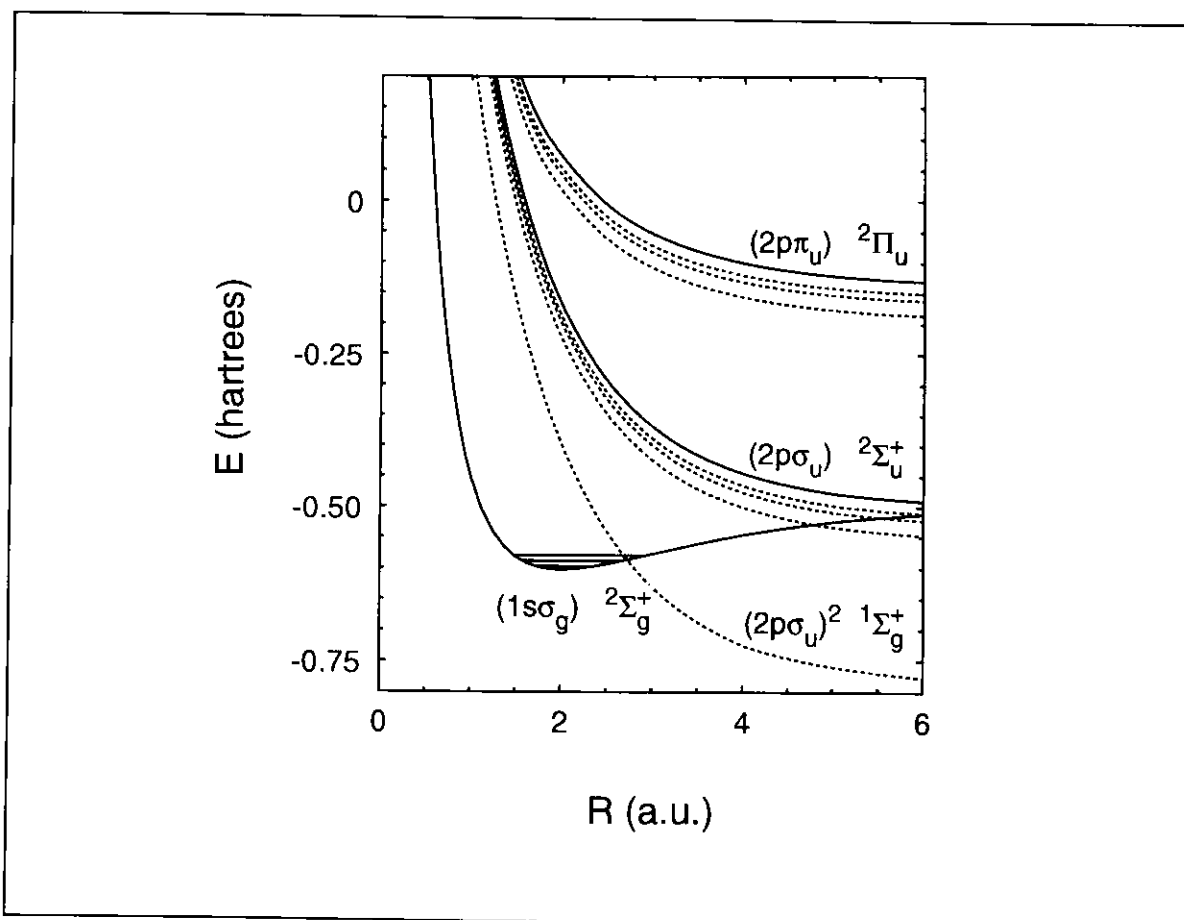


Figure 7.1 Potential curves for H_2^+ (full curves) and H_2 (dashed curves).

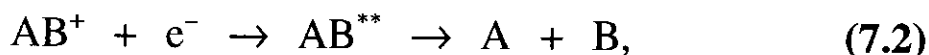
limits. The ground and first excited electronic states of H_2^+ are therefore referred to as $1s\sigma_g \ 2\Sigma_g^+$ and $2p\sigma_u \ 2\Sigma_u^+$, respectively. In the case of H_2^+ , where we have only one electron, the 'coupling' to find Λ and S is trivial, and we always find $\Lambda=\lambda$ and $S=1/2$. For this reason, we will skip the last part of the designation and in the following refer to states of H_2^+ as $1s\sigma_g$, $2p\sigma_u$, etc.

Some of the concepts described in this section are illustrated in fig.7.1, which shows the electronic ground state and the lowest two ungerade excited states, together with some doubly excited dissociating states of neutral H_2 .

7.3 The DisR processes

The electron-electron interaction can cause doubly excited electronic states of neutral molecules to autoionize. Therefore also the inverse process of forming doubly excited states through dielectronic capture of a free electron to a molecular ion is possible. If the doubly excited state formed is a repulsive state, the molecule dissociates into two neutral parts. Since this dissociation is usually very rapid, there is only a very low probability for autoionization to take place before the neutrals have moved sufficiently far apart that the electronic energy has dropped below the limit for autoionization.

The scenario described above is normally referred to as *direct* dissociative recombination and is formally described as:



where AB^{**} denotes the doubly excited intermediate state of the neutral molecule.

This process is quite similar to the dielectronic-recombination process for atomic ions described in ch.5, but two important differences should be emphasized. Firstly, the dielectronic-capture process is not a resonant process for molecular ions since for a range of electron energies, a vertical transition from a vibrational level of the ion state to the doubly excited state can take place (see fig.7.1). Secondly, stabilization against autoionization is usually much more efficient than for atoms where one has to rely on a radiative transition. This is why the measured rate coefficients for DisR are typically higher than for DR.

If we disregard the possibility for the doubly excited state to re-autoionize prior to the dissociation, the DisR cross section is found to be proportional to the autoionization probability A_a divided by the electron energy E_{rel} (Mitchell 1990). To calculate the autoionization probability, matrix elements of the electron-electron potential-energy operator must be evaluated between the intermediate state and the initial state, consisting of a molecular ion in some vibrational state and a free electron. To the extent that the Born-Oppenheimer approximation holds, and the total wave functions can be expressed as products of nuclear and electronic wave functions, the nuclear part will reduce to being just an overlap integral since the operator does not depend on the nuclear coordinates. If we now assume that only this nuclear overlap integral depends strongly on energy in the energy range of interest, we get the simple model prediction

$$\sigma \propto |\langle \chi(\mathbf{R}) | \chi^+(\mathbf{R}) \rangle|^2 / E_{\text{rel}}, \quad (7.3)$$

where χ and χ^+ are the nuclear wave functions of the neutral and ion state, respectively. The squared overlap integral of eq.(7.3) is called a Franck-Condon factor.

To get a simple estimate of the energy dependence of the DisR signal, we calculated the Franck-Condon factors between the initial H_2^+ vibrational levels and the doubly excited intermediate states of neutral H_2 : $(2p\sigma_u)^2 1\Sigma_g^+$ and $2p\sigma_u(2\Sigma_u^+)3l\lambda$ (see fig.7.1). The latter of the two was chosen to represent the DisR contributions from all Rydberg levels converging to the $2p\sigma_u 2\Sigma_u^+$ level of H_2^+ . The calculation of the Franck-Condon factors was performed using the computer code BCONT (Le Roy 1989). This program takes as input the potential curves involved

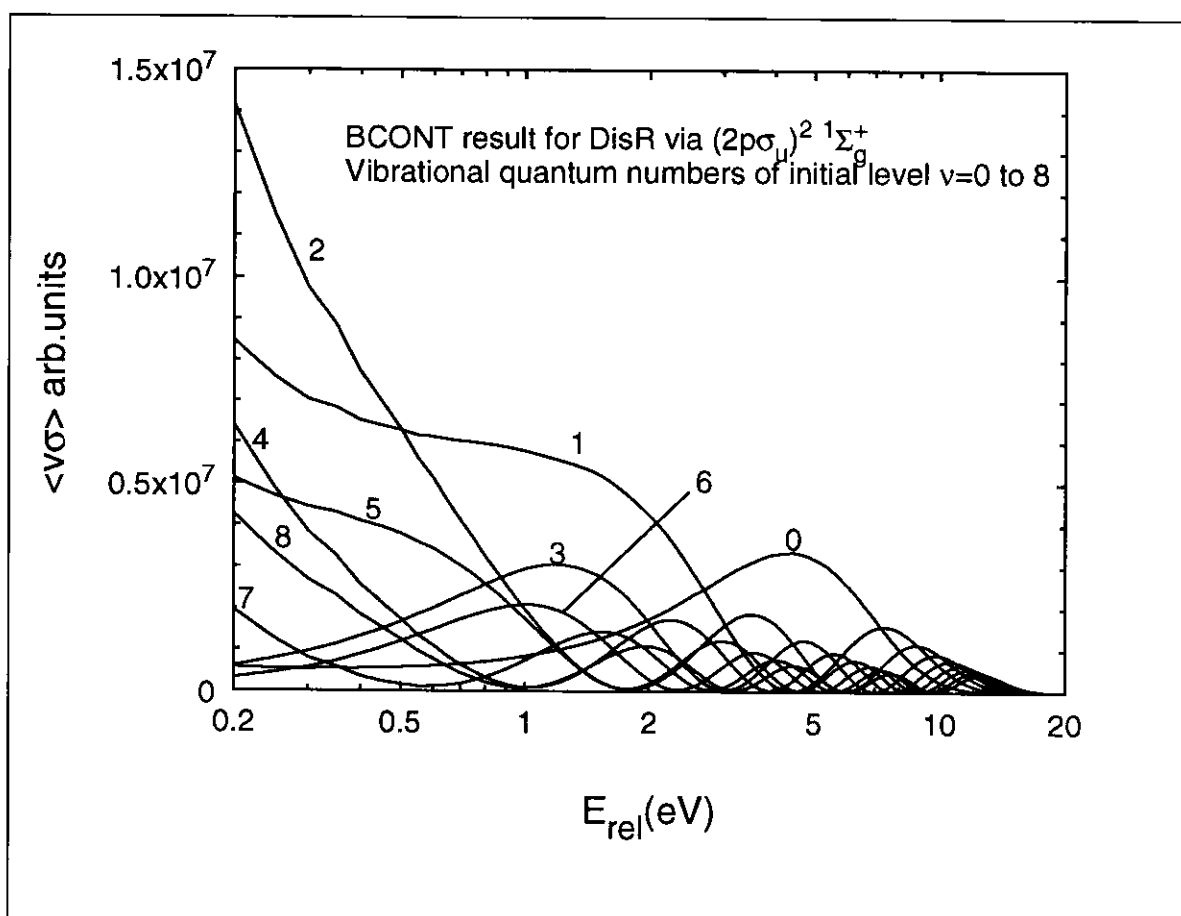


Figure 7.2 Relative rate coefficients for DisR via the $(2p\sigma_w)^2 \ ^1\Sigma_g^+$ intermediate state as a function of the relative energy for different initial vibrational levels.

and the reduced mass. The radial nuclear wave equation is then solved for both the ion and neutral states. After this, the Franck-Condon factors can be calculated as a function of energy for all vibrational initial levels. We used the potential curves calculated by Guberman as input for BCONT (Guberman 1983).

The results of this calculation in terms of the experimental rate coefficient found by convoluting the calculated cross sections with the expected electron-beam velocity distribution are shown in fig.7.2 and fig.7.3 for the two different, doubly excited neutral intermediate states.

The first and most important point to note when considering these results is the fact that the initial distribution on vibrational levels

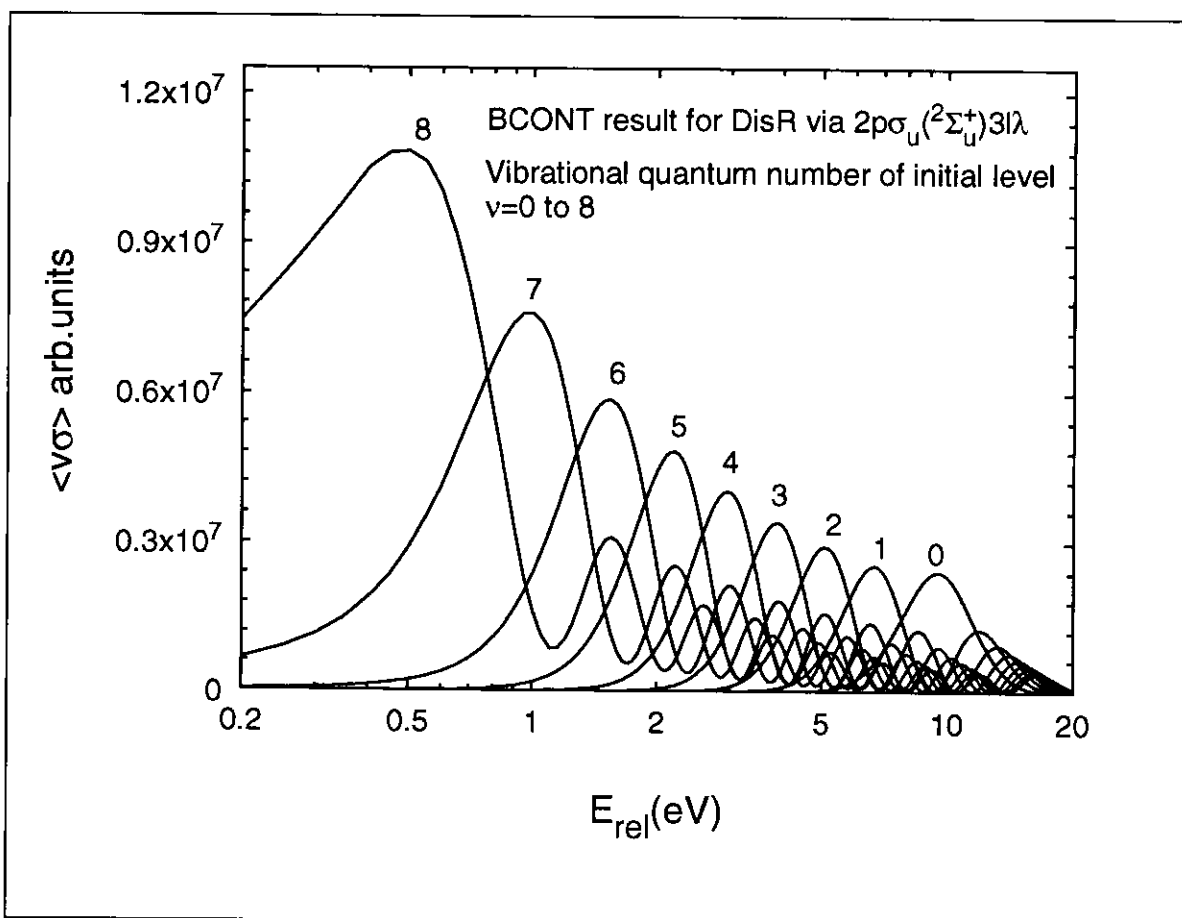


Figure 7.3 Relative rate coefficients for DisR via the $2p\sigma_u(^2\Sigma_u^+)3I\lambda$ intermediate state as a function of the relative energy for different initial vibrational levels.

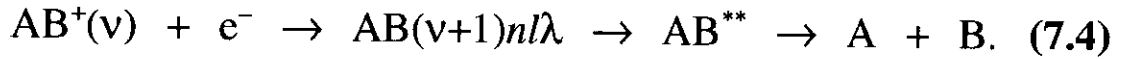
is indeed very important for the DisR spectra, and this point deserves much attention if one wants to perform experimental studies of this process. Concerning the reliability of these simple model predictions, it should be mentioned that for the energy ranges and vibrational levels, where detailed calculations are available, there appears to be qualitative agreement (Nakashima 1986, Derkits 1979). It should be emphasized that within the approximations made, one can compare the relative sizes of the contributions from different vibrational levels via the same intermediate state, but no information is given concerning the relative contributions of the two different intermediate states (in other words, the y axes of fig.7.2 and fig.7.3 are completely uncorrelated).

A specific word of caution should be added concerning the contribution from $v=0$ via the $(2p\sigma_u)^2\ ^1\Sigma_g^+$ state (fig.7.2). When carefully examining fig.7.1, it can be seen that the crossing of the resonance potential curve with that of the H_2^+ ground state lies beyond the classical turning point of the $v=0$ level. This means that for low energy, this contribution relies on quantum mechanical tunneling and therefore becomes extremely sensitive to the exact crossing point and thereby also to the exact shape of the potential curve of the doubly excited resonance state, which has an expected accuracy of a few tenths of an eV (Guberman 1982). One should therefore not rely on the value found here for the contribution from this level for $E_{rel} < 1$ eV.

The direct DisR is not the full story of the DisR process. Some complications caused by Rydberg levels converging to vibrationally excited states of the ionic electronic ground state should also be considered.

For sufficiently high principal quantum number, a Rydberg state with a vibrationally excited ion core can autoionize into a free electron and an ion with a lower vibrational quantum number. There is a propensity rule ($\Delta v = -1$) for this process. Larger steps in v are not excluded, but the autoionization probability drops typically two orders of magnitude when going to $\Delta v = -2$ (Lefebvre-Brion 1986). The time-reversed process will be a resonant capture to a Rydberg state, with an excited core of a low-energy electron. If the potential curve of this Rydberg state is crossed by a repulsive curve of the same symmetry, there will be a coupling to this repulsive state and therefore a finite probability for dissociation via this curve. This type of dissociation via coupling to a repulsive state is called pre-dissociation, and the entire

process of capture by vibrational excitation followed by pre-dissociation is called *indirect* dissociative recombination. The formal description is



Since both the initial and final states of this process are identical to those of the direct process (eq.7.2), interference effects between these two processes have been predicted theoretically (Nakashima 1986) and observed experimentally (Van der Donk 1991).

The indirect process causes narrow structures superimposed on the signal from the direct process. These structures were too narrow for us to resolve in our H_2^+ experiment and are therefore not considered in this presentation, but with the improved resolution obtainable with the adiabatic expansion technique described in sec.3.2, this type of structure should become observable.

7.4 The ASTRID H_2^+ experiment

The H_2^+ ions were formed in a low-pressure plasma ion source of the Nielsen type (Nielsen 1957). If we neglect the influence of other collision processes in the ion source and assume that all the H_2^+ ions are formed in electron-impact ionization of H_2 molecules in the vibrational ground state, the relative population of the vibrational states of H_2^+ will be determined by the Franck-Condon overlap factors between the vibrational ground state of H_2 and the different vibrational levels of H_2^+ . The relative populations have been calculated (Dunn

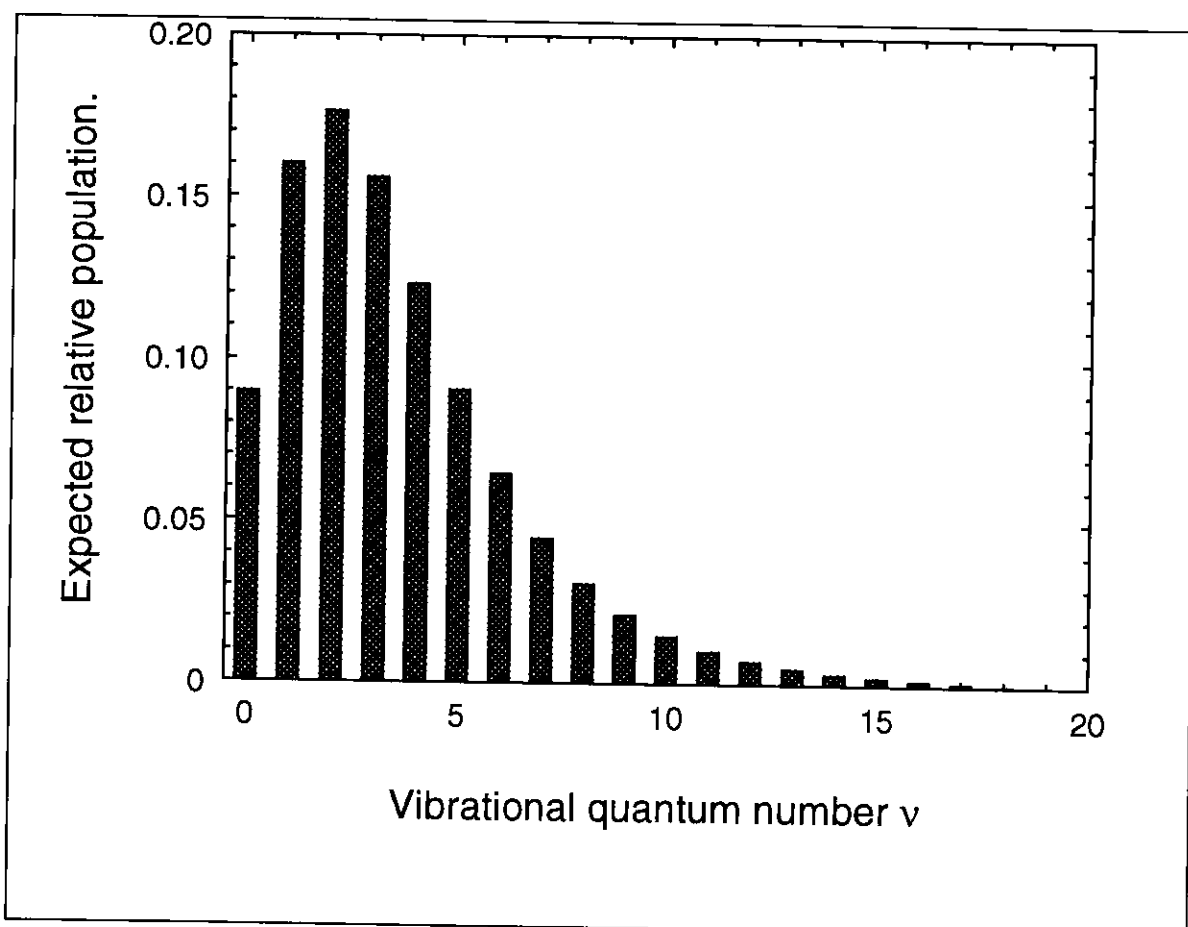


Figure 7.4 *Expected relative population of vibrational levels of H_2^+ as a function of the vibrational quantum number v , assuming the ideal ion-source conditions described in the text.*

1966) and are presented in fig.7.4.

From the point of view of the interpretation of the experimental results, it is desirable to reduce the number of vibrational levels populated during the DisR measurement. As the H_2^+ molecule does not have a permanent electric dipole moment, the spontaneous decay to lower vibrational levels of the ions stored in the ring is too slow to influence the vibrational distribution during the measurement. A certain amount of selective survival of the ions in low vibrational levels will be expected since the cross section of the dominant process of destruction of stored particles, the excitation in residual-gas collisions to the repulsive $2p\sigma_u$ state, is expected to increase with v . This is

related to the fact that for higher v , less energy must be transferred to the molecular ion in the collision.

In order to achieve a more efficient and well controlled selection of the H_2^+ ions present during the measurement, we applied a 50 mW continuous-wave 280 nm laser beam to photo-dissociate ions in higher vibrational levels. The laser system was designed for studies of laser cooling of Mg^+ ions in ASTRID. The dye laser, which is pumped by an argon-ion laser, produced a beam at a wave length of 560 nm with a power of ~ 600 mW. This beam was then injected into an external-

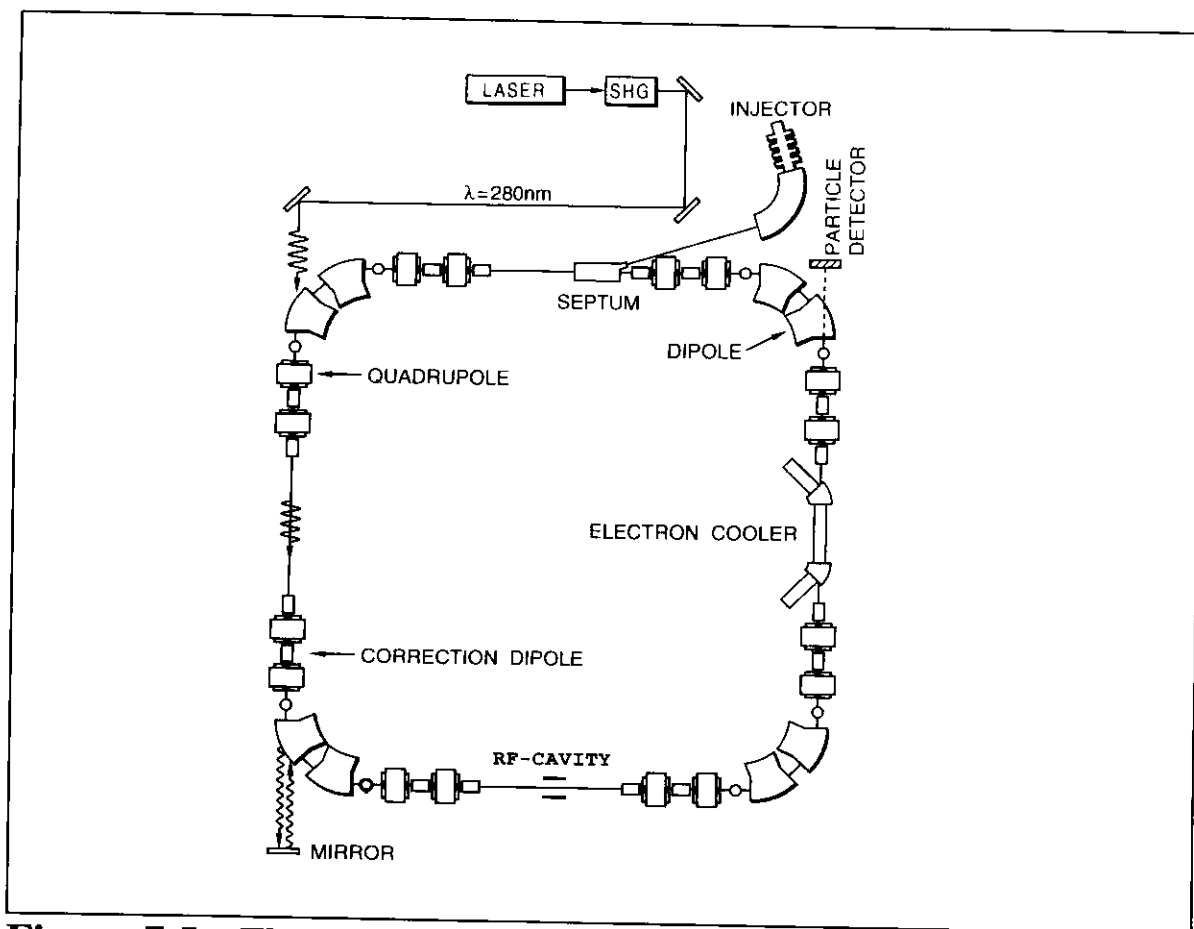


Figure 7.5 *The experimental setup for the measurement of DisR with ions in low vibrational levels, as obtained by photo-dissociating H_2^+ ions in high vibrational levels.*

ring resonator where the 280 nm light was produced by second-harmonic generation in a KDP crystal (Nielsen 1994). The laser beam with a diameter of 5 mm was injected into the straight section of the storage ring opposite to the electron cooler co-propagating with the ion beam. At the end of this straight section, the laser light was reflected back through the ring to obtain also a counter-propagating beam. A sketch of the experimental set-up is shown in fig.7.5.

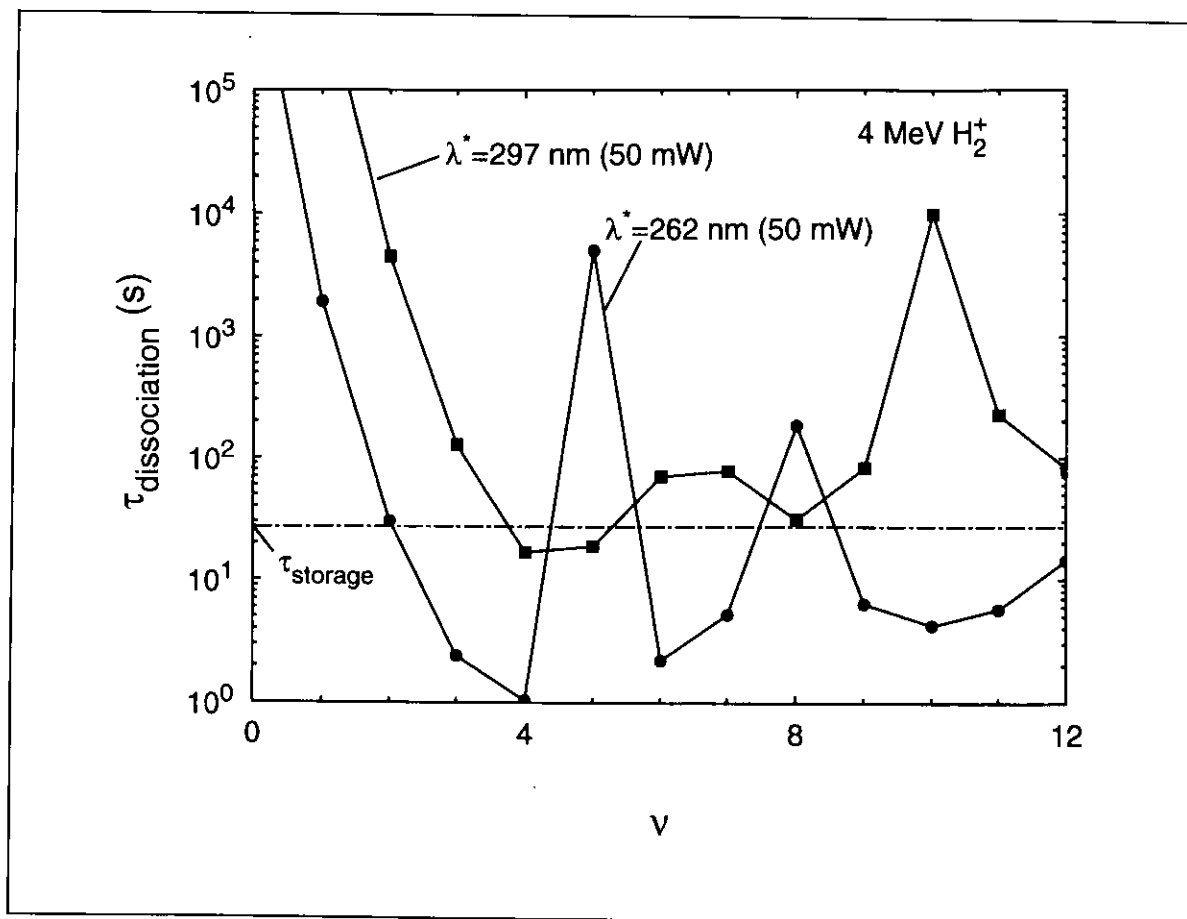


Figure 7.6 Dissociation times for the vibrational states ($v \leq 12$) of H_2^+ . For comparison, the average storage lifetime is also shown.

The photon energy of 4.45 eV exceeds the dissociation energy of 2.79 eV for H_2^+ , but the photo-dissociation cross section only becomes non-negligible when excitation to the $2p\sigma_u$ state becomes possible. Using tabulated theoretical photo-dissociation cross sections

for the different vibrational levels as a function of wave length (Dunn 1968a, 1968b), we calculated the lifetimes with respect to photodissociation at the Doppler-shifted wave lengths corresponding to the co- and counter-propagating beams (taking into account that the stored ions spent only a fraction of the time in the straight section where the laser was applied). The results obtained assuming perfect overlap are shown in fig.7.6.

With the assumptions made above, we see that after about one minute, we can reach a situation where the ions are found almost exclusively in the lowest two vibrational levels. Very long dissociation times are seen for particular cases (for example for the effect of the blue-shifted laser on the $v=5$ level). This is due to the nuclear wave function of the particular level having a node at the internuclear distance where the energy needed for a transition to the repulsive state is equal to the photon energy.

After injection into the storage ring at a kinetic energy of 150 keV, the ion beam was accelerated for 5 s to reach a kinetic energy of 4 MeV appropriate for the measurement (see sec.3.2). After acceleration, the ion current was 1-2 μA , as estimated from the magnitude of the total signal observed on one set of electrostatic pick-up plates. At this energy, the storage lifetime of the beam was 26 s at an approximate average storage-ring pressure of $3 \cdot 10^{-11}$ mBar (primarily H_2). 10 s after the injection, the electron cooler was switched on at the acceleration voltage corresponding to zero relative energy, which was previously determined by observing the revolution frequency of the stored ions, as given by the Schottky spectrum. Electron cooling was then performed for 10 s until the actual measurement was started. The electron current was typically about 3 mA.

The neutral particles formed in the electron-cooler straight section of the storage ring were detected at a 4 cm diameter surface-barrier detector. The output signal from this detector is proportional to the energy dissipated in it. We could therefore distinguish DisR events where two neutral hydrogen atoms, each possessing 2 MeV kinetic energy, gave rise to a 4 MeV signal from the dominating gas-collision process of dissociation without capture, which led to formation of only one neutral hydrogen atom and therefore only a 2 MeV signal. No 4 MeV signal was seen when the electron cooler was switched off, indicating that the possible background contribution from electron capture in residual-gas collisions was negligible.

The actual measurement was performed by modulating the electron acceleration voltage between the cooling voltage and the voltage corresponding to the desired energy at a frequency of 25 Hz. The DisR counts detected during a 20 ms measurement period and those detected during a cooling period were separately recorded as a function of time after start of the measurement in time bins of 2.4 s. The rate coefficient could then be determined relative to the rate coefficient at cooling energy.

The rate coefficient at cooling energy was determined from a separate measurement where the electron energy was kept fixed at cooling energy. The estimated ion current as evaluated from the pick-up signal was noted for each injection, and the storage lifetimes corresponding to the four different conditions: cooler ON/OFF, laser ON/OFF, were measured. With this information, the ion current at the time of measuring could be deduced. Since also the electron density was known, the rate coefficients at cooling energy could be determined. The results were $\langle v\sigma \rangle_{\text{laser}} = 5.6 \cdot 10^{-9} \text{ cm}^3/\text{s}$ and $\langle v\sigma \rangle_{\text{no laser}} = 8 \cdot 10^{-9}$

cm³/s. The uncertainty on the *ratio* of these two values were estimated to be approximately 25%, whereas the absolute value could be off by a factor of 2. Within the large errors of the estimates, no conclusive evidence of a time dependence on these values could be found.

During a recent experiment on electron-impact detachment of negative atomic hydrogen ions, we discovered that due to an incorrect ion-orbit correction of the influence of the electron cooler toroid field, neutral particles formed in the electron cooler can have a slightly different angle with respect to the vacuum chamber than neutrals formed elsewhere in this straight section. For this reason we cannot exclude the possibility that a certain fraction of the neutrals formed were not detected. In the following figures, we use the values that we found for the rate coefficient in units of cm³/s, but label the y-axis 'arb. units'.

7.5 Results and discussion

The DisR rate coefficient deduced from data taken in two different time windows (34.4s-36.8s after injection and 56s-65.6s after injection) measured *without applying the laser* is shown in fig.7.7 as a function of the relative energy. Typical statistical errors are shown for one point on each of the two curves.

Regarding fig.7.7, we first note that the data from the two time windows appear to be quite similar. We interpret the observed spectrum as follows:

The low-energy part (0 eV - 2 eV) is dominated by capture into the $(2p\sigma_u)^2\ ^1\Sigma_g^+$ repulsive state (fig7.2). As all vibrational levels can

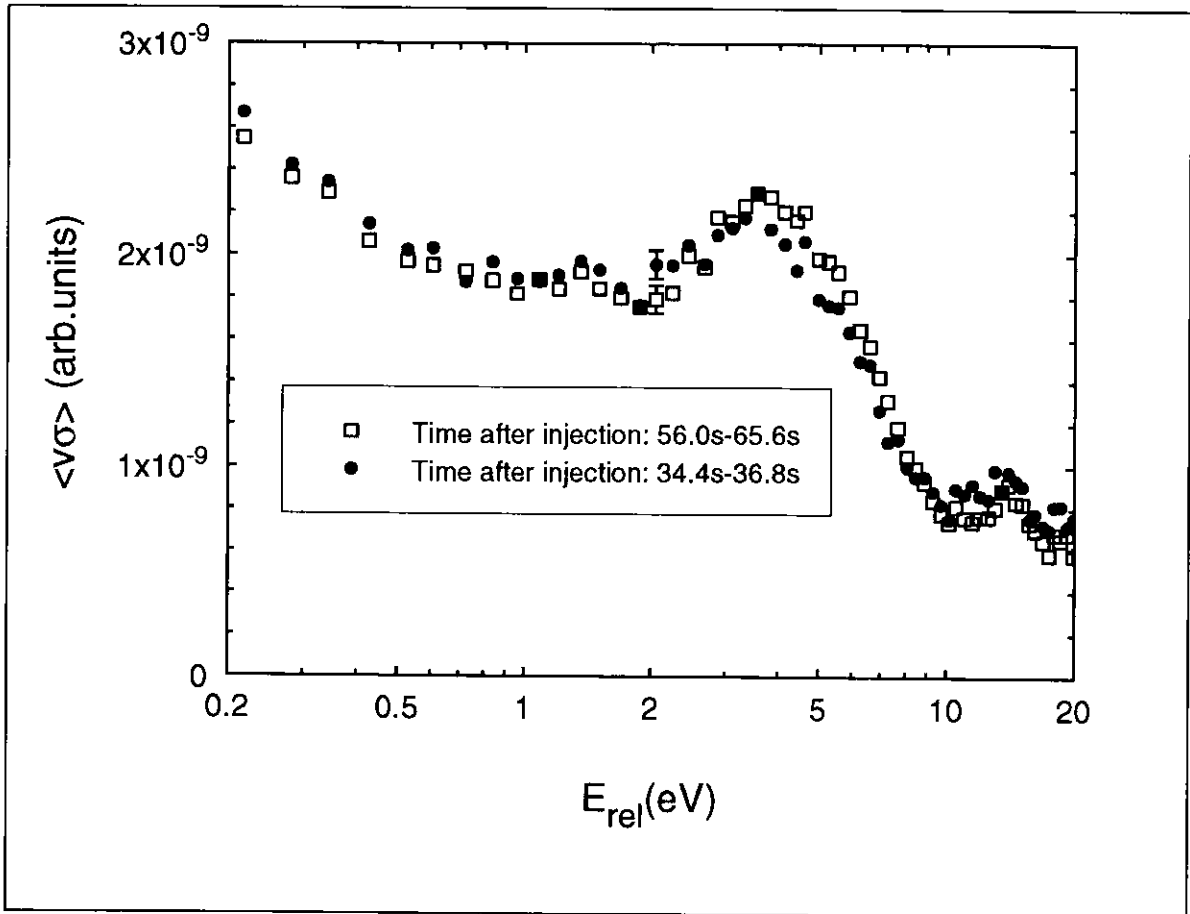


Figure 7.7 *The measured DisR rate coefficient when no laser photodissociation was applied. Shown are data taken in two different time windows after injection 34.4s-36.8s and 56.0s-65.6s.*

contribute to the signal in this energy range, we make no conclusions regarding the vibrational distribution from this.

The dominant feature in the spectrum is the broad structure ranging from about 2 eV to 10 eV, with a maximum around 4 eV. This structure we ascribe to be mainly due to capture processes into Rydberg levels converging to the $2p\sigma_u$ state of H_2^+ . According to the model prediction for this (fig.7.3), the energetic positions of the main contributions from each vibrational level depend monotonically on the vibrational quantum number. We can therefore get a rough estimate of the vibrational distribution by comparing our data with the model prediction in this region of energy. On the basis of such a comparison,

we estimate that the majority of the ions are found in levels with vibrational quantum numbers in the range of 1 to 4. In particular, the levels with $v=2$ and $v=3$ are strongly populated. There is apparently only little (if any at all) population in the $v=0$ level. There is probably some population in levels with $v>4$, but this information is very difficult to extract since the dominant contribution from these levels is at low energy where recombination via $(2p\sigma_u)^2\ ^1\Sigma_g^+$ is expected to dominate. In summary, it appears that this vibrational distribution resembles the expected relative populations of fig.7.4, perhaps with a slight shift towards higher vibrational quantum numbers.

The structure at about 15 eV we ascribe to recombination via Rydberg levels converging to the $2p\pi_u$ state of H_2^+ , for which no model calculation has been performed.

With no information on the relative magnitudes of the contributions from $(2p\sigma_u)^2\ ^1\Sigma_g^+$ (fig.7.2) and from the Rydberg levels converging to the $2p\sigma_u$ state of H_2^+ (fig.7.3), an entirely different interpretation, involving a very different vibrational distribution, would appear to be just as well justified as the interpretation presented above. To illustrate this point, we assume for a moment that the contribution from $(2p\sigma_u)^2\ ^1\Sigma_g^+$ is completely dominating (which is **NOT** the case). With this assumption in mind, we make a fit to our data with a linear combination of the contributions from $(2p\sigma_u)^2\ ^1\Sigma_g^+(v=0,1,2,3)$. It so happens that a reasonable fit is obtained yielding 70% $v=0$, 20% $v=1$, 10% $v=2$, and 0.3% $v=3$! But as already mentioned, the assumption that the contribution from the Rydberg levels can be neglected is not correct. This can be seen from the result of a DisR measurement with HD^+ performed at the TSR in Heidelberg (Forck 1993). HD^+ has a permanent electric

dipole moment and is therefore expected to relax to the $v=0$ level quite rapidly. Furthermore, the DisR spectrum of $\text{HD}^+(v=0)$ is expected to be very similar to that of $\text{H}_2^+(v=0)$. In the HD^+ experiment, the rate coefficient observed at 10 eV (corresponding to the maximum $v=0$ contribution via Rydberg levels) exceeded that observed at 4 eV (where there is a 'bump' in the $(2p\sigma_u)^2\ ^1\Sigma_g^+(v=0)$ contribution) by a factor of five! We therefore conclude that this alternative interpretation was based on an invalid assumption and therefore incorrect.

This (in my humble opinion) incorrect interpretation was recently applied in a measurement of DisR for D_2^+ at the Stockholm storage ring CRYRING (Larsson 1994), leading the authors to conclude that more than 65% of the D_2^+ ions was found in the $v=0$ level after 22 s of storage.

In the Stockholm D_2^+ experiment, as in our results presented in fig.7.7, the maximum of the broad structure was found at about 4 eV. The fact that they claim to have their ions in the vibrationally lowest levels, whereas we do not, is not due to very different experimental results (the results are in fact quite similar), but merely to the different interpretations, as described above. What appears to be a real mystery, however, is a result of DisR of H_2^+ performed at the TSR (Zajfman 1993). In this experiment, the maximum DisR signal was found at an energy as high as 9 eV, which is almost as high as for HD^+ , indicating that the degree of vibrational excitation is substantially lower than for the expected relative population shown in fig.7.4. The authors ascribe the low vibrational excitation to residual-gas collisions, but if the vibrational distribution for H_2^+ gets displaced towards lower v upon storage in the TSR, there is of course no reason why the same thing should not happen in ASTRID. I do not have very good explanation

of the difference between the two experimental results for H_2^+ , but it appears that special conditions in the ion sources, leading to vibrational distributions different from the expected relative populations of fig.7.4, would be a reasonable guess.

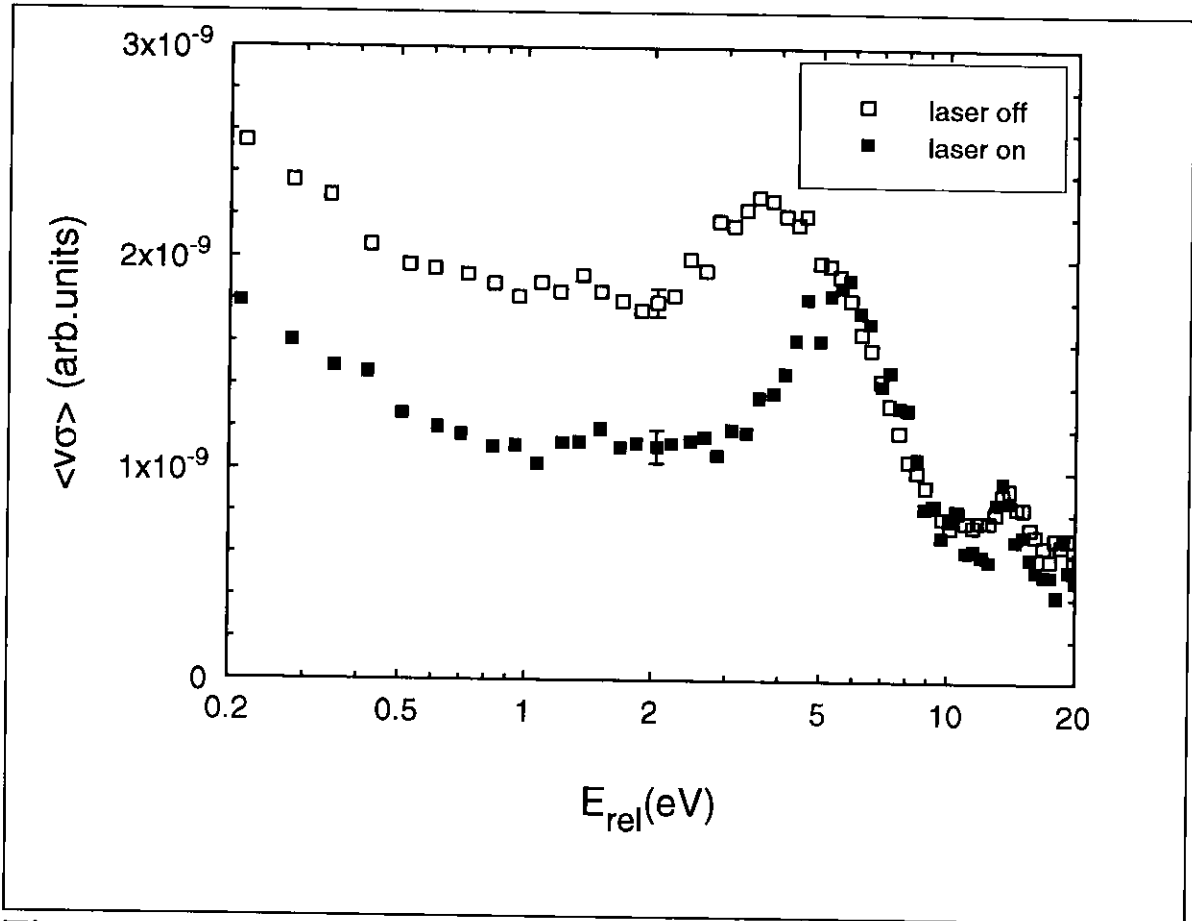


Figure 7.8 *The measured DisR spectrum with and without the application of laser photodissociation. Both sets of data are from the time window 56.0s-65.6s after injection.*

In fig.7.8, we present the DisR spectrum obtained in the time window 56.0s-65.6s after injection, with the laser running all the time to eliminate the population in the higher vibrational levels. For comparison, we also show the spectrum obtained in the same time window without the laser. Again a single point on each curve has been assigned an error bar, indicating the typical statistical uncertainty.

When comparing the two results, we see that in the low-energy

region, the rate coefficient is reduced, and the two structures around 5 eV and 15 eV have become narrower. As before we use the structure at around 5 eV, which we ascribe to recombination via the Rydberg levels converging to the $2p\sigma_v$, as the key to deduce the vibrational distribution. Comparing these data to fig.7.3, we find that now we have about equal populations in the $v=1$ and $v=2$ levels, whereas the populations in the $v=3$ and $v=4$ levels appear to have vanished. From fig.7.6, we would expect that also the population in $v=2$ could be removed, but in the estimates leading to fig.7.6, we assumed a hundred per cent overlap, which is not likely as the ion and laser beams are of about the same size. With an imperfect overlap, we may have a situation where the populations in $v=3$ and 4 can be completely depleted, whereas the $v=2$ population is only partly removed, in agreement with the observed DisR spectrum shown in fig.7.8.

To summarize the above discussion, we present in fig.7.9 the data in the energy range of 2 eV to 10 eV without and with laser photo-dissociation, together with the expected leading contributions to the observed structures labelled by the vibrational quantum number of the initial level responsible for the particular structure.

In the present experiment the feasibility of applying a photodissociation technique to obtain an ion beam with reduced vibrational excitation has been demonstrated. For future experiments one could try to perform the photodissociation at the maximum energy in ASTRID, which is 75 MeV for H_2^+ . At this energy the blue-shifted laser light will have a wave length of 212 nm due to the much stronger doppler shift. At this wave length all levels but the $v=0$ level will be photo-dissociated quite rapidly. This could provide a detailed test of whether the

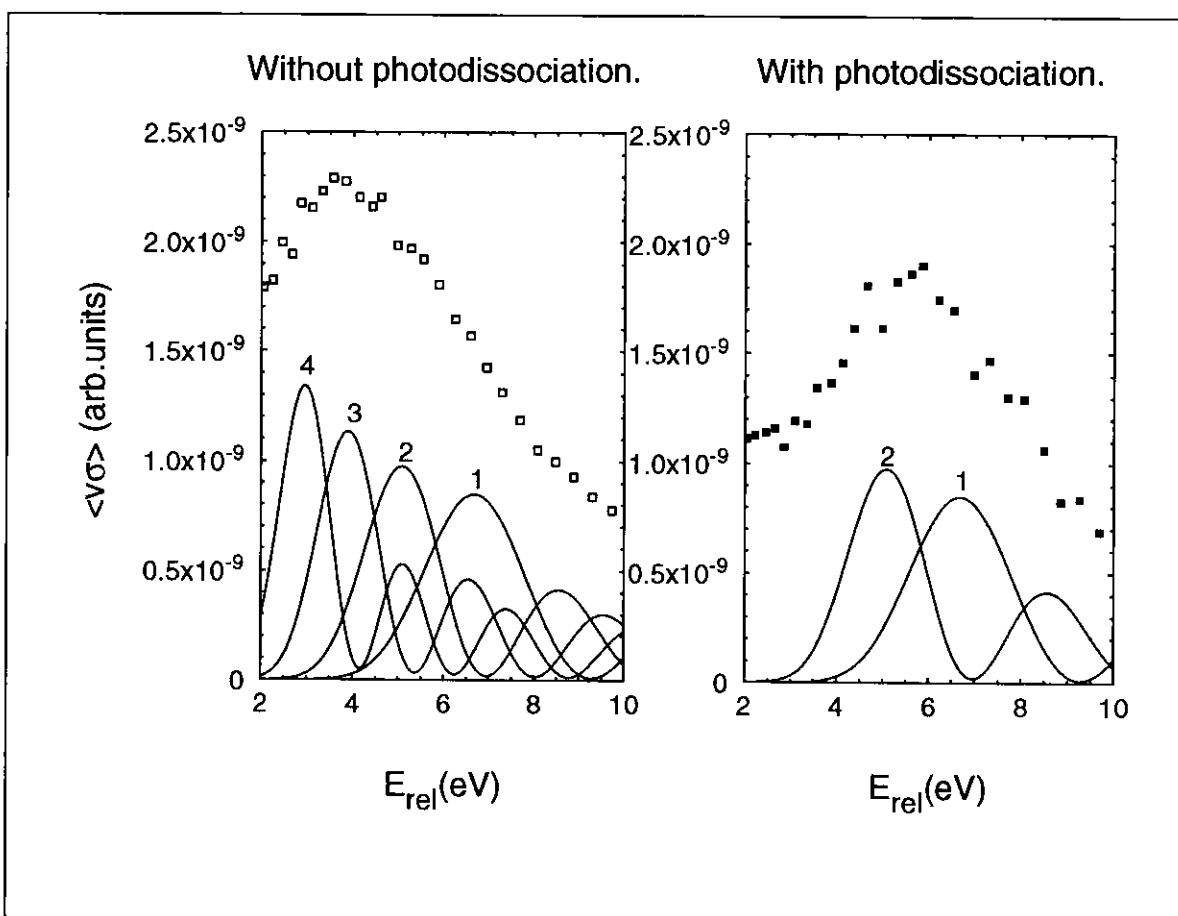


Figure 7.9 The DisR spectra found without and with the application of the laser photodissociation technique. Also shown are the expected leading contributions to observed structures.

DisR spectra for $v=0$ are really identical for HD^+ and H_2^+ . Having provided a DisR spectrum for pure $v=0$ the next logical step would be to do the same for $v=1$. This can be achieved by choosing the laser wave length in such a way that there is a minimum in the cross section for photodissociation of ions in the $v=1$ level and at the same time a substantial cross section for photo-dissociating ions in the $v=0$ level. Such a wave length exists, unfortunately it is as short as 115 nm making continuous wave laser operation a difficult task.

In the above discussion the role of *rotational* excitation has not been discussed. It is generally believed that when the ions are

produced from planar molecules the degree of rotational excitation will be rather limited. For this reason rotations are not often discussed in the DisR community (except that they are nice jokes to refer to when you do not understand your data!). Recently the first calculations taking rotations into account in DisR of H_2^+ have been published (Takagi 1993), and a proposal have been made to study DisR in ASTRID for very highly rotationally excited H_2^+ ions formed from methane gas rather than from hydrogen (Mathur 1994).

Z Amitay, D Zajfman, and P Forck (1994) (In course of publication)

D Auerbach, R Cacak, R Caudano, T D Gaily, C J Keyser, J Wm McGowan, J B A Mitchell, and S F J Wilk (1977) J.Phys.B 10, 3797

N G Adams, D Smith, and E Alge (1984) J.Chem.Phys. 81, 1778

D Bates (1950) Phys.Rev. 78, 492

M A Biondi and S C Brown (1949) Phys.Rev. 76, 1697

B H Bransden and C J Joachain (1983): Physics of Atoms and Molecules, Longman Scientific & Technical

C Derkits, J N Bardsley, J M Wadehra (1979) J.Phys.B 12, L529

G H Dunn (1966) J.Chem.Phys. 44, 2592

G H Dunn (1968a) Phys.Rev. 172, 1

G H Dunn (1968b) JILA report #92

P Forck, M Grieser, D Habs, A Lampert, R Reppow, D Schwalm, A Wolf, and D Zajfman (1993) Phys.Rev.Lett. 70 426

S L Guberman (1983) J.Chem.Phys. 78, 1404

M Larsson, M Carlson, H Danared, L Broström, S Mannervik, and G Sundström (1994) J.Phys.B 27, 1397

H Lefebvre-Brion and R W Field (1986): Perturbations in the Spectra of Diatomic Molecules, Academic Press (In particular ch.7 on autoionization)

R J Le Roy (1989) Comp.Phys.Comm. 52, 383

D Mathur, M Krishnamurthy, and P Gross (1994) (in course of publication)

J B A Mitchell (1990) Phys.Rep. 186, 215

K Nakashima, H Takagi, and H Nakamura (1986) J.Chem.Phys. 86, 726

J S Nielsen (1994) To be published in Optics Letters

K O Nielsen (1957) Nucl.Inst.&Meth. 1, 289

B Peart and K T Dolder (1974) J.Phys.B 7, 236

H Takagi (1993) J.Phys.B 26, 4815

P Van der Donk, F B Yousif, J B A Mitchell, and A P Hickman (1991) Phys.Rev.Lett. 67, 42

D Zajfman, P Forck, M Grieser, D Habs, R Reppow, D Schwalm, and A Wolf (1993), Abstract of Contributed Papers, XVIII ICPEAC, Århus 1, 383

8. Summary

In the present thesis, studies of recombination processes applying the technique of merged beams of fast ions and electrons are described. The main advantage of this technique is that the low relative velocity of ions and electrons necessary for these investigations can be achieved, at the same time as the velocity of the ions relative to the molecules of the residual gas is high. The high ion velocity leads to a very low reaction cross section for the leading contribution to the background signal, the capture of electrons in collisions with residual gas molecules.

The experimental technique is described in ch.3, emphasizing the electron beam velocity distribution and its relation to the energy resolution of the experiments. The presentation of the process of electron cooling is aimed at introducing this process as a tool for merged-beams experiments in storage rings rather than investigating the process itself.

The non-resonant process of radiative recombination is discussed in ch.4. Results of measurements of this process for non-fully stripped ions, showing evidence of incomplete screening, are presented. The process of laser-induced recombination is also considered in this chapter.

Experimental investigation of dielectronic recombination is presented in ch.5. Results of measurements of this process for He-like ions from the Aarhus single-pass experiment and the Heidelberg storage ring experiment are compared.

In ch.6 recombination is reduced from being the aim of the investigation to being a tool for high-precision measurements of the lifetimes of the $1s2s\ ^3S$ metastable states of He-like ions of boron, carbon, and nitrogen, performed at the Heidelberg storage ring.

The experiment described in ch.7 is concerned with the process of dissociative recombination of molecular hydrogen ions. The discussion of this experiment emphasizes the distribution of population on the different vibrational levels of the ions in the initial state. In particular, a laser photo-dissociation technique was introduced to reduce the number of initial levels in the experiment.

9. Dansk Resumé (Summary in Danish)

Nærværende afhandling beskriver studier af rekombinationsprocesser i eksperimenter med hurtige sammenfaldende stråler af ioner og elektroner. Denne teknik har sin væsentligste styrke ved, at den lave relative hastighed mellem ioner og elektroner, der er nødvendig for disse undersøgelser, kan opnås samtidig med en høj hastighed i forhold til restgassen. Dette medfører, at reaktions-tværsnittet for den væsentligste kilde til baggrundssignalet, elektronindfangning ved kollisioner med restgas-molekyler, reduceres med en overordentlig stor faktor.

Hovedparten af det eksperimentelle arbejde præsenteret i afhandlingen er udført ved hjælp af elektron-køleren ved Institut for Fysik og Astronomi, Aarhus Universitet. For den tidligst udførte del af dette arbejde var elektron-køleren installeret ved tandem-acceleratoren, mens de seneste eksperimenter er udført med elektron-køleren monteret på lagerringen ASTRID (Aarhus STORAGE RING, Denmark). Desuden præsenteres resultater opnået i løbet af et seks måneders studieophold ved "Max-Planck-Institut für Kernphysik" i Heidelberg, Tyskland.

Hovedvægten er lagt på beskrivelsen af studier af processerne dielektronisk rekombination (DR) og den molekylære rekombinationsproces dissociativ rekombination (DisR).

I DR processen indfanges en fri elektron til en positiv atomar ion ved samtidig anslåelse af en allerede bundet elektron til en dobbelt-anslået tilstand, som derefter med en hvis sandsynlighed henfalder ved udsendelse af et lys-kvant. Denne proces er studeret for ioner med to

til seks elektroner i begyndelsestilstanden. Specielt er der lagt vægt på diskussionen af DR med en metastabil tilstand i et to-elektron system som begyndelsestilstand. Specielt er levetiden af sådanne metastabile tilstande målt ved at studere signalet fra DR-eksperimentet som funktion af tiden efter en injektion i Heidelberg-lagerringen, TSR.

For den variant af DisR-processen, som er studeret i afhandlingen, er selve indfangningsprocessen principielt identisk med første skridt af DR-processen, men for denne molekylære proces afgives overskudsenergien fra indfangningsprocessen, ved at molekylet dissocierer. Denne proces er studeret for molekylære brint-ioner. Specielt er en laser-fotodissociationsteknik til begrænsning af antallet af vibrationelle tilstande populært i eksperimentet beskrevet.

10. Acknowledgments

During the years, several people have contributed in different ways to what has now evolved to this Ph.D.-thesis. I want to thank them all.

First of all I wish to thank my supervisor, Lars Andersen, who taught me many practical tricks in the laboratory and with whom I have had many interesting discussions concerning our experiments and the interpretation of our results. Also Jakob Bolko and Lise Vejby-Christensen, my fellow students in the recombination group, should be mentioned.

I would like to thank the ASTRID group, Søren Pape Møller, Niels Hertel, and Torben Worm, for being available at practically any hour for telephone consultation in case of ring problems. Neither Finn Abildskov's contribution concerning the data taking system should be forgotten. Practically everybody in the electronics workshop has at some point contributed to these experiments. In particular, I would like to thank Arne Petersen and Per Christensen. For the photo-dissociation part of the H_2^+ experiment a special thanks to Jørgen Nielsen and Jeff Hangst who provided the laser light.

Of course no ASTRID experiments would be performed if not for Vagn Toft and his vacuum crew.

A special thanks to Andreas Wolf for inviting me to come to Heidelberg and for collaborating on the TSR experiments and the writing of [VI]. I would like to thank all the physicists, technicians, and students working at the TSR facility who helped me during these

experiments. In particular, I want to mention Joachim Kenntner, Thomas Schüßler, Ulrich Schramm, Peter Forck, Dieter Habs, and Dirk Schwalm.

Several times, when I have had a question of theoretical nature concerning the experiments, I have received good advice from Knud Taubjerg.

I want to thank Peter Balling, Deepak Mathur, and Alice Grandjean for reading, correcting, and commenting on this thesis from the points of view of their different lines of expertise.

Finally, the help and encouragement of Marianne and Heidi has been invaluable to me.